NASA Contractor Report 3411

Modular Reflector Concept Study

D. H. Vaughan

NASA

Modular Reflector Concept Study
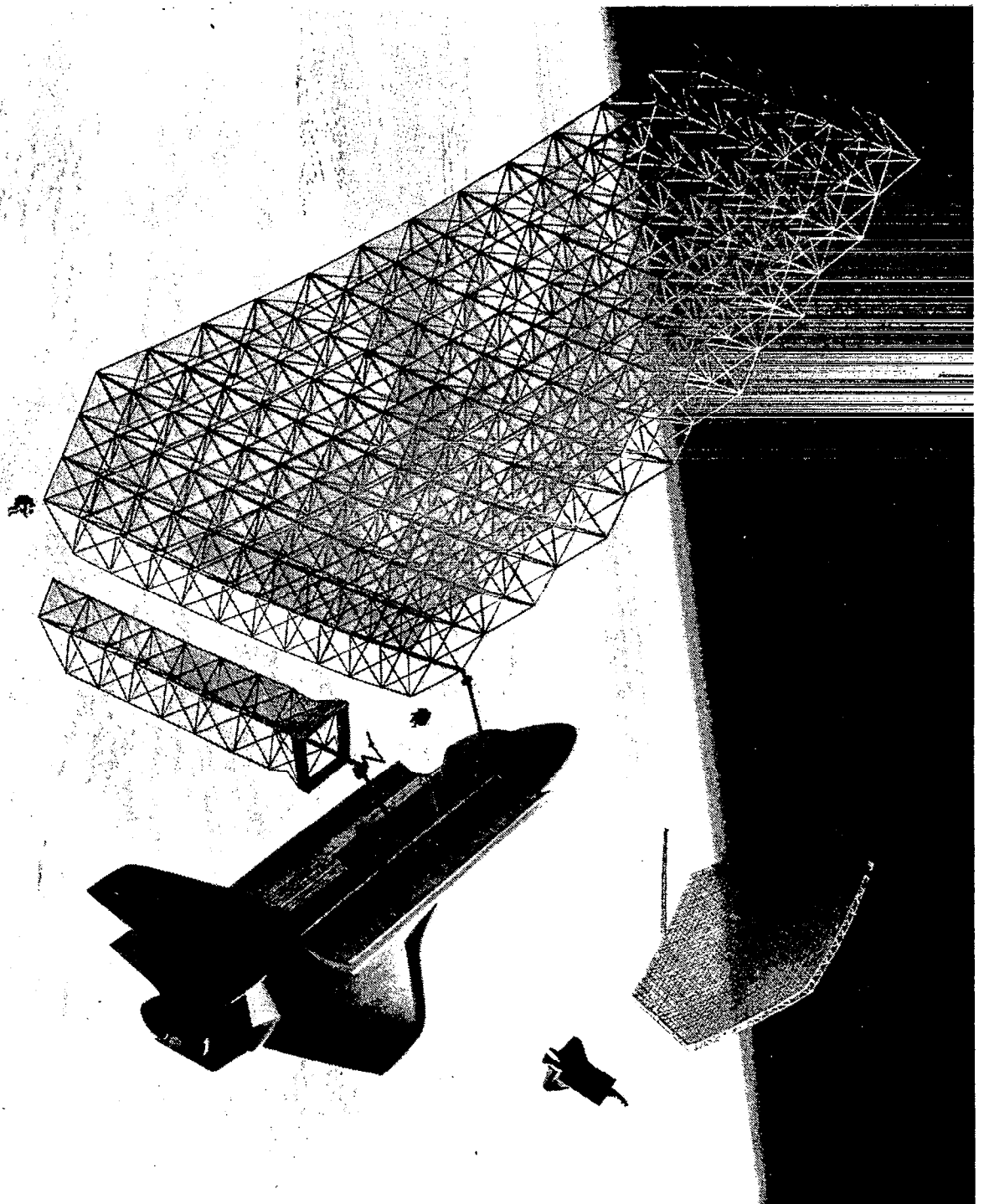
DEPLOYMENT/ERECTION OF A MOD-PETA (J) MODULAR REFLECTOR

Modular Reflector Concept Study

D. H. Vaughan
General Dynamics Corporation
San Diego, California

N/\S/
National Aeronautics
and Space Administration

**Scientific and Technical
Information Branch**

1981

FOREWORD

This study was conducted by General Dynamics Convair Division for NASA-LaRC in accordance with Contract NAS1-15753.

The principal study results were developed from April 1979 through December 1979 followed by documentation. Reviews were presented at LaRC in September 1979 and in February 1980.

Dr. Michael F. Card was the NASA-LaRC Technical Representative.

The study was conducted in Convair's Advanced Space Programs. The program was supervised by the Director of Advanced Space Programs (Dept. 950-0), initially J. Hurt then D. Jones.

Computer analysis tasks were performed by Steve Valenta and Alex Leondes. Frank Leinhaupel provided the theoretical evaluation of shape errors attributable to flat facets. Professor Adnan Nayfeh of the University of Cincinnati assisted in geometry optimization.

For further information contact:

Dr. Michael F. Card   Desmond H. Vaughan
Chief, Structural & Mechanical Division   Study Manager
Mail Stop 244   Mail Zone 42-6730
NASA-LaRC   General Dynamics Convair Div.
Hampton, Virginia 23665   P. O. Box 80847
(804) 827-3121   San Diego, California 92138
                                           (714) 277-8900, Ext. 2633

TABLE OF CONTENTS

TABLE OF CONTENTS, Contd

LIST OF FIGURES

LIST OF FIGURES, Contd

LIST OF FIGURES, Contd

LIST OF FIGURES, Contd

LIST OF FIGURES, Contd

LIST OF TABLES

SECTION 1

INTRODUCTION

The primary objective of this study is to investigate the feasibility of constructing large space structures, specifically a 100 meter paraboloidal radio frequency (RF) reflector, by individually deploying a number of relatively small structural modules, and then joining them to form a single, large structure in orbit.

The advantage of this approach is that feasibility of a large structure may be demonstrated by ground and flight tests of a few smaller and less costly substructures (modules). Thus, initial development costs are substantially reduced and a high degree of reliability can be obtained without initial commitment to construction of a very large system.

The three candidate structural concepts illustrated in Figure 1-1 are investigated:

1. The Deployable Cell Module (DCM)

2. The Paraboloidal Extendable Truss Antenna adapted to modular assembly (Mod-PETA)

3. The Modular Extendable Truss Antenna (META)
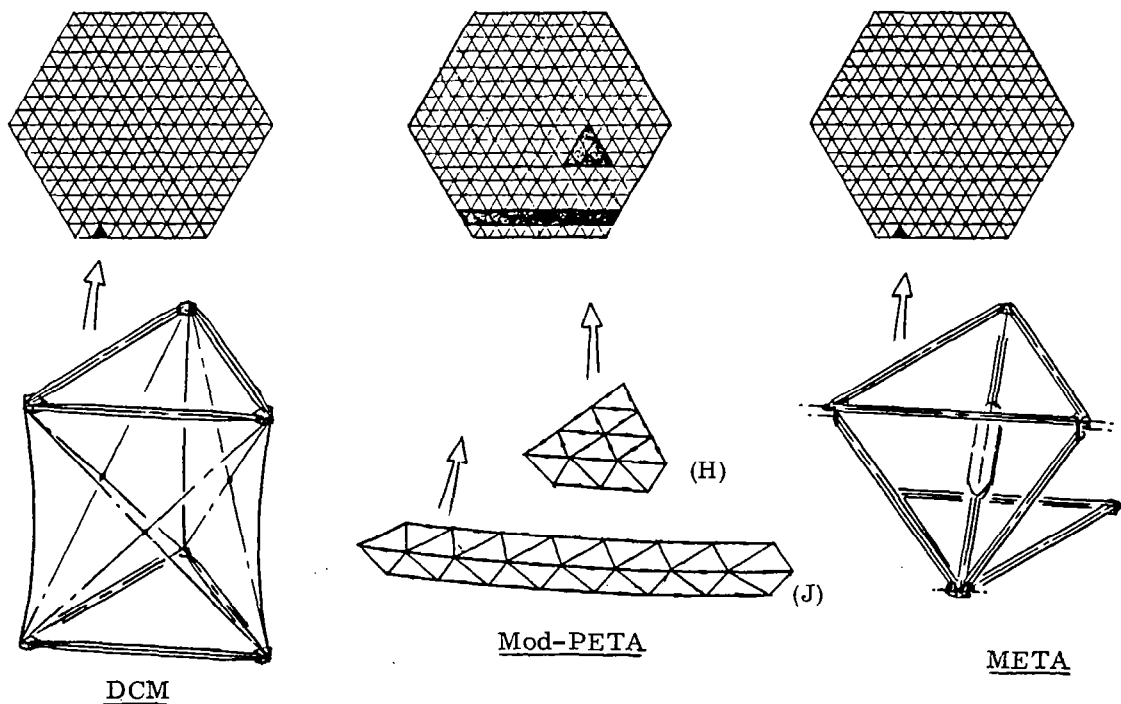
Figure 1-1. The Three Candidate Structural Concepts

1-1

In each of these concepts the reflector structure is made up of a series of substructures (modules), each module supporting an equivalent section (facet) of the RF reflective surface. Each module is individually packaged in a compact envelope for launch, extended to its deployed configuration in orbit, and subsequently joined to neighboring modules to create a single, large, integrated structure. The facets are thus aligned, edge-to-edge, producing a single large surface.

Investigation has been conducted of the means by which the structural concepts, including a reflecting surface, can be packaged and deployed in an automated fashion. Structural weights and packaging efficiencies have been compared. Practical means and method-ology of joining modules using the Space Shuttle Orbiter as a base have been studied, and equipment required to support construction has been described.

The general conclusion drawn from this study is that combining mechanical deployment with modular assembly in a step-by-step sequence is a feasible, low cost, low risk approach to in-space construction of large space structures.

The study also shows that deep truss concepts consisting of tubular, structural elements arranged in three-dimensional triangulation are well suited to this application and provide structures of outstanding rigidity, stability, structural efficiency, and size potential. For all concepts the estimated natural frequency (f_1) exceeds 1.7 Hz for the 100 meter assembly.

It is concluded that all three candidate structures (DCM, Mod-PETA, and META) are feasible structural concepts for the in-space assembly of a 100 meter diameter paraboloidal reflector for operating at 1 GHz radio frequency.

Critical evaluation factors are shape accuracy and stability, packaging efficiency, in-space deployment/assembly, and cost. None of the three candidate concepts has been found to possess critically unacceptable characteristics. Thus, for specific missions all three concepts should be assessed against the specific requirements of the mission for determination of the most applicable concept. Each concept has individual features, peculiarities, and limitations that may or may not be critical for specific missions and modes of operation. The most significant of these are summarized thus:

- All three concepts are capable of adequately providing structural support to a 100 meter diameter reflective surface (f/d=1.00) for operation at 1 GHz ($\delta = \lambda/50$) in the space environment.

- Transportation by Space Shuttle for assembly of deployable structural modules is feasible for all three concepts.

- The sizing and proportioning of the DCM and META modules are severely constrained by the available payload diameter which directly limits module size and attainable structural depth.

- The PETA concept is much less constrained by envelope considerations. It provides a wide range of design sizing options permitting optimization for a wide range of reflector sizes and applications.

- The DCM and META concepts require the space assembly of a large number of small modules. Space assembly functions are small scale but highly repetitive. The number of modules required to assemble structures exceeding 100 meters in diameter may be unacceptably large. For a diameter of 119 meters the module count would exceed 1000.

- The Mod-PETA concept requires the space assembly of a smaller number of larger modules. Space assembly operations are moderately repetitive, but relatively complex. Growth potential beyond 100 meter diameter is good.

- The DCM structure has a high component part count, depends upon sustained preloading for structural stability, and uses tension ties as primary structural elements. This preloading detracts from the ability of the structure to tolerate applied (external) loads, and may cause material creep.

- The Mod-PETA concept provides a less complex structure of superior performance and characteristics from a smaller payload volume, which translates into fewer orbiter flights.

- The Mod-PETA concept is burdened by duplication of structural members at the modular interfaces, which increases the part count by approximately 35%.

SECTION 2

DEPLOYABLE CELL MODULE (DCM) CONCEPT

2.1 DEFINITION OF A 100 METER DCM REFLECTOR

The reflector configuration shown in Figure 2-1 is optimized for the minimum number of component structural modules. Figure 2-2 shows the typical module configuration.

Due to the desired paraboloidal shape of the reflector (f/d=1.0) the component structural elements of the modules vary slightly in length. The double dimensions shown in Figure 2-1 and 2-2 indicate the limits of this variation, which is generally within ±2.06% of the median dimension. Optimization ensures that the largest module, when packaged as shown in Figure 2-3, is compatible with transverse stowage in the Space Transportation System (STS) Orbiter payload bay diameter. Space is allowed for the stowage pallet as shown in Figure 2-4.

2.2 DESIGN CONSIDERATIONS

The two triangular frames and the six cross ties are the prime structural elements of the module. The structural performance of the total reflector is dependent on the strength and stiffness of these elements. The three prebuckled column members that separate the two triangular frames act as compression springs and provide a simple means of preloading the prime structural elements. The geometric stability of the DCM module is dependent upon this preloading, which puts the six cross ties in a state of sustained tension, and the triangular frames in sustained compression. In practice the magnitude of this required preloading must be determined for each specific application to satisfy two critical requirements: 1) preloading must be sufficient to ensure that the tension in the six ties remains positive for all conditions of externally applied structural loading, and 2) preloading must not be so large as to exceed allowable column strength of the triangular frame elements (tubes) under conditions of additive applied structural loading.

It is thus seen that external, operational loading of the structure is a critical consideration in the detail design of all elements of the structure. Other critical considerations include:

- Required stiffness characteristics of the reflector.

- Handling loads in the module elements during packaging, deployment and integration of the modules.

- Thermal stresses and strains, due to shadowing and non-uniform solar heating, in the completed reflector structure.

3.50 m

DCM STRUCTURAL MODULES
(721)

200m RADIUS

A

3.5908 MAX.
3.4490 MIN.
TYPICAL

108 m
MODULES (31)
POINT-TO-POINT

3.5908 MAX
3.4490 MIN

3.6527 MAX.
3.5084 MIN.

2.0732 MAX
1.9912 MIN.
TYPICAL

A

A—A

SCALE												
METERS	10	0	10	20	30	40	50	60	70	80	90	100
FEET	25	0	25	50	75	100	150	200			300	
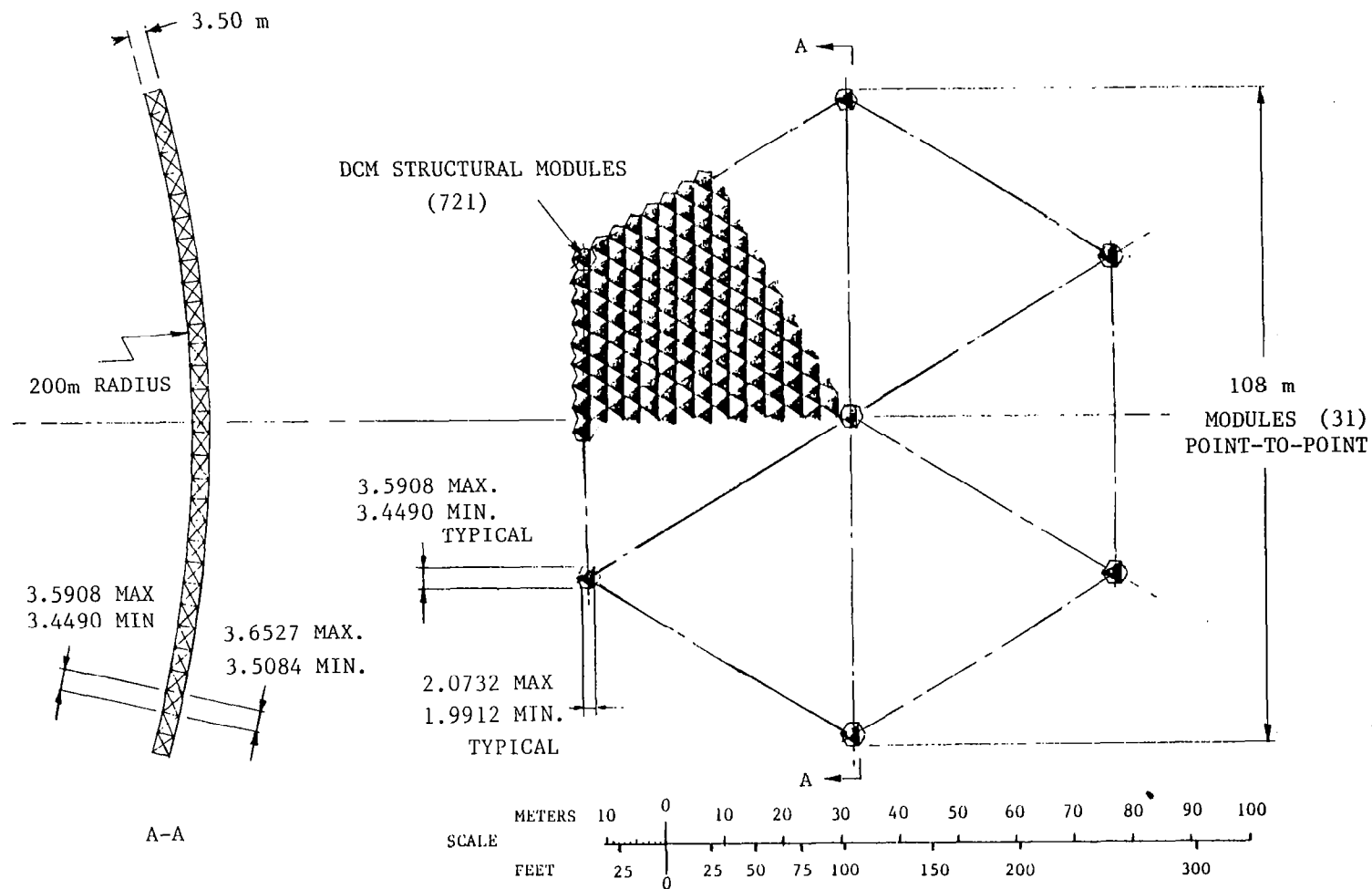
Figure 2-1. DCM—100 Meter, 721 Module, Reflector, Study Case C-1

GRAPHITE EPOXY TUBE
3.1cm (1.2 IN.) SQUARE
0.91mm(.036 IN.) WALL
TYPICAL (6) PLCS

MODULE-TO-MODULE
STRUCTURAL INTERFACE (12)

SPRING COLUMN (3)
(BOWED OR TELESCOPIC)

REFLECTIVE SURFACE
SEGMENT (FACET)

STRUCTURAL INTERFACE (NODE)
FITTINGS (6)

TIE LINES (6)
(METALLIC OR COMPOSITE)

REFLECTIVE SURFACE
SEGMENT (FACET)
200m RAD. SPHERICAL
OR FLAT.

3.5908 m
3.4490 m

3.6527m
3.5084m

2.0732m
1.9912m

4.1464 m
3.9824 m

3.50 m

MINOR FRAME
(CONCAVE FACE)

MAJOR FRAME
(CONVEX FACE)

Figure 2-2. DCM — Typical Module in Deployed Configuration, Study Case C-1

GRAPHITE EPOXY TUBE
3.1cm (1.2 IN.) SQUARE
0.91mm (.036 IN.) WALL
TYPICAL (6) PLCS

7.04 cm (2.77 IN.) OVERALL, SPHERICAL FACET
6.20cm (2.44 IN.) OVERALL, FLAT FACET.

REFLECTIVE SURFACE
(SPHERICAL OR FLAT)

REFLECTIVE SURFACE SEGMENT (FACET)

BACK FRAME

FRONT FRAME

3.50m
(137.8 IN.)

3.6527m
3.5084m

3.5908m
3.4490m

2.0732
1.9912

6.10 cm (2.4 IN.)
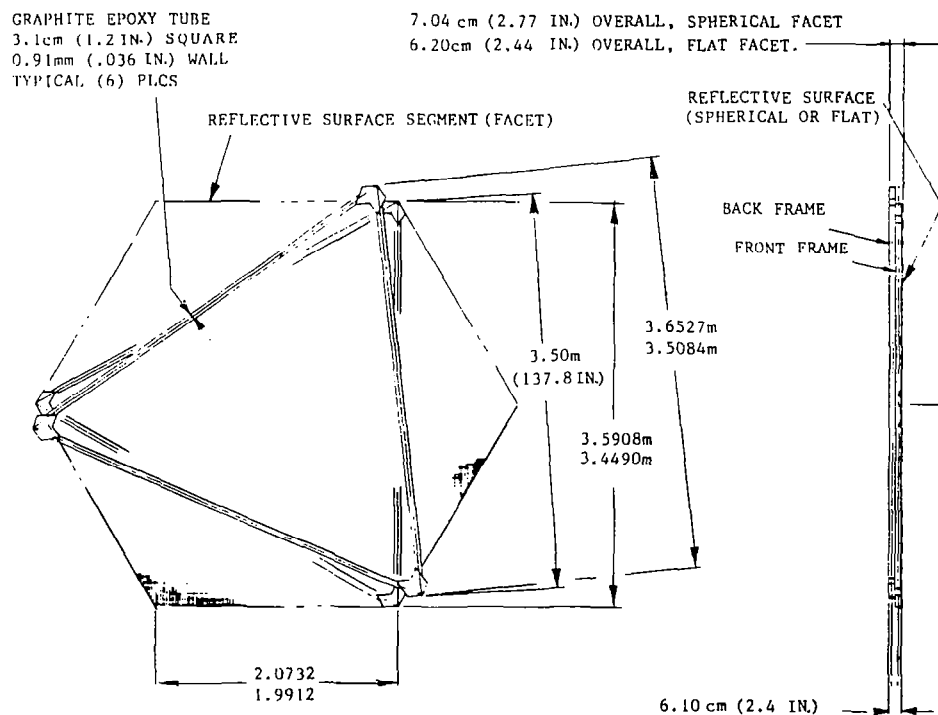
Figure 2-3. DCM - Typical Module in Stowed Configuration, Study Case C-1

2-3

7.6cm (3.0 IN) MIN. CLEARANCE

PAYLOAD ENVELOPE
4.572m (15 FT) DIA.
REF.

3.653m
(143.8 IN.)
MAX.

3.591m
(141.38 IN.)
MAX.

DCM MODULE.
MIN. PROFILE
MAX. PROFILE

INTERFACE SHOES, UPPER

PALLET SUPPORT TRUNNION

3.8cm(1.5 IN.) MIN.

¢ CONCAVE FRAME
  MIN. PROFILE
  MAX. PROFILE

¢ CONVEX FRAME
  MIN. PROFILE
  MAX. PROFILE

PAYLOAD SUPPORT PALLET

6.0cm (2.4 IN.) CLEARANCE

INTERFACE SHOE, LOWER

PALLET SUPPORT TRUNNION

ORBITER FUSELAGE, REF.

6.20cm (2.44 IN.)
FLAT FACET.

DCM MODULE,
TYPICAL

7.04cm (2.77 IN.)
SPHERICAL FACET

INTERFACE SHOES,
UPPER

REFLECTIVE FACETS

PAYLOAD SUPPORT PALLET

INTERFACE SHOES,
LOWER

ORBITER MID-FUSELAGE

Figure 2-4. DCM — Stowage of Packaged Modules in Orbiter Payload Bay

Such considerations with respect to specific system requirements must be the basis for sizing the structural elements.

Of critical importance is selection of an appropriate slenderness ratio (L/ρ) for the tubular, structural elements of the triangular frames. This characteristic obviously has direct impact on achievable packaging density, which directly determines the number of Orbiter flights required to support a specific application. Figure 2-5 shows packaging density (number of modules per payload) versus slenderness ratio (L/ρ) for the packaged configuration shown in Figure 2-3.
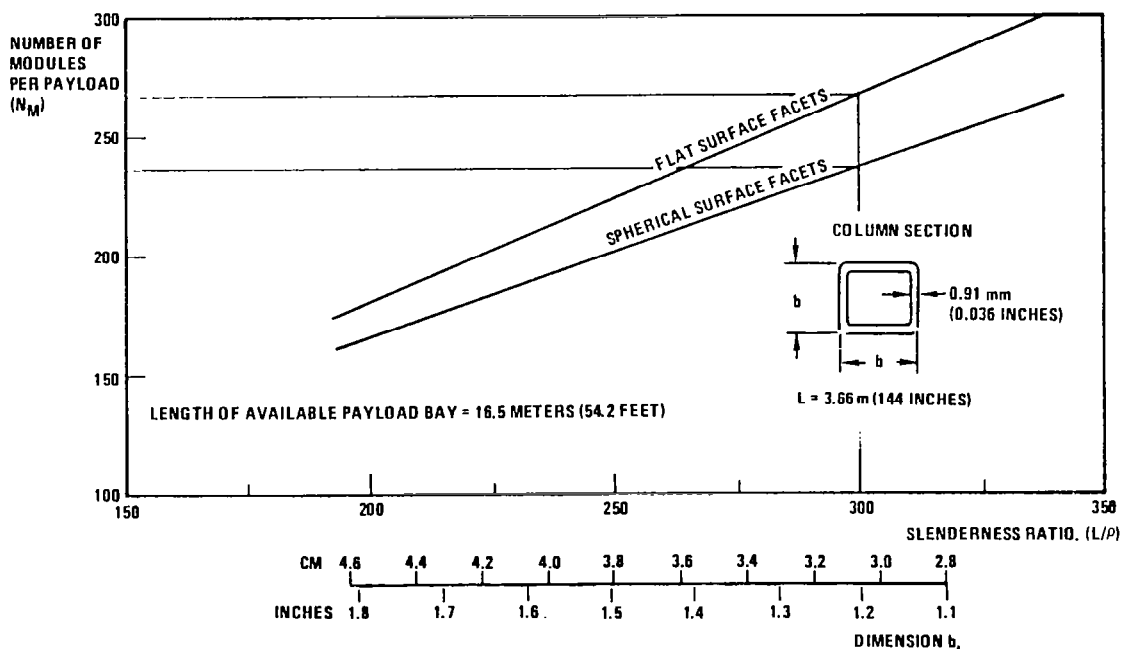
Figure 2-5. Packaging Density is Dependent on Selected Slenderness Ratio of Module Elements (Struts)

Curves are plotted both for modules with flat reflective facets, which adds an increment of 1.0 mm (0.04 inch) to the overall thickness of the packaged module, and for modules with concave (200 meter spherical radius) facets, which adds an increment of 9.4 mm (0.37 inch). Figure 2-6 shows the number of Orbiter flights required to carry into orbit the 721 modules of a 100 meter diameter reflector (see Figure 2-1). Obviously, maximizing L/ρ is desirable in order to minimize the number of flights. The limit is set by considerations of structural strength versus predicted loading. The typical structural section shape selected for the tubular members that comprise the triangular frames is illustrated. The square shape maximizes packagability for the selected L/ρ value, and also facilitates fabrication.
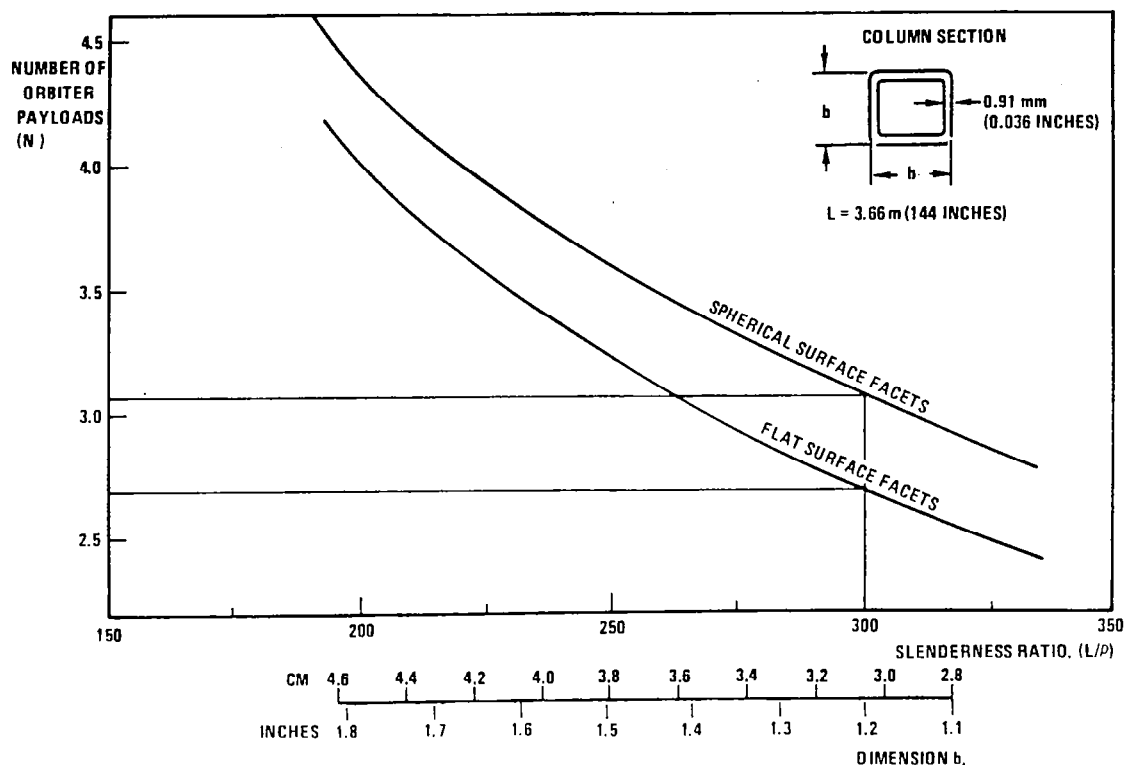
Figure 2-6. Selection of High Slenderness Ratio (L/ρ) Reduces Number of Orbiter Payloads (N) Required for Assembly of 100-Meter Diameter Reflector, 721 Modules

2.2.1 MATERIAL SELECTION. Thermal stability of the candidate structures is an important consideration in their evaluation, and is highly sensitive to material selection.

The selection of graphite epoxy for the principal structural elements is primarily justified by its low coefficient of thermal expansion (CTE) and its high stiffness-to-weight ratio.

Since the structure is destined for operation in the zero-g environment, operational structural loads generally tend to be low and critical loading conditions tend to be associated more with the dynamics of handling, boost, deployment, and assembly. Minimum wall thicknesses are frequently found to be adequate for such structures, and their exact value is then dictated more by the design of the cross-plied laminate than by predicted loading.

Carbon fibers have a characteristic negative CTE value, and this effect predominates in unidirectional graphite epoxy laminates.

In a pseudo-isotropic graphite epoxy laminate, the matrix has a greater influence and the CTE value becomes positive. A pseudo-isotropic GY70/X30 laminate (0, 45, 90, 135)$_{sn}$ typically exhibits the following in-plane properties.

2-6

$$F_{tu} = 165 \text{ to } 255 \text{ MN/m}^2 \ (24\text{k to } 37\text{k lb/in}^2)$$

$$E = 108.3 \text{ GN/m}^2 \ (15.7\text{M lb/in}^2)$$

$$CTE = (+0.18 \pm 0.18) \ 10^{-6} \text{ m/m/deg K } [(+0.10 \pm 0.10) \ 10^{-6} \text{ in/in/deg F}]$$

$$\rho = 1771.5 \text{ kg/m}^3 \ (0.064 \text{ lb/in}^3)$$

In the design of struts and columns, the primary interest is in the axial properties of the tube material and isotropy loses its usual significance. It is then desirable and feasible to tailor the material layup orientation to give the tube the mix of axial properties that best suits the specific design requirements. A typical example is presented below in which the fiber direction is biased toward the axial direction. Test results show a significant improvement in axial stiffness and strength but a shift in CTE to a negative value. This laminate consists of four plies of GY70 in $(30, 0_2, -30)_T$ orientation and is characterized thus:

$$F_{tu} = 206 \text{ MN/m}^2 \ (30\text{k lb/in}^2)$$

$$E_t = 207.5 \text{ GN/m}^2 \ (30.1\text{M lb/in}^2)$$

$$E_c = 166.2 \text{ GN/m}^2 \ (24.1\text{M lb/in}^2)$$

$$CTE = (-2.0 \pm 0.13) \times 10^{-6} \text{ m/m/deg K } [(-1.05 \pm 0.07) \times 10^{-6} \text{ in/in/deg F}]$$

This laminate, increased in thickness to a symmetrical layup of eight plies $(\pm 30, 0_4, \mp 30)_T$, is selected for the DCM structural elements. The negative CTE value is brought effectively to zero by the compensation technique described below.

Where the operational application requires the structure to have a high degree of shape stability in the space environment, its sensitivity to temperature change must be correspondingly low. This is accomplished by designing the effective length of the metal structural components (e.g., node fittings and strut end fittings) so that their positive expansion (ΔL) counters the negative expansion ($-\Delta L$) of the composite elements, giving the total structure an effective overall CTE that is theoretically zero.

The selected material for the metal components is titanium, by virtue of its high strength to weight ratio, its relatively low CTE, and its noncorrosive interface compatibility with graphite epoxy.

The properties of titanium are taken to be:

$$CTE = 8.64 \times 10^{-6} \text{ m/m/deg K } (4.8 \times 10^{-6} \text{ in/in/deg F})$$

$$\rho = 4428.8 \text{ kg/m}^3 (0.16 \text{ lb/in}^3)$$

$$F_{ty} = 1000 \text{ MN/m}^2 (145\text{k lb/in}^2)$$

$$F_{cy} = 1062 \text{ MN/m}^2 (154\text{k lb/in}^2)$$

$$E_t = 110.3 \text{ GN/m}^2 (16.0\text{M lb/in}^2)$$

$$E_c = 113.1 \text{ GN/m}^2 (16.4\text{M lb/in}^2)$$

Using the above thermal compensation design technique, it is determined that if the effective, node-to-node column length (L) consists of composite 0.82L long and titanium 0.18L long, then the theoretical CTE over length L is zero.

Tests conducted over the temperature range of 117 deg K to 394 deg K (-250 deg F to +250 deg F) have shown the CTE of a graphite epoxy composite to vary $\pm 0.41 \times 10^{-6}$ m/m/deg K ($\pm 0.23 \times 10^{-6}$ in/in/deg F) with the positive deviation occurring at the higher temperatures and the negative deviation at the lower temperatures.

Fabrication tolerances account for a further potential CTE deviation of up to $\pm 0.8 \times 10^{-6}$ m/m/deg K ($\pm 0.10 \times 10^{-6}$ in/in/deg F).

These two considerations are the principal causes of deviation from the designed zero CTE and give the following RSS value for actual CTE:

$$CTE = \sqrt{(0.41 \times 10^{-6})^2 + (0.18 \times 10^{-6})^2}$$

$$= 0.45 \times 10^{-6} \text{ m/m/deg K } (0.25 \times 10^{-6} \text{ in/in/deg F})$$

Further, this mix of composite and titanium components typically results in the following effective structural properties, node-to-node.

$$E = 131.4 \text{ GN/m}^2 (19.05\text{M lb/in}^2)$$

$$\rho = 1873.9 \text{ kg/m}^3 (0.0677 \text{ lb/in}^3)$$

These EQUIVALENT values (shown boxed above) are used in all subsequent structural concept mass properties calculations and performance analyses.

2.2.2 <u>STRUCTURAL SIZING</u>. Static structural stiffness is a function of material modulus, section area of the elements, and structural depth

$$\left(I \cong \sum_{i=1}^{N} A_i \, y_i^2 \right)$$

Stiffness is a significant consideration for applications involving loading of the structure while the antenna is operating, such as load inputs to produce angular acceleration for tracking purposes.

Stiffness characteristics under dynamic conditions are dependent on material properties, mass distribution, and structural depth. Natural frequency tends to be insensitive to element section areas since the stiffness benefit gained by increasing section areas is essentially negated by corresponding increase in mass.

Structural strength is a function of material properties and structural sizing. It is significant when conditions such as high-rate tracking, retargeting, and orbital transfer produce critical structural loading.

In practice, discrete thickening of certain structural elements of the reflectors may be required to reduce transient stress levels resulting from the secondary loading conditions mentioned above, but this would be localized and not significant to overall mass properties characteristics.

2.2.2.1 <u>Sizing of Tubular Column Members (Struts)</u>. The data presented above (also see Figures 2-5 and 2-6) are parametric only to the extent that the radius of gyration of the section (ρ) is a variable. L/ρ is a readily visualized indicator of column stability, strength, and structural efficiency. The figures apply specifically to modules whose structural elements have the section shown, with L, t, and E_{11} as constant values. Thus, each value of L/ρ has a corresponding value of b, where b is the overall width of the section, and is the parameter that determines achievable density of packaging. The intent of such data is to aid the user in determining the *number of Orbiter payloads* required to support construction involving a given number of modules of given column strength, or, conversely, in determining the *column strength* of a given number of modules sized for a given number of Orbiter payloads.

The constant L = 3.66 meters (144 inches) and is the optimized value for compatibility with the payload envelope diameter (see Figure 2-4).

The constant t, wall thickness, = 0.91 mm (0.036 in.) is derived from the eight 0.11 mm (0.0045 in.) plies of the laminate selected above. This is a preferred but not mandatory thickness value. Other values for t are feasible and, if selected, would require modification of the data presented in Figures 2-5 and 2-6. Increased wall thickness would permit reduction of b without reduction of

ρ, but structural efficiency would be lower. In other words, if "t" were increased in value then packaging density is improved, but there is a weight penalty and associated degradation of structural dynamic performance. The converse is true if "t" is reduced in value.

Figure 2-7 therefore illustrates the preferred baseline structural section. The characteristics and properties of the section are:

Length (L)	=	3.66 m (144 in.)
Wall (t)	=	0.91 mm (0.036 in.)
Width (b)	=	3.1 cm (1.2 in.)
Radius (r)	=	3.0 mm (0.12 in.)
L/ρ	=	300
P_{cr}	=	2131N (480 lb)
Weight	=	0.57 kg (1.257 lb)
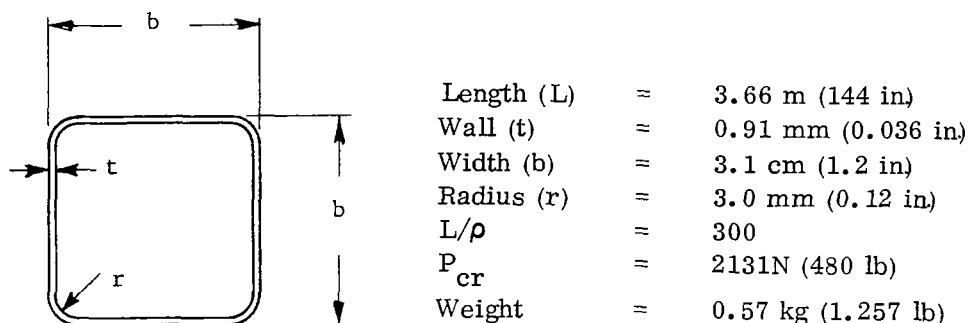
Figure 2-7. Typical Structural Section Geometry

Figure 2-8 shows the column strength (P_{CR}) of a 3.66 meter (144 inch) length of such square section tubing where "b" is the variable.
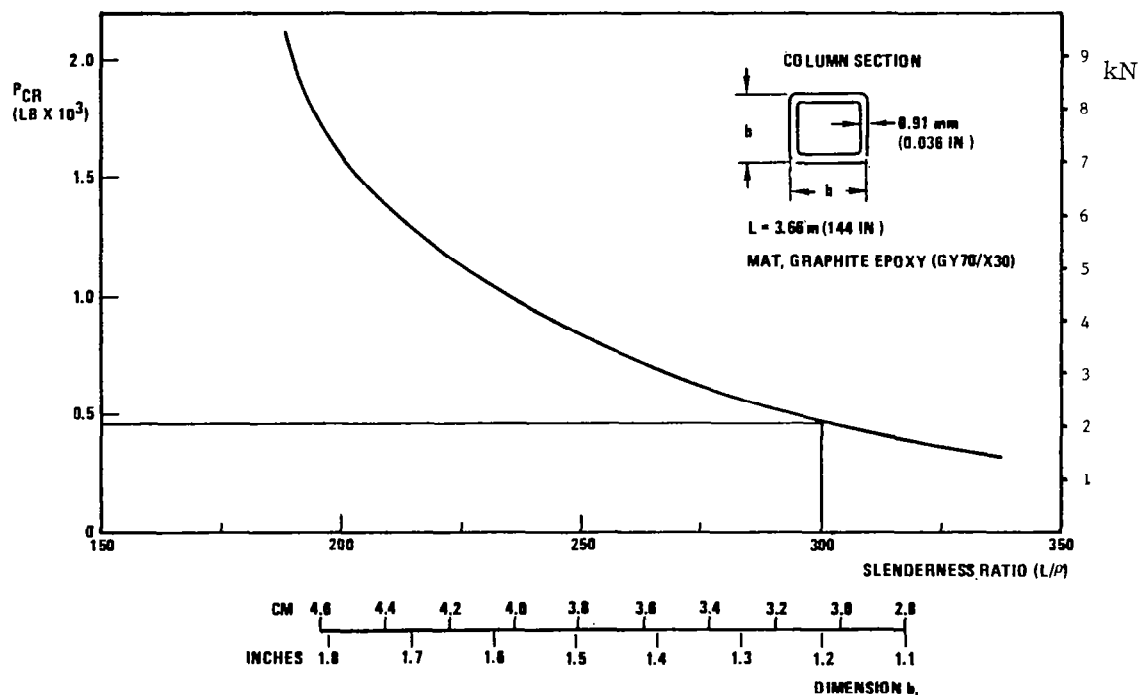
Figure 2-8. Column Strength Versus Slenderness Ratio (L/ρ)

2.2.2.2 Sizing of Tension Ties. Since the DCM concept depends o₁
preloading for its structural stability, the magnitude of such preloa
sizing of its structural elements must be compatible with specific mi
ments. However, for purposes of this study, it is assumed that ma
surface element load is 2230N   (500 lb). Due to the curvature of t
(spherical radius = 200 meters) surface struts typically have an an₁
tion of 0.97 degree to the plane of the nodes (see Figure 2-9a). T]
surface strut load of 2230N   (axial compression) the corresponding
buckled column load needed to maintain positive tension in each set
is 2230 sin 0.97 = 38N (8.5 lb) (Figure 2-9a).

Note that since each column provides pretensioning for two sets of ₍
ties the actual design spring load for this element must be 38N × 2

With the surface struts unloaded, this spring load will be reacted ir
equilibrium, producing a tension of 55N (12.4 lb) in each tie, 41N (
each inner surface member, and 39N (8.8 lb) in each outer surface
Figure 2-9b). This represents a steady-state preloading, which is a
characteristic of the DCM concept.

Figure 2-9. Design Loads — DCM Structures

2-11

Figure 2-10 shows a concentrated external load (L) applied as shown to a single structural node point. The six tie lines that support the node fittings go into tension, transferring the load to six node fittings on the upper face of the structure. Each of these node fittings has a vertical load capacity of 76N × 3, which corresponds to the preloading exerted by the three "buckled" columns beneath each node fitting.
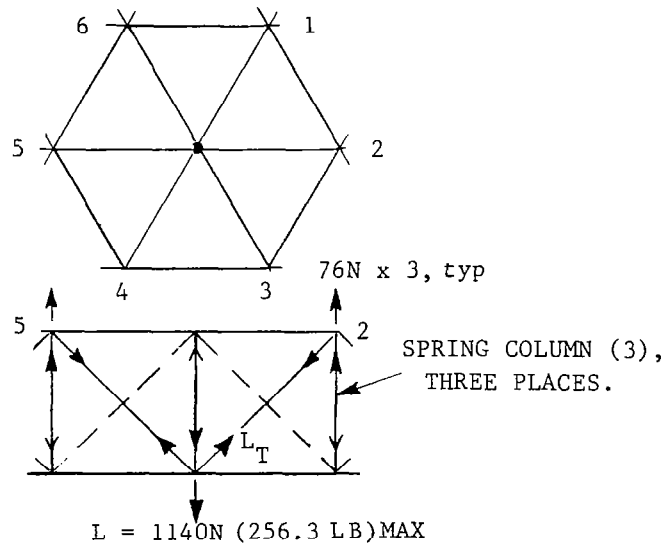
Figure 2-10. Point Loading is Limited by Capacity of Spring Columns

Thus, maximum allowable value of applied load (L) is given by:

$$L_{max} + 228N = (6)(228)N$$

$$L_{max} = 1140N \ (256.3 \ lb)$$

This calculation is simplified by neglecting the curvature of the structure and assuming it to be flat. The slight inaccuracy in the calculation that results is not considered significant for purposes of sizing.

Thus, load in each of the six ties:

$$L_T = preload + \frac{L_{max}}{6 \cos 45 \ deg}$$

$$= 55N + 269N$$

$$= 324N \ (73 \ lb)$$

If stress in tie is limited to $6.9 \, MN/m^2$ ($1000 \, lb/in^2$), cross sectional area of tie (A_T) is:

$$A_T = \frac{324}{6.9 \times 10^6} = 47 \times 10^{-6} m^2 \, (0.0721 \, in^2), \, i.e., \, \underline{0.7 \, cm \, (0.27 \, in.) \, square}$$

The application of tension tie lines as primary structural elements in high stability space structures is undeveloped and must be considered a high risk technology area. Design requirements for such an application are: high strength to weight ratio; high axial stiffness and low bending stiffness; low expansion coefficient (CTE). Conventional cable design utilizes high performance material in small section size to permit compact coiling. However, conventional materials do not satisfy the thermal stability requirements of most space structure designs. Dimensional stability under applied load requires adequate AE product (i.e., cross-sectional area × Young's modulus of the material). Dimensional stability under thermal loading requires a low coefficient of thermal expansion (CTE). Neither of these requirements is characteristically satisfied by conventional highly stressed ties. A small diameter, relatively long tension tie just adequate for the load conditions would not exhibit exceptional stiffness. Thus, stiffness requirements are likely to drive the tie design to diameters significantly larger than minimum. Selection of suitable materials for the ties is a major concern. Cables of Invar or molybdenum, if they can be made, would have reasonable thermal stability, but relatively low specific stiffness. Such materials as graphite, quartz, or E-glass must be considered. These fibers used in composite (fine rod) form could meet all requirements except bending flexibility. Coiling for stowage may not be possible to the desired compactness, and creep and permanent set during coiled storage could present problems upon deployment. Using these fibers in loosely bundled "tow" form, with no bonding matrix, would greatly increase coiling capability. However, load transfer from the fiber ends to end fittings would present a challenging design problem, and progressive breakage of individual fibers due to local bending effects is likely.

For the purposes of DCM concept evaluation, the structural cross ties are assumed to be graphite epoxy rods. For performance analyses the compensated equivalent material property values derived for the tubular (strut) elements (Section 2.2.1) are used.

Since the ties act in crossed pairs, each is assumed to have half the cross-sectional area of the typical tubular element.

2.2.3 <u>BUCKLED COLUMN MEMBER</u>. As discussed above, the sustained spring force (P) required of the installed column is 76N (17.0 lb).

The buckled column is assumed to have the rectangular section shape shown in Figure 2-11.

NEUTRAL AXIS

$h = 0.64$ cm (0.25 IN)

$b = 1.27$ cm (0.50 IN.)
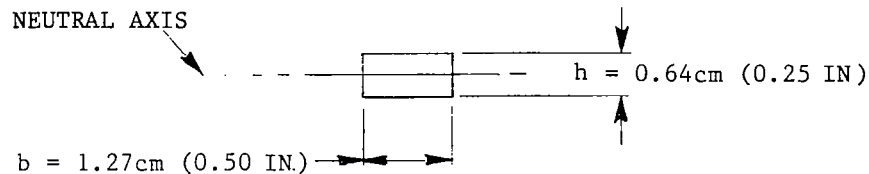
Figure 2-11. Buckled Column Section

where

$$I = \frac{b\,h^3}{12} = \frac{1.27\,(0.64^3)}{12} = 0.0277 \text{ cm}^4$$

For its high structural efficiency and stiffness, the selected material is the graphite epoxy laminate (±30, 0_4, ∓30)$_7$ having the properties listed in Section 2.2.1.

It is conceivable that the installed length of the buckled column will vary slightly due to manufacturing tolerances or due to post assembly strain in other structural components. Further, if the 76N limit load is exceeded, the buckling of the column will increase. It is therefore of interest to determine the general relationship between values of axial load (P) that exceed 76N, and the resultant column deflection; i.e., the spring rate.

Past analytical work performed at General Dynamics in this general area[1] is applied below to determine this relationship.

In its installed, prebuckled state (see Figure 2-12) the effective length of the column and its mid-point lateral deflection (y_e) are taken to be 3.5 meters (137.8 in.) and 15.2 cm (6.0 in.) respectively. Free length (unbuckled) is therefore 3.516 meters (138.5 inches).

---

[1]Wilson, P.E. and Spier, E.E., "Nonlinear Bending of a Stress Corrosion Specimen," Trans. ASME J. of Engineering for Industry, February 1966.
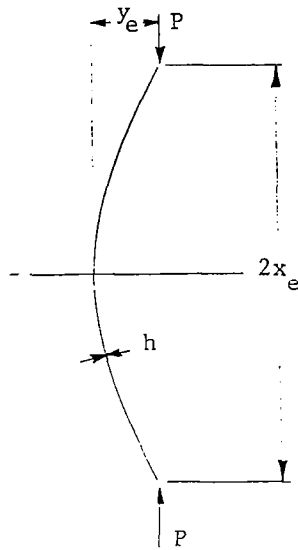
Figure 2-12. Buckled Column in Deflected State

$$\bar{y}_e = \frac{y_e}{L+l} = \frac{15.2}{351.6/2} = 0.0865$$

$$\bar{x}_e = \frac{x_e}{L+l} = \frac{350.0}{351.6/2} = 0.995 \text{ calculated}$$

$$(= 0.994 \text{ per Figure 8 of Reference 1})$$

$$\bar{\sigma} = (1 - v^2) \frac{\sigma L}{Eh} = 0.10 \text{ (from Figure 5 of Reference 1)}$$

$$\therefore \text{maximum bending stress, } (\sigma) = \frac{\bar{\sigma}Eh}{(1 - v^2)L} = \frac{0.10 \ (186.9 \times 10^9) \ 0.0064}{3.516/2}$$

$$= 67.9 \text{ MN/m}^2 \ (9.85\text{k lb/in}^2)$$

where

$$E = \frac{(207.5 + 166.2)}{2} \text{ GN/m}^2 = 186.9 \text{ GN/m}^2 \ (27.1 \text{ M lb/in}^2)$$

$\lambda^2 = PL^2/2D = 1.11^2$ (from Figure 6 of Reference 1) = 1.23

Calculation for end force (P):

Flex, rigidity (D) $= \dfrac{Eh^3}{12(1-v^2)} = \dfrac{(186.9 \times 10^9)\,0.0064^3}{12} = 4081.9$ N/m

Note. This represents an approximate solution. For a more exact and correct solution the value for E would be derived from a bending analysis based on lamina theory.

$\therefore$ unit end force (P) $= \dfrac{\lambda^2 2D}{L^2} = \dfrac{1.23\,(2)\,4081.9}{(3.516/2)^2} = \underline{3249\text{N/m}\ (18.5\ \text{lb/in})}$

These and other similarly derived values of σ and P for various values of y_e are presented in Table 2-1.

Table 2-1. Unit End Load and Stress at Various Deflection Values

Deflection (y_e)	meters (inches)	0.025 (1.0)	0.152 (6.0)	0.300 (12.0)	0.457 (18.0)
Maximum bending stress (σ)	MN/m^2 (k lb/in^2)	13.6 (1.97)	67.9 (9.85)	122.7 (17.80)	203.4 (29.50)
Unit end force (P)	N/m (lb/in)	3190 (18.2)	3249 (18.5)	3290 (18.8)	3380 (19.3)

These tabulated values indicate the gradual increase in load that occurs as the column is compressed and the concurrent, more dramatic, increase in bending stress and bending deflection. At 0.457 meter (18 inches) deflection, extreme fibers are close to ultimate stress and effective column length has reduced from 3.516 meters to 3.37 meters.

Weight per column is:

$W_c = b\,h\,L_c\,p = 1.27\text{ cm} \times 0.64\text{ cm} \times 3.516\text{ m} \times 1771.5\text{ kg/m}^3 = 0.5\text{ kg }(1.1\text{ lb})$
(0.5 in.) (0.25 in.)(138.5 in.) (0.064 lb/in^3)

Allowing a factor of 1.4 for weight of end fittings the total weight of all 2163 buckled columns is: 0.5 (2163) 1.4 = $\underline{1514\text{ kg }(3338\text{ lb})}$.

2.2.4 THE TELESCOPIC COLUMN MEMBER. A possible alternative to the buckled column is illustrated in Figure 2-13 and evaluated below. It is simply a spring-loaded, telescopic tube. Over most of its length it is a thin-walled round tube. At one end, a second, short, inner tube is provided with an end fitting for attachment to the structural node point. A spring is assembled in such a way that it tends to expel the inner tube from the primary tube, thus applying the required preloading force to the structure. The installation can be lightweight and compact and would have a reasonable structural efficiency. Its performance would be more predictable than a buckled column. As already stated, the deployment phases of the DCM module involve a rotation of one frame relative to the other. It amounts to approximately 114 degrees and requires that the three buckled columns be provided with universal swivel joints at their ends to relieve torsion. In the alternative telescopic column, this torsion is relieved by simple counterrotation of the two component tubes about their common axis. Thus, simple pivot joints suffice as the end fittings.

A feature is designed-in that takes advantages of the counterrotation and greatly facilitates deployment of the module from the packaged configuration by avoiding the buildup and release of elastic strain energy described above. The elastic energy buildup problem is avoided by locking the telescoping columns in a precompressed condition during packaging, before launch. The lock is released
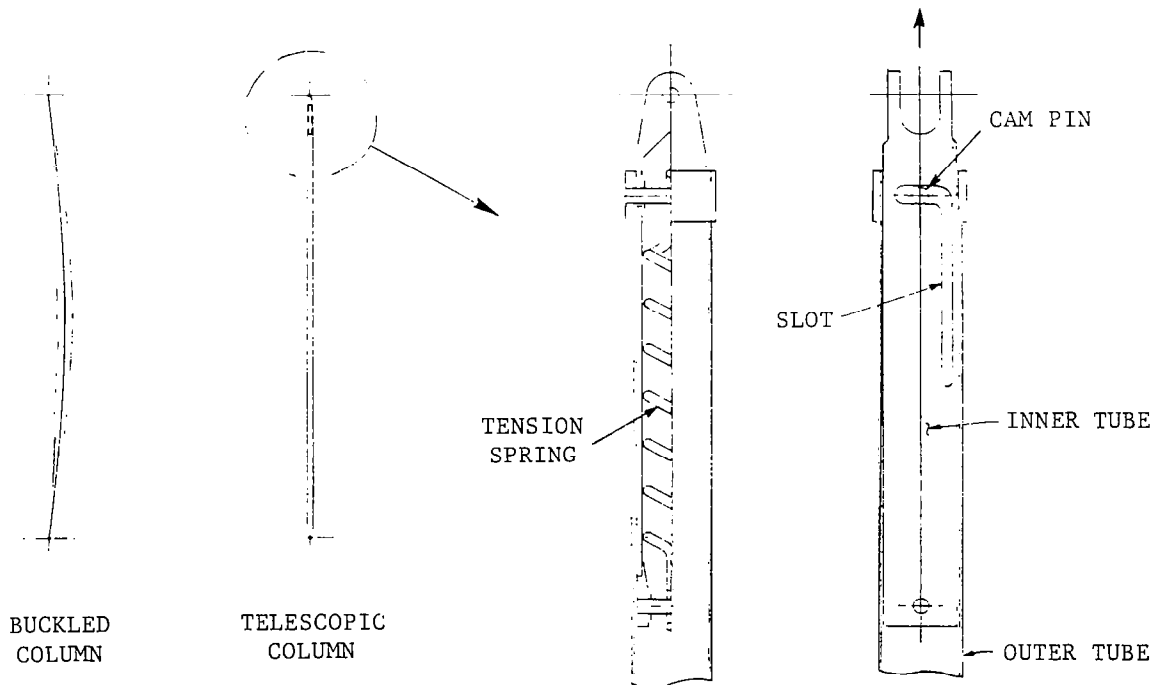
Figure 2-13. Telescopic Element with Automatic Spring Release at Full Deployment is Feasible Alternative to Buckled Column

2-17

by the counterrotation of the two component tubes and occurs only at the very end of the module deployment phase. This lock/release capability can be provided by a simple slotted cam shown, in principle, in Figure 2-13. Thus, the inner tube rotates within the outer tube until, at the point of full module deployment, the cam pin aligns with the vertical slot feature and the tension spring drives the inner tube upwards. The module tie lines become taut and arrest the motion just short of the limit of travel of the cam pin in the slot.

Since this member is not a prime structural element, thermally stable materials are not necessary. Therefore, if considered beneficial, the mechanical components, at least, could be metallic without detriment to the "thermal stability" of the structure. Aluminum alloy is assumed to be the selected material.

For consistency with the structural loading discussed in Section 2.2.2.2, the spring loading is set at 76N (17.0 lb) with the column compressed to an effective length of 3.5m (137.8 in.). For this relatively low value of axial loading a minimum wall thickness of 0.5 mm (0.02 in.) is adequate and the column slenderness ratio (L/ρ) may approach 400.

$$\rho = \frac{-3.5}{400} = 0.875 \text{ cm}$$

thus mean tube diameter (d) $= \dfrac{0.875\ (2)}{0.707} = \underline{2.475 \text{ cm } (0.97 \text{ in.})}$

$$I = \pi/4 \left[\left(\frac{2.515^4}{2} \right) - \left(\frac{2.413^4}{2} \right) \right] = 0.3 \text{ cm}^4 \ (0.007 \text{ in}^4)$$

$$P_{Euler} = \frac{\pi^2 E I}{L^2} = 150.1\,N \ (33.8 \text{ lb})$$

Area of tube cross section (A): $= \pi Dt = \pi 2.475\ (0.05) = 0.39 \text{ cm}^2 \ (0.06 \text{ in}^2)$

Weight of tubing per column (W_c): $= L(1.25)\ A\rho_A$

$$= 3.5(1.25)(0.039/100^2)(2768)$$

$$= \underline{0.472 \text{ kg } (1.04 \text{ lb})}$$

Note: The 1.25 factor allows for tube overlap, and ρ_A is density of aluminum $= 2768 \text{ kg/m}^3 \ (0.10 \text{ lb/in}^3)$

Allowing a factor of 1.5 for end fittings, spring and lock/release device the total weight of all 2163 telescopic columns is: 1.5 (2163) 0.472 = <u>1531 kg</u> (3376 lb).

2.2.5 <u>CONCLUSIONS</u>. The buckled column is a structurally feasible means of providing the required preloading. It is simple, but relatively high bending and twisting stresses may occur during deployment. These stresses also result in various reactant forces that complicate requirements for deployment handling of the DCM module.

The alternative, telescopic column approach is preferred, in spite of its relative complexity, due to the following advantageous characteristics.

- Since the telescopic extension mechanism is not triggered until the final increment of deployment of the DCM module, there are no significant forces opposing deployment, and handling requirements are greatly simplified. Columns are locked in spring-loaded condition before launch. Applied compression, during deployment, is not required.

- Since they are compressed for packing they extend upon deployment — thus increasing structural depth. The reverse is true for the buckled column.

- Pure column characteristics (no bending) result in low stress levels.

- Material properties are not critical. (There is no impact on structural thermal stability.)

- No weight penalty.

2.3   QUANTITIES AND MASS PROPERTIES

The true, projected, 'bore axis view' geometry of the total, 31 bay DCM Study Case C-1 reflector (ref. Fig. 2-1) is presented in graphic output form in Figure 2-14.

The mass properties of this reflector are presented in Table 2-2.

Input data for the synthesis program, including material properties data (consistent with values selected in Section 2.2.1) are listed in Table 2-3, and presented in both I.S.U. (Metric) and conventional (English) units. Several of the input values presented in Table 2-3 will appear to differ from actual values found in the design definition. Such values are "equivalent" values generated to allow for design peculiarities not recognizable by the computer program. For example, the square section tube selected for the design, reference Figure 2-7, is input as equivalent round tube since the program input must be in terms of DIAMETER.

Certain other input parameters are drastically modified, in order to suppress them so that the analysis will be based on other, preferred parameters. An example of this is the input value of the ratio of length to radius of gyration, which is suppressed so that the value for surface strut minimum diameter dominates.
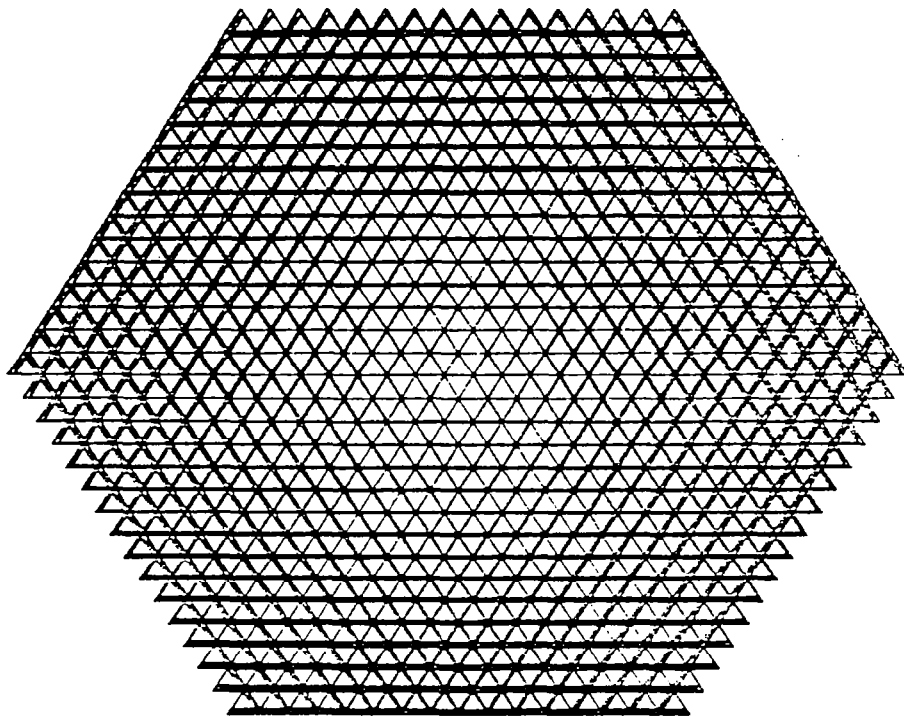
Figure 2-14. Graphic Output Defines Geometry of DCM Study Case C-1

Table 2-2. Synthesis Program Output Defines Mass Properties and Element Lengths for DCM Study Case C-1

```
INPUT PARAMETERS  31 MAY              95.3 M (  312.6 FT )ACROSS FLATS
                  ±±±±±± L/RHO ±±±±±± D/T 1.050 F/D     0.0 % CONTINGENCY
```

COMPONENTS	UNIT WEIGHT KILOGRAMS	(POUNDS)	NUMBER REQUIRED	WEIGHT KILOGRAMS	(POUNDS)
STRUTS	.60E+00	(.13E+01)	10815	.65402E+04	(.14421E+05)
UPPER SURFACE	.72E+00	(.16E+01)	2163	.15522E+04	(.34227E+04)
COLUMNS	.69E+00	(.15E+01)	2163	.15026E+04	(.33133E+04)
CROSS-TIES	.44E+00	(.97E+00)	4326	.19068E+04	(.42245E+04)
LOWER SURFACE	.73E+00	(.16E+01)	2163	.15785E+04	(.34807E+04)
SPIDER ASSEMBLY	.13E+01	(.28E+01)	1536	.19639E+04	(.43304E+04)
UPPER SPIDER	.13E+01	(.28E+01)	768	.98194E+03	(.21652E+04)
LOWER SPIDER	.13E+01	(.28E+01)	768	.98194E+03	(.21652E+04)
STANDOFFS	0.	(0.	) 768	0.	(0.)
MESH INSTALLATION				.89515E+03	(.19738E+04)
MESH				.45439E+03	(.10019E+04)
MESH CONTROL SYSTEM				.44076E+03	(.97188E+03)
CONTINGENCY			0.	(0.	)

TOTAL WEIGHT	9399.	(20725.)

X-C.G. CENTIMETERS (INCHES)	.45706E-08	(.17994E-08)
Y-C.G. CENTIMETERS (INCHES)	.36505E-09	(.14372E-09)
Z-C.G. CENTIMETERS (INCHES)	.17097E+03	(.67311E+02)
IXX KILOGRAM METER SQ. (SLUG FT2)	.63394E+07	(.46721E+07)
IYY KILOGRAM METER SQ. (SLUG FT2)	.63394E+07	(.46721E+07)
IZZ KILOGRAM METER SQ. (SLUG FT2)	.12572E+08	(.92653E+07)
IXZ KILOGRAM METER SQ. (SLUG FT2)	.20900E-06	(.15403E-06)
IXY KILOGRAM METER SQ. (SLUG FT2)	-.50841E-07	(-.37470E-07)
IZY KILOGRAM METER SQ. (SLUG FT2)	.22134E-05	(.16313E-05)

MISCELLANEOUS GEOMETRY	UPPER SURFACE	CROSS-TIES	LOWER SURFACE
STRUT DIAMETER CM (IN)	3.69 (1.45)	.77 (.30)	3.69 (1.45)
STRUT THICKNESS CM (IN)	.09144(.03600)		.09144(.03600)
AVG. STRUT LENGTH M (IN)	3.62 (142.)	5.05 (199.)	3.68 (145.)
MAX. SURF. STRUT LENGTH CM (IN)		377.3 (	148.6)
AVG. COLUMN LENGTH M (IN)		3.50 (	138.)
MESH AREA SQ METERS (SQ YDS)		7974.0 (	9537.1)
CRITICAL LOAD (PCR) NEUTONS (POUNDS)		1638.2 (	368.3)

2-20

Table 2-3. Synthesis Program Input Data for DCM Study Case C-1

LASS PREPROCESSOR REAL MODEL INPUT ITEMS IN METRIC (S.I.) UNITS

Value	#	Name	Description
* 95.270	1	RFDM	-RADIO FREQUENCY DIAMETER (METERS)
* 1.0000	2	SHAPE	-SHAPE FLAG: 1=PARABOLA, 2=SPHERE, 3=FLAT
* 1.0500	3	FOVERD	-FOCAL LENGTH TO RF DIAMETER RATIO
31.000	4	NBAYS	-NUMBER OF BAYS IN REAL DISH STRUCTURE
31.000	5	ANBAYS	-ANALYSIS NUMBER OF BAYS
0.	6	THETA	
1.96000E-02	7	SODM	-MESH STAND-OFF DISTANCE (METERS)
0.	8	MOUNTF	
0.	9	REMOVF	
7.0000	10	NMODE	-NUMBER OF MODE SHAPES (0=NO SAP MODELS)
3.5000	11	XANACM	-STRUCTURAL DEPTH (M)
0.	12	YANACM	
0.	13	ZANACM	
0.	14	TUBTYP	
1.00000E+06	15	SLOR	-SURFACE STRUT LENGTH OVER RADIUS OF GYR RATIO
* 1.00000E+06	16	SDOT	-SURFACE STRUT DIAMETER OVER THICKNESS RATIO
* 1.31350E+11	17	SSYMM	-SURFACE STRUT YOUNGS MODULUS (NEUTONS/SQUARE METER)
3.68700E-02	18	SMINDM	-SURFACE STRUT MINIMUM DIAMETER (METERS)
9.14400E-04	19	SMINTM	-SURFACE STRUT MINIMUM THICKNESS (METERS)
0.	20	SPCRM	
1.0000	21	SHAR	-COLUMN SPRING CONSTANT, NOTE:(LB/IN)
4.50000E-07	22	SHLR	-SURFACE STRUT THERMAL COEFFICIENT (1/KELVIN)
0.	23	SHMOD	
4.50000E-07	24	DLOR	-CROSS-TIE THERMAL COEFFICIENT (1/KELVIN)
* 4.50000E-07	25	DDOT	-COLUMN THERMAL COEFFICIENT (1/KELVIN)
* 1.31350E+11	26	DSYMM	-CROSS-TIE YOUNGS MODULUS (N/M**2)
7.69800E-03	27	DMINDM	-CROSS-TIE DIAMETER (M)
0.	28	DMINTM	
0.	29	DPCRM	
0.	30	DIFROD	
3.03380E+10	31	DSSM	-SURFACE STRUT SHEAR MODULUS (N/M**2)
1874.0	32	SRHO	-SURFACE STRUT DENSITY (KILOGRAMS/CUBIC METER)
0.	33	SSBRU	
.69470	34	SEFRU	-COLUMN WEIGHT PER ELEMENT (KG)
0.	35	SHLACE	
1874.0	36	DRHOM	-CROSS-TIE DENSITY (KG/M**3)
0.	37	DSBRU	
0.	38	DEFRU	
0.	39	DLACE	
0.	40	UWSTOM	-UNIT WEIGHT OF STAND-OFF (.1 METERS LONG) (KILOGRAMS)
.98500	41	SRWM	-SPIDER REFERENCE WEIGHT (KILOGRAMS)
5.70000E-02	42	UWMESH	-UNIT WEIGHT OF MESH (KILOGRAMS/SQUARE METER)
1.9700	43	UWMCSR	-MESH SYSTEM TO MESH ONLY WEIGHT RATIO
0.	44	UTCONT	-WEIGHT CONTINGENCY (ALL WEIGHT*(1+UTCONT))
0.	45	MESHBK	

INPUT DATA IN CONVENTIONAL (ENGLISH) UNITS

Value	#	Name	Description
* 312.56	23	RFD	-RADIO FREQUENCY DIAMETER (FEET)
* 1.0000	19	AMP	-SHAPE FLAG: 1=PARABOLA, 2=SPHERE, 3=FLAT
* 1.0500	17	FCN	-FOCAL LENGTH TO RF DIAMETER RATIO
31.000	18	ANBAYS	-ANALYSIS NUMBER OF BAYS
0.	21	AN	
.77165	22	SOD	-MESH STAND-OFF DISTANCE (INCHES)
0.	27	MF	
0.	5	FLAG	
7.0000	20	AM	-NUMBER OF MODE SHAPES (0=NO SAP MODELS)
137.88	28	XANAC	-STRUCTURAL DEPTH (IN)
0.	29	YANAC	
0.	30	ZANAC	
0.	39	TUBES	
1.00000E+06	11	TRRS	-SURFACE STRUT LENGTH OVER RADIUS OF GYR RATIO
* 1.00000E+06	13	TTRS	-SURFACE STRUT DIAMETER OVER THICKNESS RATIO
* 1.90460E+07	25	SSM	-SURFACE STRUT YOUNGS MODULUS (POUNDS/SQUARE INCH)
1.4516	33	DMINS	-SURFACE STRUT MINIMUM DIAMETER (INCHES)
3.60000E-02	34	TMINS	-SURFACE STRUT MINIMUM THICKNESS (INCHES)
0.	41	PCR	
1.0000	8	SPLAR	-COLUMN SPRING CONSTAN (LB/IN)
4.50000E-07	9	HLR	-SURFACE STRUT THERMAL COEFFICIENT (1/KELVIN)
0.	24	HM	
4.50000E-07	12	TRRD	-CROSS-TIE THERMAL COEFFICIENT (1/KELVIN)
* 4.50000E-07	14	TTRD	-COLUMN THERMAL COEFFICIENT (1/KELVIN)
* 1.90460E+07	26	DSM	-CROSS-TIE YOUNGS MODULUS (PSI)
.30307	32	DMIND	-CROSS-TIE DIAMETER (IN)
0.	35	TMIND	
0.	43	DPCR	
0.	40	FROD	
4.39900E+06	38	QSM	-SURFACE STRUT SHEAR MODULUS (PSI)
6.77020E-02	1	RHOT	-SURFACE STRUT DENSITY (POUNDS/CUBIC INCH)
0.		UBST	
1.5318	36	USE	-COLUMN WEIGHT PER ELEMENT (LB)
0.	7	SPLR	
6.77020E-02	44	DRHOT	-CROSS-TIE DENSITY (LB/IN**3)
0.	3	UBDT	
0.	37	UDE	
0.	4	UWSTO	-UNIT WEIGHT OF STAND-OFF (POUNDS/FOUR INCHES)
2.1718	10	SRW	-SPIDER REFERENCE WEIGHT (POUNDS)
1.6809	15	UWMSV	-UNIT WEIGHT OF MESH (OUNCES/SQUARE YARD)
.9700	16	UWMCSR	-MESH SYSTEM TO MESH ONLY WEIGHT RATIO
0.	6	CONTPR	-WEIGHT CONTINGENCY (ALL WEIGHT*(1+CONTPR))
0.	42	ANSM	
1.0000	31	RRATIO	-RATIO OF REAL TO ANALOGOUS MODEL NUMBER OF BAYS

*Modified to compensate for geometry aberration; does not correspond to actual parameter.

2.4 METHODOLOGY AND SUPPORT EQUIPMENT

As previously described, the stowed modules are individually supported in three shoes: one at bottom center and one either side just above the horizontal center-line. Three similar transport belt subsystems operate in unison to advance the modules toward the dispending end of the support cradle (see Figure 2-4). For each module there are three carriages that transfer module support loads to channel section rails or troughs mounted on the cradle primary structure. Since all modules vary in size, the support shoes are individually located on the carriages to suit the modules.

2.4.1 TWIN MANIPULATOR SYSTEM. Two similar manipulator systems are provided. They are mounted as a complete subsystem on a special pallet at the front end of the payload bay (Figure 2-15). The pallet contains all necessary control systems for the two manipulators. Multiple electric connectors permit plug-in of Orbiter power and remote control leads. Control and operation of the manipulators are primarily by automation, but the crew is provided the option of manual override for the more critical operations or for correcting possible malfunctions. Closed-circuit TV, pressure sensors, and proximity sensors provide the crew with continuous monitoring capability. All monitoring and control operations are conducted from within the shirt-sleeve environment of the crew compartment. Crew EVA capability provides discretionary backup for direct monitoring and troubleshooting.
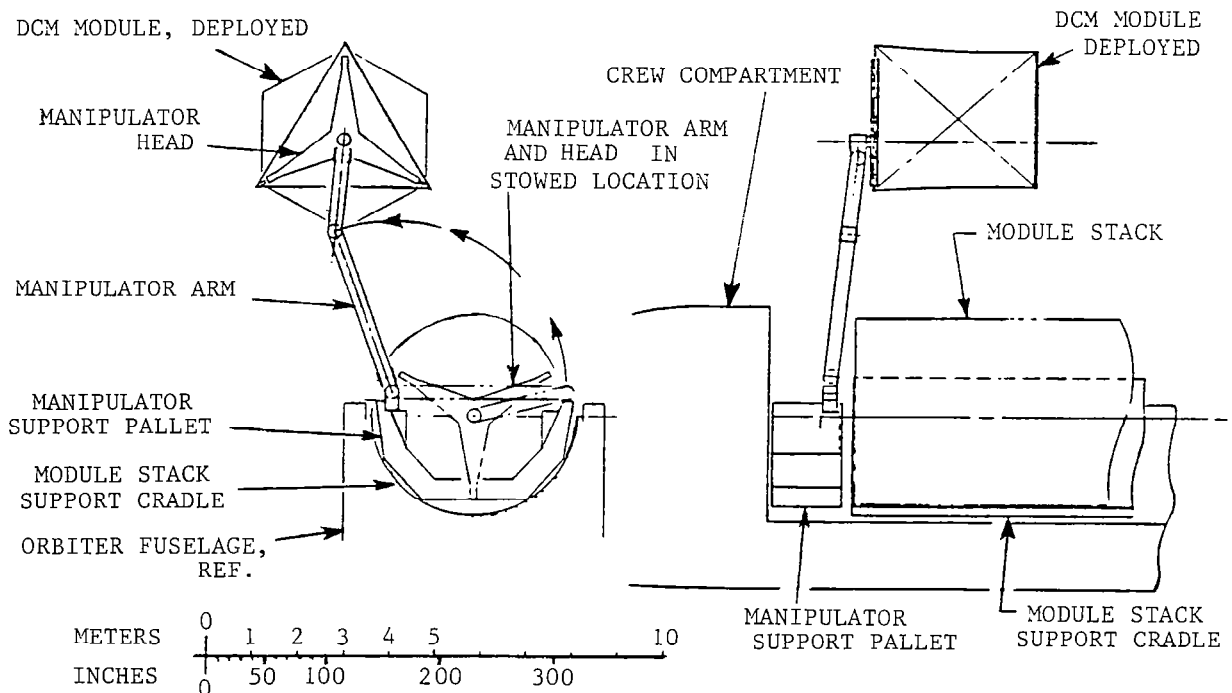
Figure 2-15. Manipulator System Performs all Required Module Handling

2-22

Each manipulator arm is provided with a three-spoked "head" designed to fit within the triangular frames of the modules. Upon command a probe extends from the tip of each of the three spokes to engage mating recesses in the three inner corners of the module frame. Since all modules will vary dimensionally, the degree of probe extension varies for each module. By this means the manipulator securely engages each module of the stack in turn, withdraws it from the stack, and repositions it outside the Orbiter preparatory to deployment. To provide the manipulator arms with the necessary freedom of movement each has a shoulder, elbow, and wrist joint and a reach of between 2 and 6 meters (6.2 and 19.2 feet) from its mount location.

2.4.2 MODULE STOWAGE AND DISPENSING. In the Orbiter launch configuration, the DCM modules are densely stacked within a cradle that occupies 90% of the Orbiter payload bay (see Figures 2-4 and 2-15). Each module is supported within the cradle by three "shoes": one at the bottom centerline and one more on either side just above the horizontal centerline as shown in Figure 2-4. The shoes are keyed into troughs that run the full length of the cradle and individually engage an endless belt. In orbit the modules are dispensed one at a time from the front end of the cradle. To dispense a module the three endless belts are advanced, simultaneously, a distance equal to the overall thickness of one module. As shown in Figure 2-16, this causes the entire module stack to advance a similar distance, which results in the release of the dispensed module.
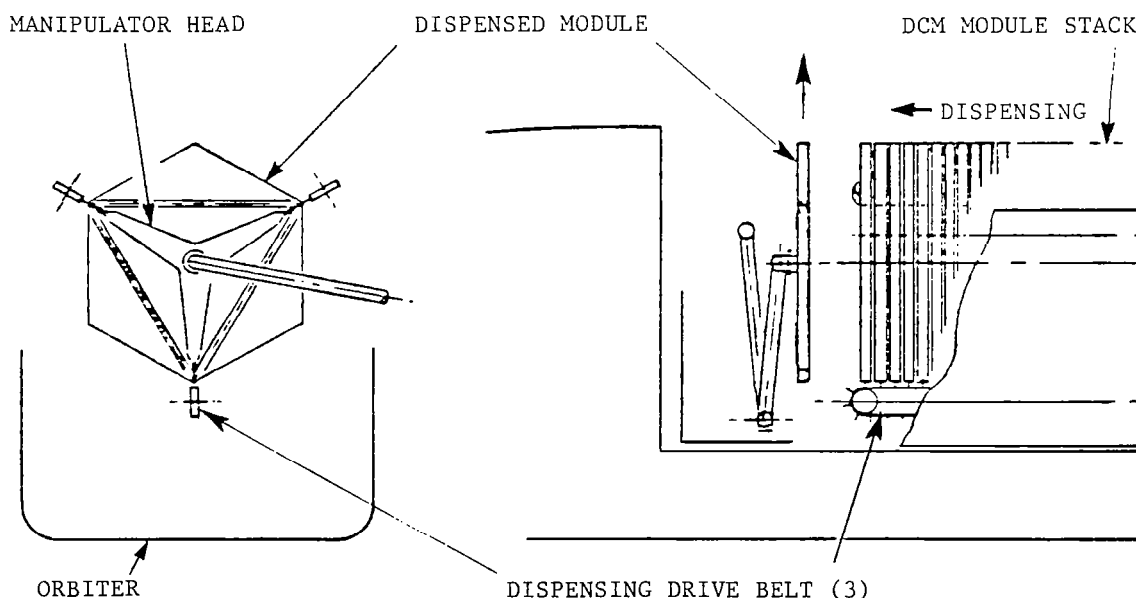
Figure 2-16. Manipulator Withdraws Packaged Module as Module Releases from Drive Belt Shoes

The three shoes rotate away from the module and move, with the endless belt, back into the body of the cradle when their function is completed.

2.4.3 MODULE DEPLOYMENT. The "packaged" module, firmly secured by the manipulator head, is now relocated to a point outside the Orbiter bay, as shown in Figure 2-15, for deployment.

Three small crank arms are mounted on the manipulator head, one at the end of each spoke. To deploy the module these cranks rotate to bear against the three telescopic elements, described in Section 2.2.4. The force applied by the cranks causes the telescopic elements to rotate about their pivotal connection to the secured frame, which moves the second frame out along an approximately helical path (Figure 2-17).

TIELINES OMITTED FOR CLARITY

CRANK ARM (3)

TELESCOPIC ELEMENT (3)

MANIPULATOR HEAD

TELESCOPIC ELEMENTS (3)

SECURED FRAME

DEPLOYING FRAME
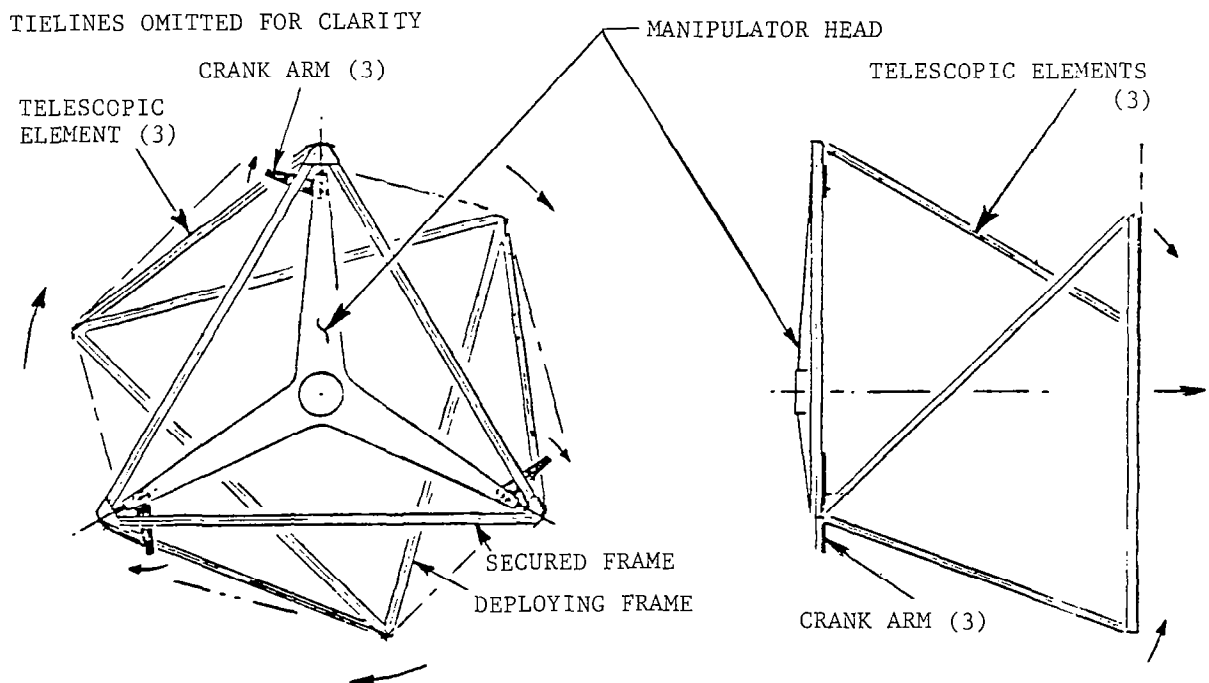
CRANK ARM (3)

Figure 2-17. Crank Arms Rotate Telescopic Elements to Deploy Module

When this phase is approximately 90% complete, spring release occurs simultaneously in each telescopic element as described in Section 2.2.4 and the module drives to its fully deployed, preloaded configuration.

2.4.4 <u>MODULE-TO-MODULE JOINING</u>. The module dispensing and deployment, described above, is repeated using the second manipulator arm to deploy a second module. The two manipulator arms are now actuated to bring the modules together in the relative attitude required for joining as presented in Figure 2-18.

ORBITER RMS SYSTEM

MODULE No. 1

MODULE No. 2
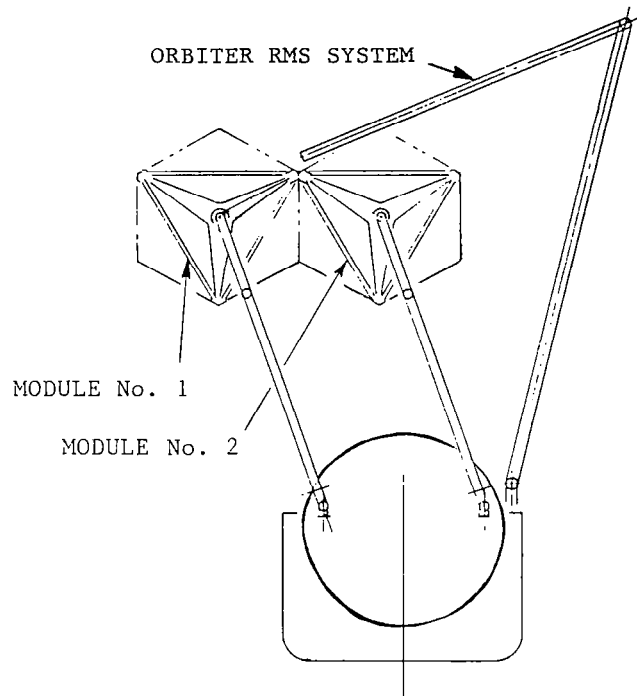
Figure 2-18. Two Modules are Deployed and Positioned Ready for Joining

Figure 2-19 shows a close-up of the interface between the nodes of the two modules.

Each node fitting presents two faying surfaces 120 degrees apart that butt to corresponding faces of adjacent node fittings as the modules are brought together for joining. Each of these faying surfaces is notched with a shear pin traversing the notch. The structural connection between modules is effected by placing a tension link across the interfaces between pins. This operation should be fully automated utilizing the Orbiter remote manipulator system (RMS) to position and insert the links from a dispensing magazine. Alternatively it may be conceivable to utilize EVA, with the astronaut performing this operation from a cherry picker seat mounted at the end of the RMS arm.

Potential approaches to the type and configuration of the locking device include spring clips, hooks, latches, rachets, collets, toggles, cams, screws with captive nuts, left-hand and right-hand threaded latches, wedges, winches — all with spring-loaded or driven automation. Sonic welding is also a potential method of joining.

The idealized functional and physical requirements for the locking device include:

- Adequate tension and shear joint strength
- Zero clearances (no slop) .
- Adequate cinch-up capability (correction of misalignment)
- Minimum complexity
- Minimum size and weight
- Equal applicability to concave and convex node fittings
- No premature actuation
- Positive lock
- No violation of packaged envelope
- Secure configuration in stowed state
- Supportive functions required of effector to be simplified and minimized (no loose parts to be added by effector)
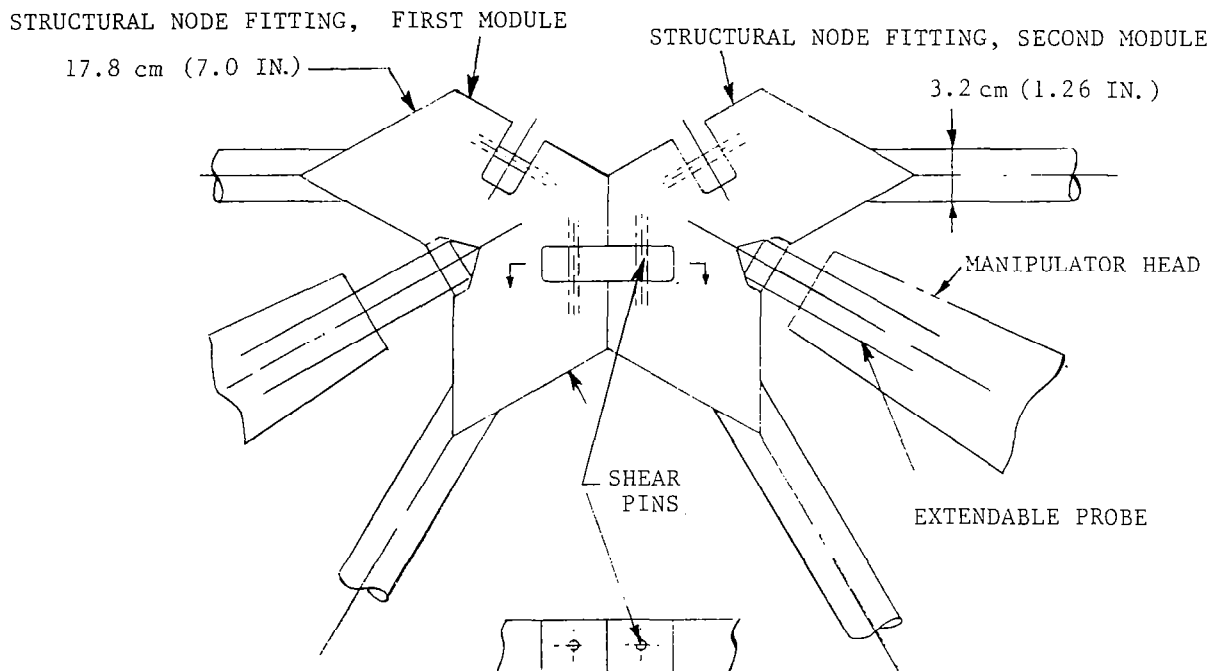
Figure 2-19. Mating Node Fittings are Clamped Across Shear Pins

All module-to-module joining operations are performed at a distance of not more than 10 meters (33 feet) from the center of the payload bay, which is well within the capability of the RMS.

Figure 2-20 shows the sequence of module addition in the progressive buildup of the total 100 meter, 721 module reflector. The 234 modules carried into orbit in the initial Orbiter payload are at the center of the reflector and are identified with center dots in Figure 2-20. It is worthy of note that this single payload provides the means and material to assemble a 60-meter (200-foot) structure.

2-26

(a)

(b)

(c)

(d)

(e)

(f)
24.6m(80.6FT)

(g)

DCM MODULES (721)

108m(354 FT) ≈ 2.6
PAYLOADS (ASSUMING
FACETS ARE FLAT,
AND $L/\rho \approx 300$

58 m (190 FT)
= ONE PAYLOAD,
REF
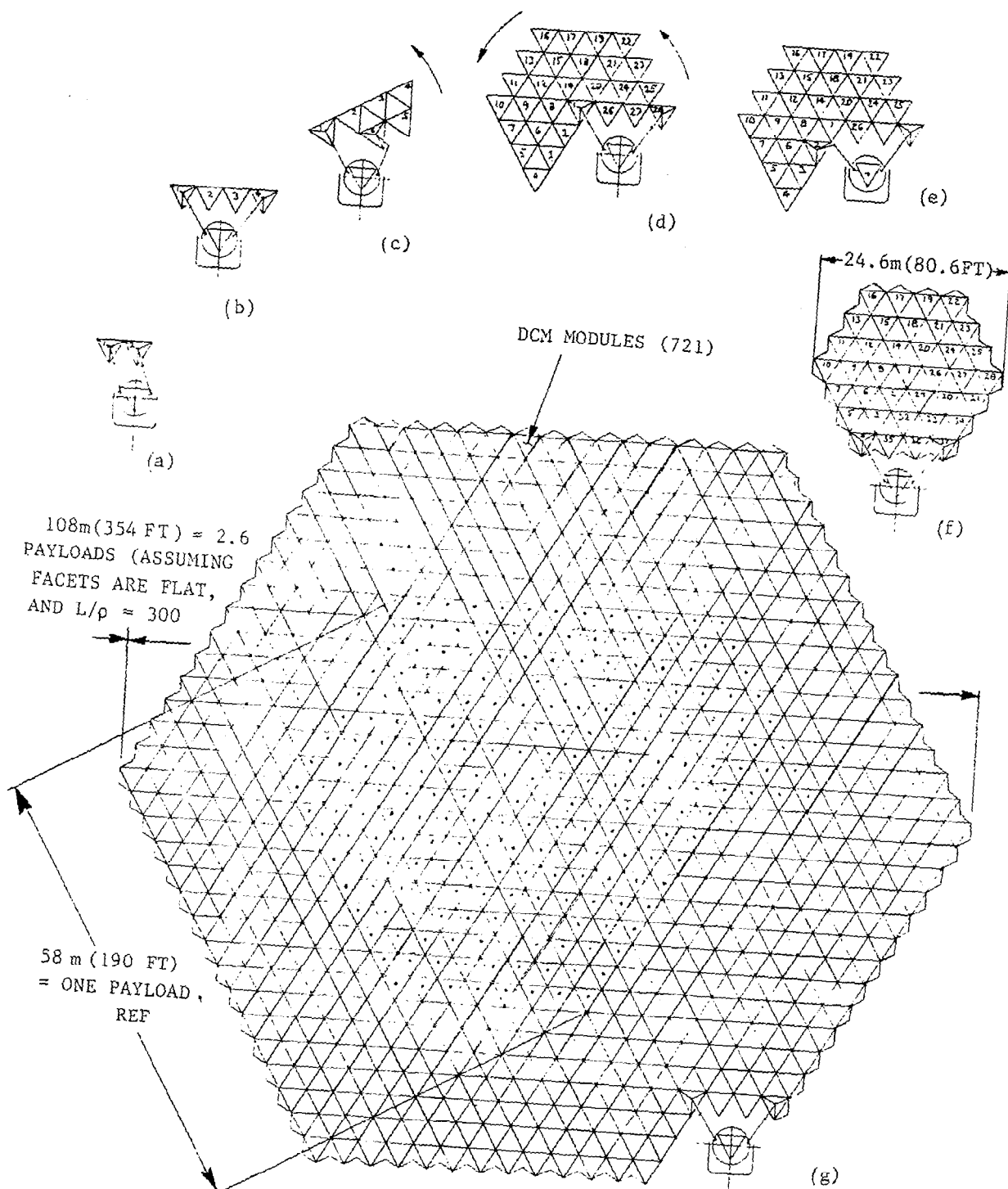
Figure 2-20. Sequence of Joining Modules to Assemble a 100-Meter
(328-Foot) Diameter Reflector

2.5 ALTERNATIVE METHODOLOGY

This section presents a method of assembly of the DCM reflector that differs from the method proposed in Section 2.4.4. The significant features of the alternative method are:

a. The Payload Support Pallet (PSP), containing the packaged structural modules and all handling and assembly support equipment, is removed as a unit from the payload bay. It is supported in an attitude and at a distance from the Orbiter that will enable observation and monitoring from the Orbiter crew compartment and that will incur minimum risk to the Orbiter.

b. All functions associated with module dispensing, deployment, and joining are performed in the immediate vicinity of the forward end of the PSP.

c. Each module deploys, in turn, while still retained by the dispensing mechanism.

d. Two, similar handling and joining arms (HJA) that extend, as required, from the payload support pallet, perform such functions as:

   1. Securing the deployed module during and after dispensing.

   2. Relocating of the deployed module to enable deployment of the following module.

   3. Alignment and positioning of adjacent modules for joining.

   4. Effecting the structural joining (latching) of the modules at their "front side" and "back side" structural node point fittings.

   5. Supporting the evolving structure as modules are added one-by-one.

2.5.1 <u>DEPLOYABLE PAYLOAD SUPPORT PALLET</u>. The stowed PSP occupies 90% of the Orbiter payload bay and contains packaged DCM modules. The provisions for support and mechanical dispensing of individual modules are as described in Sections 2.4 and 2.4.2.

In Figure 2-21 the two HJAs are shown in stowed position, retracted into the PSP structure with their effector finger probes utilized to secure them to the forward face of the PSP.

The first stage of the in-orbit deployment sequence is release of the PSP tiedown latches and elevation of the PSP from the Orbiter bay by means of two articulating support arms (Figure 2-22). These arms may subsequently be locked to establish a rigid relationship between the PSP and the Orbiter. However, to prevent excessive loading at these support interfaces as the mass moment of the evolving structure becomes large, it may be necessary to provide a sprung (non-rigid) interface that would accommodate oscillatory movements yet maintain the mean relationship at nominal. A superimposed effect would be correction of orbital tumbling by means of the Orbiter attitude control systems.

2-28

HANDLING AND JOINING ARMS (HJA)
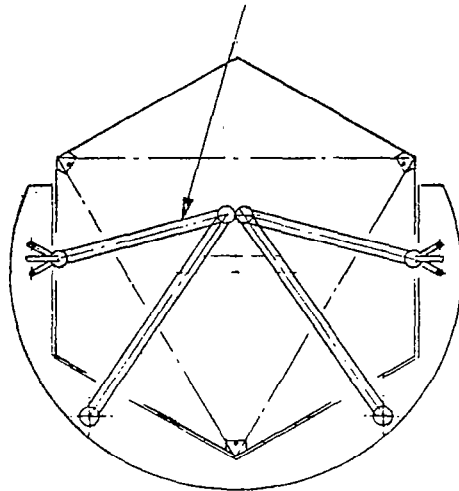
ORBITER, REF
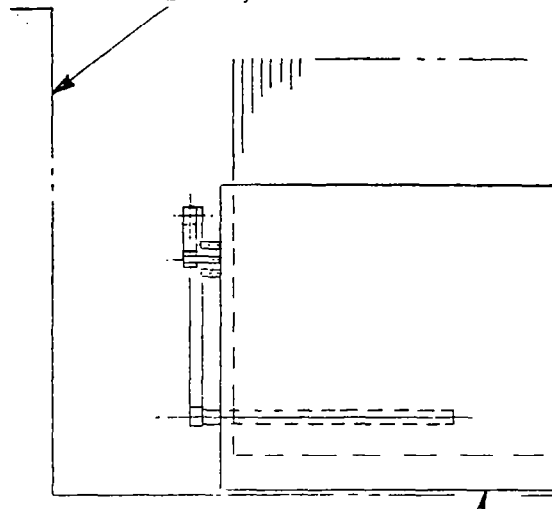
PAYLOAD SUPPORT PALLET

Figure 2-21. Stowed Pallet Occupies 90% of Payload Bay

PACKAGED MODULES, REF
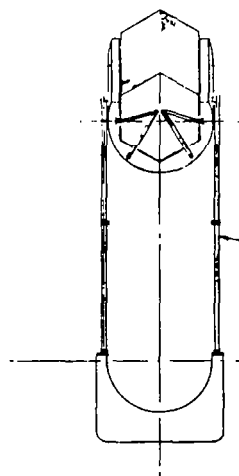
ARTICULATING
SUPPORT ARMS
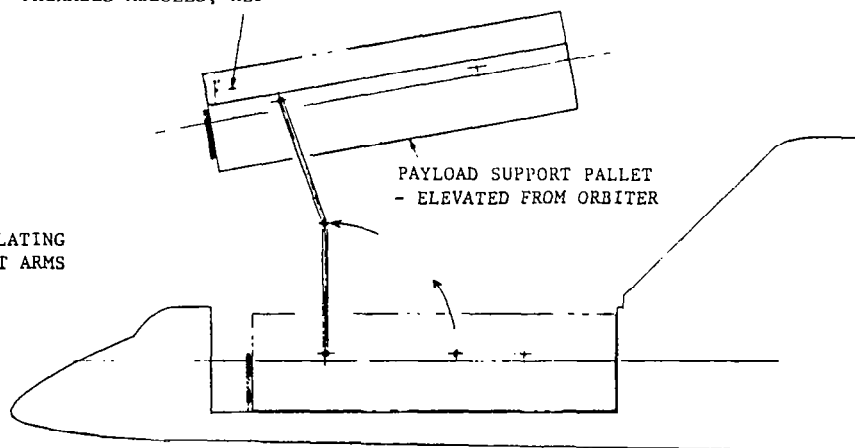
PAYLOAD SUPPORT PALLET
- ELEVATED FROM ORBITER

Figure 2-22.   Payload Support Pallet is Elevated and Supported
by Two Articulating Arms

2.5.2 <u>MODULE DISPENSING, DEPLOYING, AND JOINING</u>. In Figure 2-23 the two HJAs are shown deployed "at the ready," one to be applied to the front face of the module and the other to the back face.

LINK TRIGGER UNIT (LTU)   DEPLOYING MODULE, REF.

ENGAGEMENT FINGER PROBES   MODULE No. 1

NO. 1

EXTENDABLE HANDLING AND JOINING ARMS
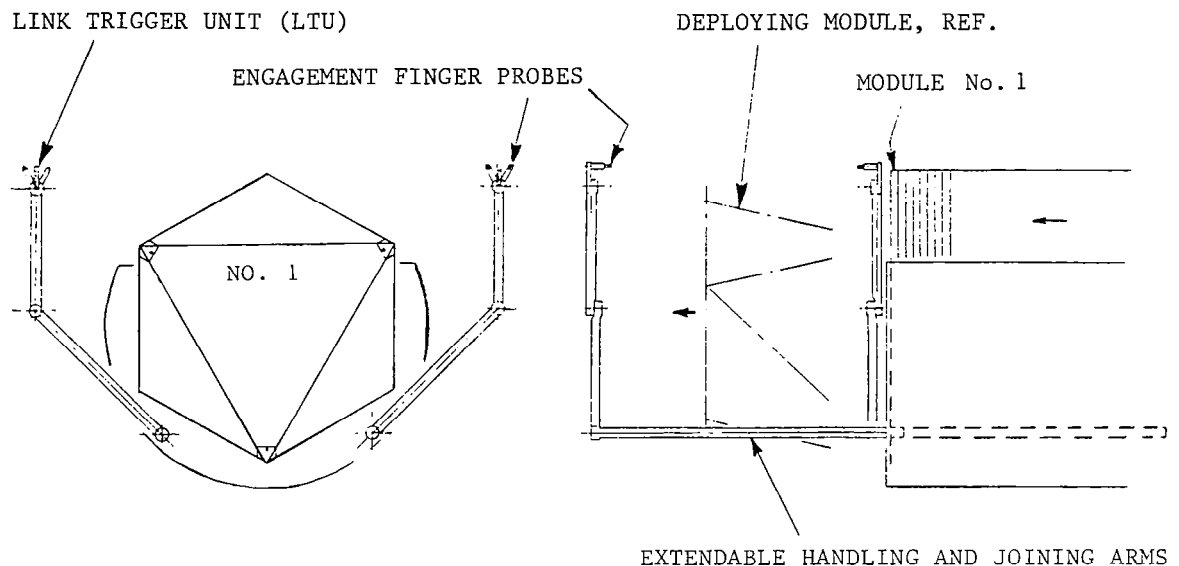
Figure 2-23.   Two Manipulators Mount on the PSP to Handle and Join
                      Deployed Modules

The module stack is advanced so that the first module (No. 1) is just short of being released. Three crank arms mounted on the front face of the PSP actuate to bear upon the three telescopic columns to effect deployment of the module. These provisions are similar to those shown in Figure 2-17, which also illustrates the module transition to deployed configuration shown in Figure 2-2.

The left-hand HJA is now articulated to engage the front, left-hand node fitting of the module as shown in Figure 2-24. This engagement is effected by extending and locking a mechanically expandable "finger" probe into a receiving feature (hole) in the node fitting. With the module thus secured, it is then released from the PSP by activating the PSP dispensing system and simultaneously extending the HJA from the PSP. HJA extension is continued until sufficient gap exists between the module and the PSP forward face to permit the second HJA to be swung in to engage the back side node fitting of the module, as shown in Figure 2-25.

The module, supported now both front and back, is traversed to the right-hand side by the synchronized manipulation of the two HJAs, as shown in Figure 2-26. This operation clears space required for the deployment of No. 2 module, which occurs in the same manner as for Module No. 1.

HJA FINGER ENGAGES
MODULE NODE FITTING

FULLY DEPLOYED
MODULE, REF.

NO. 1

R.H. SIDE ←───│───→ L.H. SIDE

VIEW LOOKING AFT

PAYLOAD SUPPORT PALLET
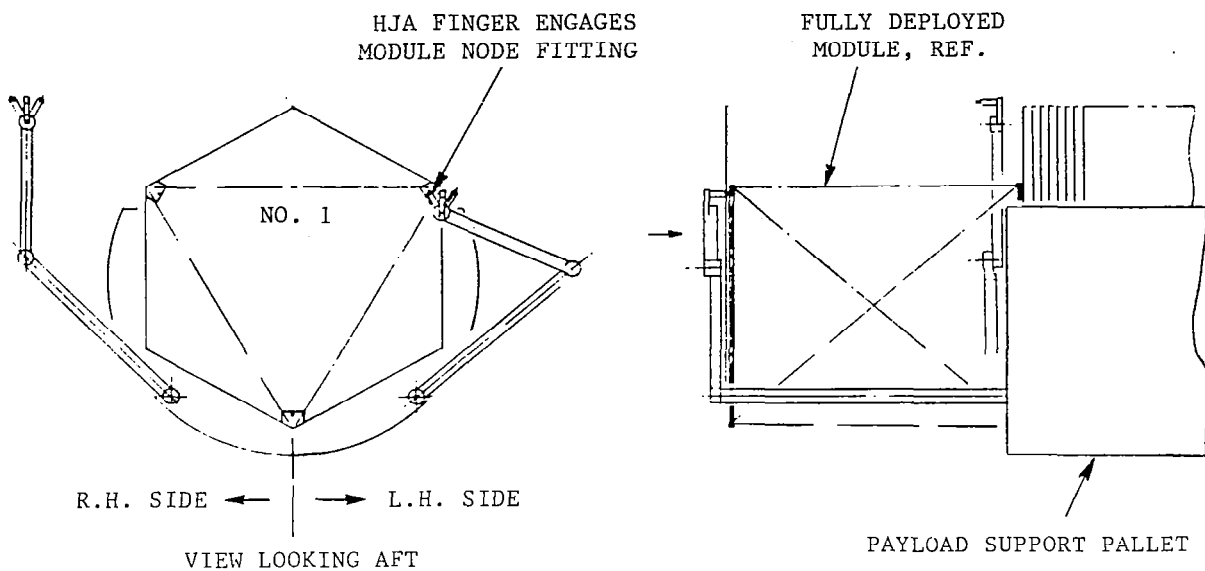
Figure 2-24.   Left-Hand Effector Engages Deployed Module

SECOND HJA ENGAGES BACKSIDE NODE FITTING

NO. 1
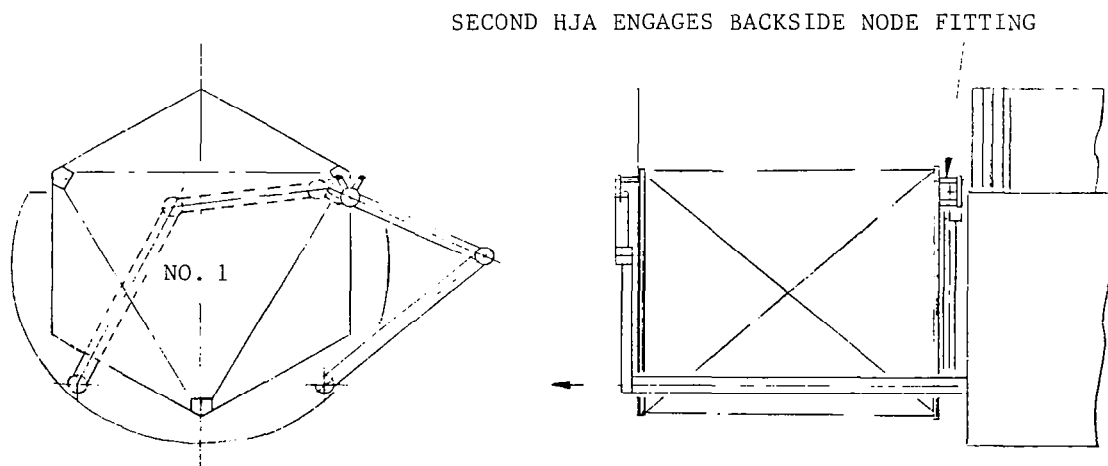
Figure 2-25.   Right-Hand Effector Engages Deployed Module

2-31

MODULE NO. 2

MODULE NO. 1

NO.1   NO.2

R.H. SIDE ◄━ | ━► L.H. SIDE
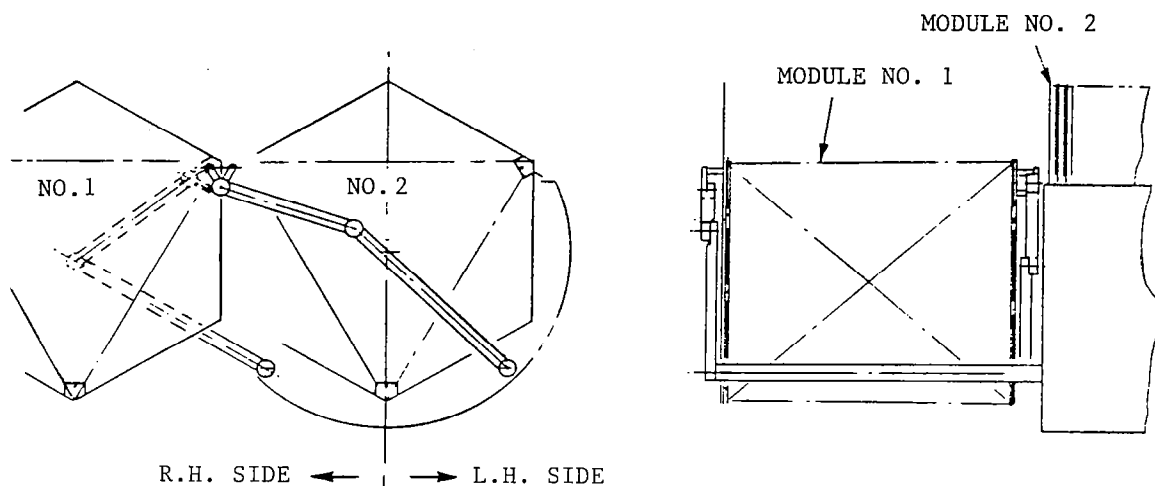
Figure 2-26. Deployed Module Relocated to Permit Deployment of Module No. 2

The two HJAs now adjust the position of Module No. 1 by retracting and trans-
lating to bring it into side-to-side engagement with Module No. 2. The second
finger probe on the left-hand HJA engages the front side node fitting of
Module No. 2. Module No. 2 is then released from the PSP by the simultaneous
actuation of the dispensing system and extension of the HJAs. When sufficient
gap exists behind Module No. 2, the effector head on the right-hand HJA rotates
about its first finger probe axis until its second finger probe aligns with and
engages the receiving feature in the Module No. 2 node fitting. As shown in
Figure 2-27, the two modules are now positively aligned and connected, both
front and back, by the two HJA heads. It now remains to perform the perman-
ent structural joining. This is effected by means of a link trigger unit (LTU)

LINK TRIGGER UNIT (LTU)

DIRECTION
OF ASSEMBLY
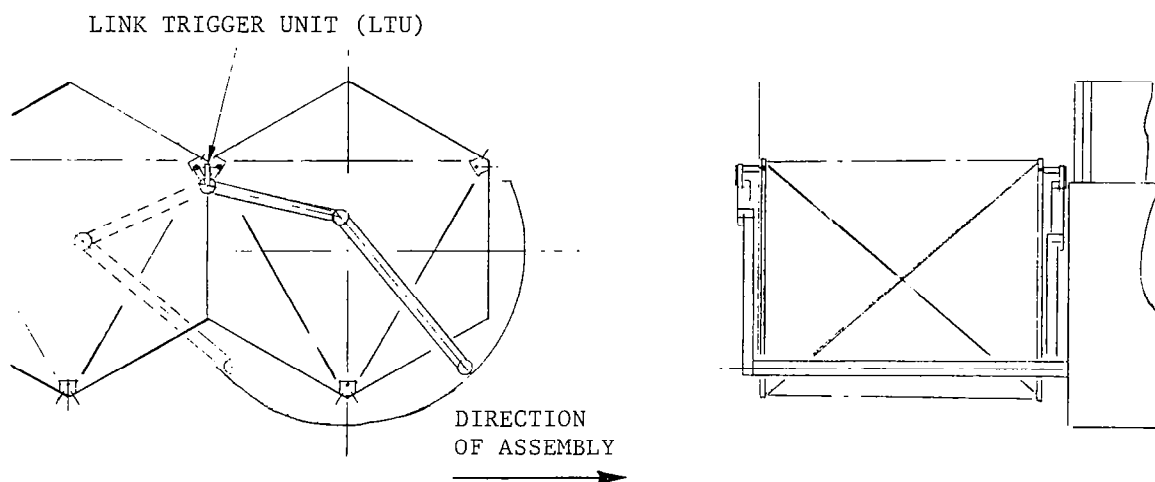
Figure 2-27. Modules No. 1 and 2 Aligned and Joined Front and Back

mounted on each HJA between the finger probes. When actuated it reaches down between the finger probes to actuate the connecting links built into each structural node fitting.

The steps described above are repeated for each module until a string of 16 modules has been assembled and paid out, becoming the first row of the reflector buildup. The seventeenth module is the first module of the second row and is handled as follows.

From the configuration shown in Figure 2-27 each HJA transfers, in turn, to reengage the end module at its lower node fitting, and then articulates back to approximately its original position. This, in effect, vacates the area for deployment of Module No. 17 and creates the required module positioning, shown in Figure 2-28. Alignment of the modules and the integration of Module No. 17 is performed in similar fashion to that described for Module No. 2.
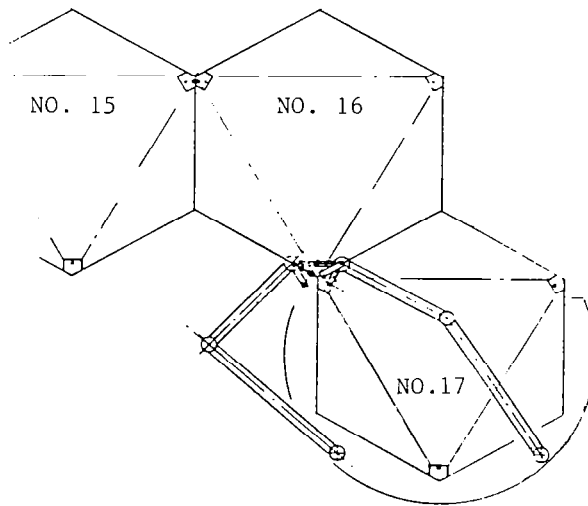
Figure 2-28. First Row of Joined Modules Relocated to Permit Deployment of Module No. 17

After the integration of Module No. 17, the direction of traverse reverses as the second row of modules is laid down below the first row. This requires reversal of the functions of the two HJAs, which is accomplished as follows:

a. Left-hand (front-side) HJA releases from right-hand node fitting of Module No. 17 and reengages at the left-hand node fitting.

b. Right-hand (back-side) HJA releases from right-hand, back-side node fitting, extends approximately 3.7 meters, reverses its effector head and engages the right-hand, front-side node fitting.

c. The left-hand HJA releases from the left-hand node fitting, swings clear, retracts approximately 3.7 meters, reverses its effector head, swings

inboard behind Module No. 17 and engages the right-hand, back-side node fitting of the module.

The net result of this maneuver is that the two HJAs have changed places, assuming the configuration shown in Figure 2-29, which is the opposite hand of that shown in Figure 2-25. Assembly can now proceed toward the left using the left-handed version of sequences described above for Modules 1 through 17.
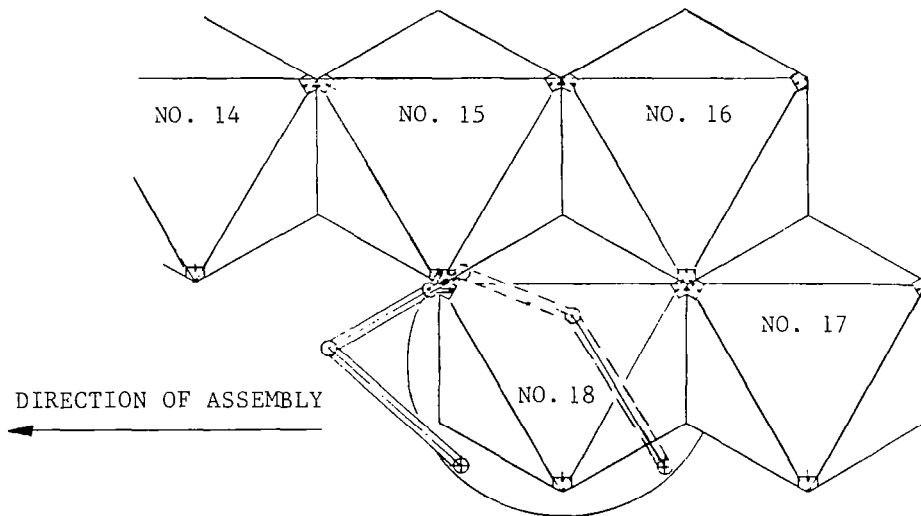
Figure 2-29. Deployment and Joining Sequence Continues in Reverse Direction

The installation of Modules 18 and on involves the connecting of additional structural interfaces per node. Whereas the joining of Modules No. 1 and 2 typically involved only two nodal fittings and one connecting interface, the integration of Module No. 18 involves three nodal fittings and three connecting interfaces since the module must be joined to the modules above (No. 15 and 16) as well as to the module adjacent (No. 17).

Thus, the total reflector structure is built up row-by-row following a zig-zag path from top to bottom as shown in Figure 2-30.

The configuration corresponding to that illustrated in Figure 2-29 is shown in greater detail in Figure 2-31.

The two handling fingers on each HJA are shown set at an angle to the center-line of the end effector. This angle is variable so that each finger can reach and engage modules not yet aligned and then pull them into alignment. The engagement is achieved by a collet feature on the end of each finger. The collet is normally contracted for minimum diameter to enable insertion of the finger into the receiving hole in the node fitting. Subsequent expansion of the collet in the hole locks the node fitting to the finger thus enabling manipulation and positioning of the module for joining.

DCM MODULE TYP.(721) PLACES

PAYLOAD SUPPORT
PALLET (PSP)

ORBITER, REF.

(1) PAYLOAD = 265 MODULES

(WITH L/ρ = 300
AND FLAT FACETS.) →

PROFILE AT COMPLETION
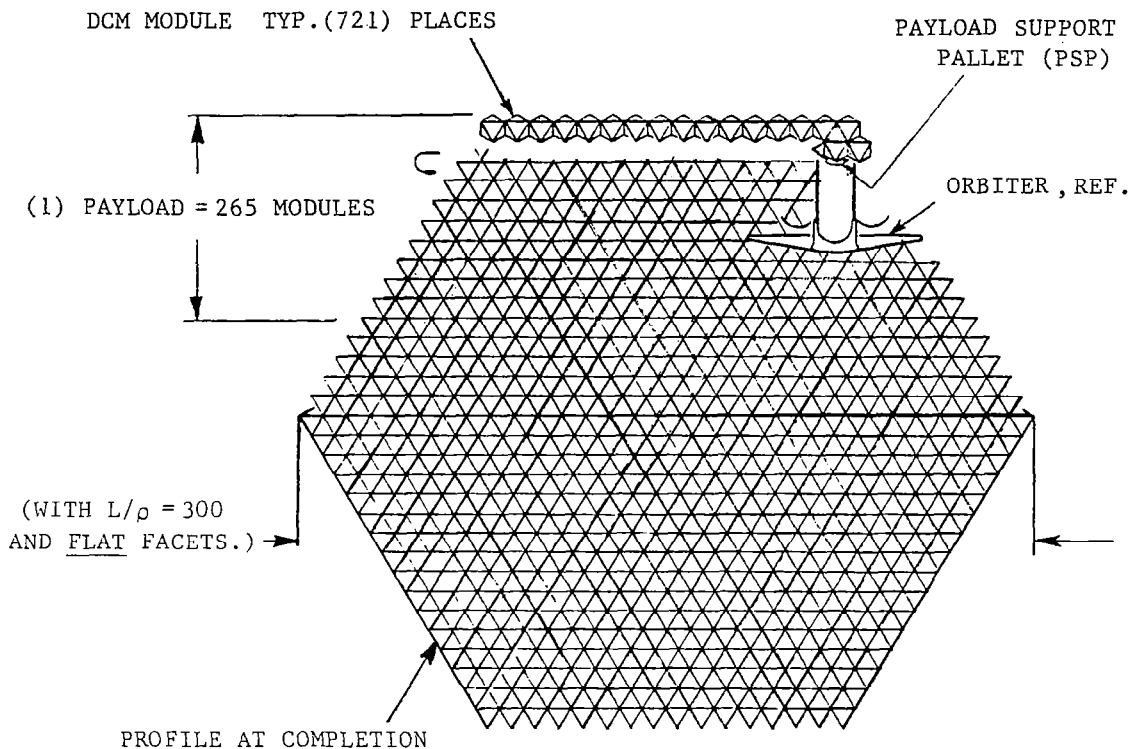
Figure 2-30. Joining Sequence Proceeds in Zig-Zag Manner to Lay Down
31 Rows of Modules

When the required alignment is achieved the link trigger unit (LTU) rotates down
to engage the node fittings and to actuate the link trigger mechanism, which
effects the mechanical joining of the structural interface. The exact logic of
this function is not defined but is visualized either as a latching link, built
into one node fitting, which extends across the structural interface to engage
the mating node fitting, or as a separate part ejected from the LTU to snap
over the anchor pins in the node fittings. For the latter approach the usual
undesirability of loose parts may be offset by the potential simplicity of the
structural features involved. (Ref. discussion in Section 2.4.4 above.)

NODE FITTING, REF.

STOWED MODULES, REF.

MODULE NO. 16

MODULE NO. 15

HANDLING
FINGER

FINGER HOLE,
REF

LINK TRIGGER
UNIT (LTU)

STRUCTURAL
LINK

HANDLING AND
JOINING ARM (HJA)

MODULE NO. 17

MODULE NO. 18

RT HD HJA   LFT HD HJA

RT HD SIDE ◄—— | ——► LFT HD SIDE

PAYLOAD SUPPORT PALLET (PSP),
REF

0

| METERS | 1.0 | | 1.0 | 2.0 | 3.0 | 4.0 | 5.0 |
| INCHES | | | 50 | 100 | 200 | 300 | |

0
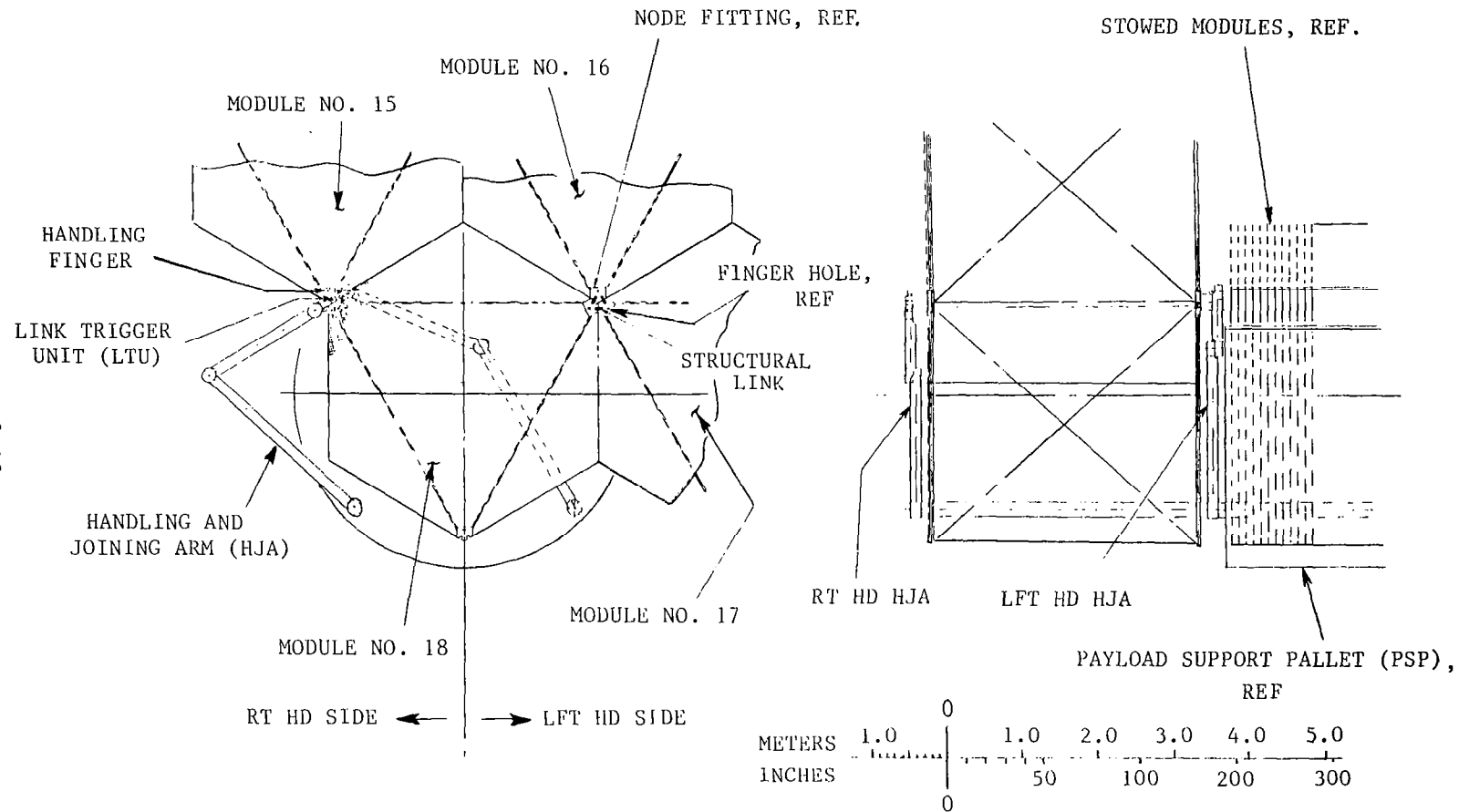
Figure 2-31. Effector Heads on the Two Manipulators Engage, Align, and Join Module Node
Fittings — Both Front and Back

2.6 ANALYSIS AND EVALUATION OF THE COMPLETED DCM REFLECTOR

2.6.1 STRUCTURAL ANALYSIS BY ADAPTING THE LASS COMPUTER
PROGRAM. The Large Advanced Space System (LASS) computer program
(Figure 2-32) was written specifically for analysis of structures having the
PETA tetrahedral truss geometry. The different geometry of the DCM structure
has required generation of a new mathematical model (Figure 2-14), plus hand-
written improvisation to maintain compatibility with LASS.
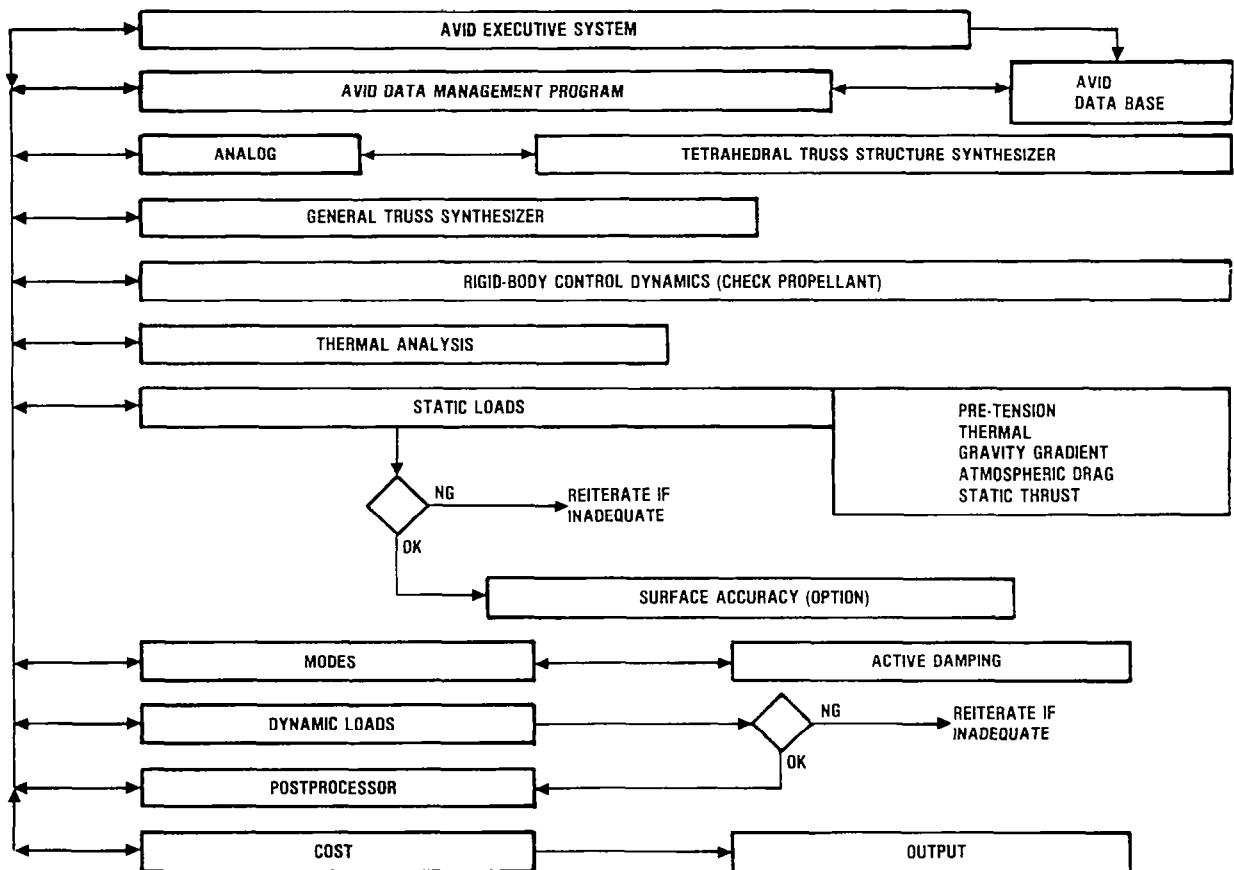
Figure 2-32. Large Advanced Space System (LASS) Computer Program
was the Principal Analytical Tool

The initial Tetrahedral Truss Structure Synthesizer (TTSS) phase of the LASS
analysis provides part counts, lengths, weights, and mass properties data as
presented in Section 2.3.

Thermal distortion analysis commences with generation of a SAP finite element model. For the given (input) thermal condition the program provides temperature data for each structural element. These temperature outputs are loaded into SAP, which outputs element loads, stresses, and displacements from nominal. Final shape accuracy output from the Surface Accuracy routine is presented both in terms of deviation from nominal shape, with respect to the x, y, z coordinate system, and as RMS deviation from an idealized "best-fit" paraboloid. Change in focal length resulting from "best-fitting" is also given.

2.6.1.1 Modeling. (Figure 2-14.) The DCM concept poses several unique mathematical modeling problems due to the nature of two of its component elements, i.e., the pretensioned diagonal cables and the pretensioning vertical columns. The column members may be either in the form of buckled columns acting as compression springs between the upper and lower structural faces, or as telescopic, compression spring struts, acting in identical fashion. Either version can be readily simulated in the mathematical model. These components are designed and sized so that the diagonal tension ties are maintained in a state of positive tension under all normal design loading modes, thermal and static. The tension ties are therefore modelled as rods, i.e., one-dimensional truss elements that react axial loading only. Any indication in the analysis that the axial loading is negative, i.e., that the ties have lost tension, could indicate local or general structural instability. This would introduce uncertainty to the analysis with respect to stresses, deflections, etc., and would require reanalysis with larger pretensioning forces.

Since the spring rate of the pretensioning column is low, the pretensioning force can be considered essentially constant over the range of expected structural deflection. Therefore, the model of the column will be characterized by relatively large preload. It is appropriate also to model these column elements as rods with ficticious properties assigned that reflect the physical characteristics; the preloading will be considered as an equivalent temperature change. This chosen approach is simple and efficient and seems to model these physical elements exactly.

2.6.1.2 Thermal Distortion Analysis

Thermal Considerations. Solar heating and the absolute heat sink of deep space combine to create a severe thermal environment for orbiting structures that results in temperature differentials between structure elements, and temperature gradients within individual elements.

Although three-dimensional truss structures characteristically exhibit exceptionally high shape stability, thermal distortions remain an important consideration.

Temperature levels in individual structural elements are primarily a function of the incident angle of solar flux (ψ) on the element. Maximum temperature values are experienced when the angle of incidence is 90 degrees, when shadowing is

minimal, and when the ratio of absorptivity (α_s) to emissivity (ϵ) for the exposed surface is high.

In a three-dimensional truss structure the component elements are typically set at various attitudes, one to another, and it therefore follows that adjacent elements will often experience widely varying angles of solar incidence. The typical overall condition is further complicated when some elements are in the full or partial shadow of other elements, and when all these effects are transient due to rotation of the structure relative to the direction of solar flux, i.e., when "barbequing."

These same considerations and effects apply to the reflective surface installation. Its components also experience various and varying temperature levels and gradients, and react according to their own individual characteristics and material properties.

Determination of the extent of structural distortions through the full range of orbital thermal conditions requires an extensive investigation that involves consideration of:

- Orbital geometry and altitude.

- Orientation of the satellite with respect to the sun and earth.

- Absorptivity/emissivity characteristics of the satellite structural surfaces.

- Earth shadowing, radiation, and albedo.

- Internal "self-shadowing" peculiarities of the satellite structural geometry.

- Thermal response of the satellite structural materials and of the structural geometry.

The magnitude of such a comprehensive investigation, performed for each of the three candidate concepts, is such that it exceeds the scope and intent of the subject study and requires that a relatively simplistic approach be adopted.

Selection of Thermal Condition for Analysis. Selection of a geosynchronous orbit imposes a relatively severe thermal condition with maximum deep space cooling of the structure and fully directional solar heating. The high orbital altitude is taken as justification to simplify the condition by neglecting earth radiation and albedo. Further, the assumption is made that earth shadowing of the structure does not occur. The orientation of the structure with respect to the sun vector is assumed constant so that the thermal condition is steady state rather than transient. This relationship, defined in terms of γ and ϕ, is shown in Figure 2-33. Values of sun vector angles, 'γ' with respect to the 'y' axis and 'ϕ' with respect to the primary axis, are chosen that judgementally produce maximum internal shadowing of the structure by the mesh surface and maximum temperature gradient across the span of the structure. Such a condition is considered likely to produce maximum values of overall thermal strains and to therefore represent, with reasonable accuracy, an actual worst-case condition.

2-39
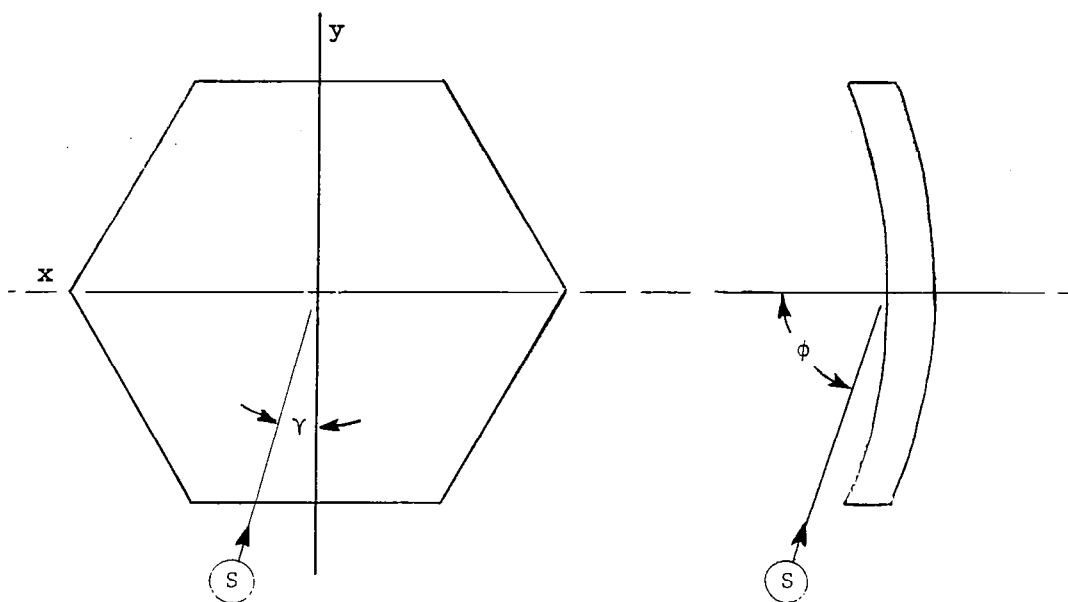
Figure 2-33. Worst Case "Side-on-Sun" Condition is Selected for Analysis

Used as input to the LASS computer program, this condition is seen to represent a fair and equal test of the thermal stability of the candidate concepts.

It is deduced from prior studies that for the subject antenna geometry (f/d=1.0) a near worst-case condition exists when ϕ=82 degrees. Then, in the lower half of the reflector, most structural members are in the general, graduated shadowing of the reflective mesh installation. The mesh itself is largely in its own shadow in the upper half of the reflector (Figure 2-33) and becomes progressively exposed in the lower half. A zone exists in the upper half of the structure where both front and back surface members are directly in the shadow of adjacent members, while the intermediate (diagonal) members are essentially fully exposed.

Selection of a value of 15 degrees for γ produces similar thermal conditions for the intermediate structural elements of all three concepts, thus maintaining equivalence of the overall thermal condition for the three concepts.

Modification of LASS CP Outputs. Since the LASS program is not written to include the effects of members falling in the shadow of other members, this effect may be artifically introduced by hand modification of the thermal analysis outputs. Such shadowing will be most significant where the sun vector is tangential to the curved (inner and outer) surfaces of the structure. Temperatures of surface members in the immediate vicinity of the great circle, thus defined, will in reality all experience a moderately low, common temperature that can be judgementally estimated by equating to the output temperature values of those members known to have a low angle of incidence to the sun vector.

A more exact but significantly more laborious task would be to recalculate, by hand, the temperature values of these shadowed members. The analyses here presented do not account for such member-on-member shadowing (this capability not yet in the program) but do account for the effects of structure shadowing by the metallic mesh reflector surface (facets).

Thermal Shape Stability — Study Case C-1. The LASS computer program analysis of DCM Study Case C-1 was performed per the input data presented in Table 2-3, Section 2.3, and the thermal condition defined above.

As for all candidate concepts, the selected structural material is graphite epoxy composite material with the mechanical properties listed in Section 2.2.1. The input values for solar absorptance (α_s) and emissivity (ϵ) were .91 and .81, respectively, which represent the surface characteristics of bare (uncoated) graphite epoxy with a roughened (diffuse) surface texture.

For the thermal condition defined above, the thermal analysis determined that the temperatures experienced by the front face struts ranged from 77.8 K (-195.4°C) to 301.1 K (27.9°C), 36% of the front face struts being below 81.9 K and 2% above 300 K. Temperatures of the back face struts ranged from 77.5 K to 301.2 K, with 20% below 81.7 K and 13% above 300 K. Temperatures for the cross bracing tension ties ranged from 66.3 K to 302.8 K, with 22.5% below 79.1 K and 9.5% above 300 K. (No temperature data output was generated for the metallic mesh reflector surface (facets)).

Figure 2-34 presents, in contour form, the normal surface displacements of the concave face of the structure with respect to a best fit paraboloid.

The overall "best fit" error (δ) is then: $\delta = 1.55$ mm (0.061 inch) RMS
Change in focal length (de-focus) is: $\Delta f = 0.14$m (5.66 inches)

2.6.1.3 Stiffness Analysis. Due to their high structural efficiency, three-dimensional truss structures characteristically exhibit high stiffness/weight ratios and, consequently, high fundamental frequencies. Equations have been evolved[2] for the sizing and characterization of tetrahedral truss platforms of hexagonal profile. The fundamental frequency of such a platform is given by the equation:

$$f_1 = \frac{25.93}{2\pi D}\sqrt{\frac{D_t g_\epsilon}{\left(M_t/A\right)_{system}}}$$

where:

- $(M_t/A)_{system}$ is the total system mass per unit area, including the mass of all structural components (tubes, end fittings, nodal joint fittings), subsystems, and payload. Total system mass is assumed to be uniformly distributed.

[2] Equations for analysis of the tetrahedral truss were developed by Walter L. Heard Jr, of NASA Langley Research Center, Virgina.

2-41

CONTOUR LEVELS
LABEL   VALUE

A   -15 E-2
B   -10 E-2
C   -5   E-2
D   0   E-2
E   5   E-2
F   10   E-2

DCM STUDY CASE C-1

(31-BAY DCM PARABOLA)

RMS DISTORTIONS

SUN VECTOR
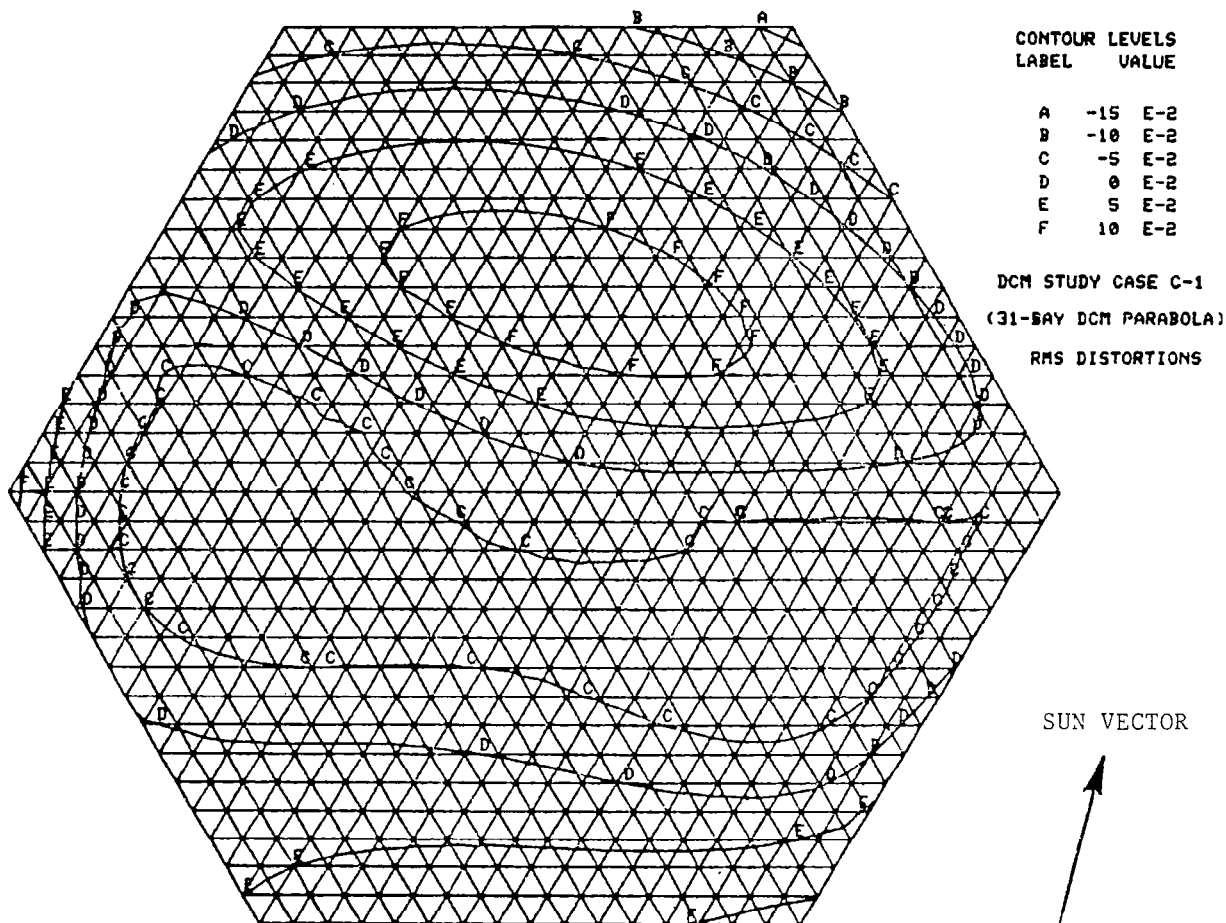
Figure 2-34. Contours of Deviations of Surface from "Best Fit" Paraboloid in Direction Normal to Surface, DCM Study Case C-1

- $D_t = \dfrac{3\sqrt{3}}{8} \; E_f \cdot A_f \cdot L_f \left[\left(\dfrac{L_c}{L_f}\right)^2 - \dfrac{1}{3} \right]$ is the structure bending stiffness

  equation, which assumes the platform idealized as a sandwich plate with isotropic face sheets and a rigid core, where:

  E_f is the Young's modulus of the face struts

  A_f is the section area of the face struts

  L_f is the node-to-node length of the typical face strut

  L_c is the node-to-node length of the typical core strut

- The constant $g_\varepsilon = 1 \dfrac{kg \cdot m}{N \cdot s^2} = 32.2 \dfrac{lbm \cdot ft}{lbf \cdot s^2}$

- D is the maximum dimension of the platform, i.e., the overall measurement across the points of the hexagonal profile.

2-42

Since the above equations are written specifically for truss platforms of the tetrahedral geometry, it is necessary to represent the DCM (core) structure by an equivalent tetrahedral geometry in the determination of the fundamental frequency of the DCM reflector. The six cross ties in the typical DCM module are therefore simulated by three "tetrahedral" core struts of equal total weight and of appropriate length to maintain the true (DCM) structural depth. Thus, whereas the typical DCM cross tie is 7.7 mm (0.3 in.) diameter and 5.05m (199 in.) long, giving a material volume per module of $0.00139\,m^3$ ($84.6\,in^3$), the equivalent "tetrahedral" core struts are 4.085m (160.8 in.) long with a section area of $0.000003\,m^2$ ($0.175\,in^2$) giving the same total material volume per module. Input parameters used for the analysis are summarized in Table 2-4: thus

$$D_t = \frac{3\sqrt{3}}{8}(1.314 \times 10^{11})\ (1.06 \times 10^{-4})(3.645)\left[\left(\frac{4.085}{3.645}\right)^2 - \frac{1}{3}\right] = 3.0415 \times 10^7$$

and   Natural frequency $(f_1) = \dfrac{25.93}{2\pi 108^2}\ \sqrt{\dfrac{3.0415 \times 10^7\ (1)}{9399/7854}} = \underline{1.78\ Hz}$

Table 2-4. Input Parameters for Analysis of DCM Reflector

Parameter		Metric Units (SI)	English Units
Maximum Dimension	(D)	108m	4251.97 in.
Equivalent Aperture Dia	(D_a)	100m	3937.0 in.
Equivalent Aperture Area	(A)	$\dfrac{(100)^2}{4} = 7854\ m^2$	$\dfrac{\pi(3937)^2}{4} = 1.217 \times 10^7 \times in^2$
Face Struts			
Young's Modulus	(E_f)	131 G Pa	$19.05 \times 10^6\ lb/in^2$
Diameter	(d_f)	0.0369m	1.45 in.
Wall	(t_f)	0.000914m	0.036 in.
Sec. Area	(A_f)	$0.000106m^2$	$\pi(1.45)\ 0.036 = 0.164\ in^2$
Length	(L_f)	3.645m	143.5 in.
Density	(ρ_f)	$1836\ kg/m^3$	$0.06633\ lb/in^3$
Core Struts			
	(E_c)	131 G Pa	$19.05 \times 10^6\ lb/in^2$
	(L_c)	4.085m	160.8 in.
	(A_c)	$0.000113m^2$	$0.175\ in^2$
	(ρ_c)	$1836\ kg/m^3$	$0.06633\ lb/in^3$
Gravity	(g_ϵ)	1	$32.2 \times 12\ in/sec^2 = 386$
Structural Mass	(M_s)	8503.8 kg	$\dfrac{18,751.2\ lb}{32.2\ (12)\ in/sec^2}$
Parasitic Mass	(M_p)	895.2 kg	$\dfrac{1973.8\ lb}{32.2\ (12)\ in/sec^2}$
Total System Mass	(M_T)	9399 kg	$\dfrac{20,725\ lb}{32.2\ (12)\ in/sec^2}$

2.6.2 CONCEPT PERFORMANCE EVALUATION. The DCM concept has packaging characteristics that limit its deployed structural depth to 3.5 meters (11.5 feet). The use of high stability composite material (graphite-epoxy) tends to compensate for this limitation and results in good structural stability. Natural frequency (f_1) is estimated to be 1.78 Hz.

Thermal instability in a typical worst-case, in-orbit thermal condition is found to be only 1.55 mm (0.061 inch) root-mean-square (RMS) deviation from the best-fit paraboloid. This value was obtained by LASS computer program analysis in which the value of the coefficient of thermal expansion (CTE) of the composite structural material was taken to be $+ 0.45 \times 10^{-6}$ m/m/deg K ($+0.25 \times 10^{-6}$ in/in/deg F).

Table 2-5 presents the achievable overall shape accuracy (excluding static loading strains that will vary according to mission). The table presents the root-sum-of-the-squares (RSS) of the following items:

1. Geometry (design) — This value represents the designed-in error that results from best fitting numerous small, flat facets to represent the paraboloid.

2. Thermal strains — Structural thermal strains are determined using the LASS computer program for an assumed worst case thermal condition. Since the reflective surface is a membrane stretched in biaxial tension within a hexagonal frame, the degree of flatness of the membrane depends upon flatness of the frame. Since the frame is small relative to the total reflector and since frame deflections will be peak deflections, their effect is small and assumed to be 10% of the magnitude of the structure thermal strain.

3. Static loading relates to externally applied loads associated with attitude control for pointing and tracking. Since these are dependent upon the requirements of specific missions and could be zero for a passive application, they are not included in the budget.

4. Measurement accuracy — The assumption is made that technology will be available to observe and determine the shape of the reflective surface of the space-assembled reflector to an accuracy of 0.03 mm (.001 inch) RMS.

5. Adjustment accuracy — The assumption is made that active adjustment capability is provided at the three facet/structure interfaces of each module and that the attitude and position of each facet can thus be moved into coincidence with a determined best fit attitude and position with an accuracy of 0.25 mm (0.01 inch) RMS.

6. Repeatability — This item allows for shifts of reference datum used for shape measurement and adjustment that may result from disassembly after 1g checkout and reassembly in orbit. If no active, post-space assembly, shape tuning capability were provided, this would be mainly a function of the repeatability of the accurate mating of modular interfaces. To illustrate: poor repeatability of bolted interfaces due to excessive bolt clearances is improved by the engagement of tapered shear pins.

7. RSS correction (10%) — This adjustment recognizes that the magnitude of reflective surface shape errors tends to be minimum at the center of the reflector where illumination is highest and maximum toward the periphery where illumination is least. (A-10 dB illumination taper is assumed).

Table 2-5. Error Budget and Achievable Shape Accuracy - DCM

Item	δ mm (inch) RMS
1. Geometry (design) — Common flat facets	2.6 (0.102)
2. Thermal Strains — Structure	1.55 (0.061)
— Mesh system (10%)	0.16 (0.006)
3. Static Loading Strains	—
4. Measurement Accuracy	0.03 (0.001)
5. Adjustment Accuracy	0.25 (0.01)
6. Repeatability	0.76 (0.03)
Total RSS (half path error)	3.14 (0.12)
RSS correction (10%)	0.31 (0.012)
Adjusted total RSS (δ)	2.83 (0.11)
	= $\lambda/107.4$ at 1 GHz
	= $\lambda/7.2$ at 15 HGz
	= $\lambda/50$ at 3.7 Hz
	= $\lambda/16$ at 11.6 Hz

Structural performance is seen to be more than adequate for operation at 1 GHz but marginal at 15 GHz. The total weight of the 100-meter reflector is 9399 kg (20,725 lb).

Stowage of the DCM modules is found to be reasonably dense — requiring 2.6 Orbiter payloads. The methodology of deployment and assembly is straightforward and is characterized by relatively small scale operations in the immediate vicinity of the Orbiter payload bay. These operations involve a mechanical handling sequence for each module that is highly repetitive since 721 individual modules have to be deployed and assembled to form the 100 meter reflector structure. This relatively large number of modules results in the following statistics.

Total number of structural tubes and ties is 10,815 and the total number of structural connections to be effected in space is 8460. Allowing 20 minutes per module, total assembly time would be approximately 240 hours, i.e., 10 days of continuous effort in fully automated mode.

Overall structural stability of the completed reflector is dependent upon maintenance of positive tension in the 4326 cross bracing ties. This, in turn, is dependent upon the preloading force exerted by the 2163 spring-loaded columns being of sufficient magnitude to exceed the opposing effects of all operational modes of applied, external loading, e.g., attitude control, tracking, and orbital transfer. Thus, the tubular structural elements must be designed to react applied loads *plus* the preloading.

If the mission requirements involve high values of applied load, the preloading would need to be correspondingly high and the design would tend to become strength critical. A convenient way of adjusting the design to meet the strength requirements is by increasing the wall thickness of the tubular components. It thus follows that, for a strength critical design, a weight penalty would be attributable to the existence of structural preloading.

There is also possible cause for concern over long-term effect of continuous pre-loading on the composite structural material. If the tubular components or the cross ties changed length due to creep, the ties would tend to slacken and the structure would tend to flatten with corresponding increase in focal length. Further, if the "creep" was not uniformly distributed, degradation of reflector shape accuracy would result.

With the objective of reducing the number of DCM modules required to assemble a 100 meter reflector, consideration has been given to the possibility of providing the typical DCM module with an additional stage of mechanical deployment that would increase deployed size. Theoretically this could be achieved by providing each of the six tubes that comprise the two triangular frames the capability of extending telescopically. A 75% expansion could result. However, this is not seen to be practical for the following reasons:

- If the telescoping action in all six tubes were not perfectly synchronized, bending could be induced and jamming of the telescopic action could occur.

- The existing simple concept of a nondeploying, flat reflective facet supported in biaxial tension within a rigid, hexagonal frame would have to be replaced by a deployable surface concept. It is not readily visualized how this could be accomplished.

- The above considerations represent a major increase in mechanical complexity, and reliability of deployment would be significantly reduced.

- No increase in structural depth would result if buckled columns were employed as intermediate members. The alternative telescopic columns could be redesigned to increase depth approximately 30%. In either case, the tie lines would be longer, would assume a shallower angle, and would thus be required to carry higher loads. Reduced shear stiffness of the structure would result.

- Support equipment required for deploying and joining the modules in space would be correspondingly larger, heavier, and more complex, requiring more stowage space.

- If flat, the larger (hexagonal) facet would have a deviation from the best fit paraboloid of $\delta = 8.0$ mm (0.315 in.) RMS, a three-fold increase. Substituting this value into the error budget presented in Table 2-5 results in a degradation of the adjusted total RSS to 8.2 mm (0.32 in.), i.e., $\delta = \lambda/36.6$. at 1.0 GHz.

SECTION 3

ALTERNATIVE STRUCTURAL CONCEPTS

3.1 MODULARIZED PARABOLOIDAL EXTENDABLE TRUSS (Mod-PETA)

3.1.1 DEFINITION OF 100-METER REFLECTOR. The 100-meter, modularized
PETA reflector shown in Figure 3-1 consists of 96 individual, triangular struc-
tural modules joined at their edges to form a single, integrated structure. To
achieve matched geometry at the structural interfaces modules are alternately
"male" and "female."

The structural system of the PETA design is, in essence, a mechanical assembly
of tubular structural members joined at their ends and arranged to form a multi-
plicity of tetrahedrons. The pivotal capability of the end joints, and the mid-
span hinges that are provided certain members, enables the structure to be mech-
anically folded into a high density package in which all members lie in parallel
orientation (Figure 3-2). The mid-span hinges may be spring loaded so that when
circumferential restraints are released from the package, the structure automati-
cally unfolds radially until it locks-up in its fully deployed configuration (Figure
3-3). A flexible reflective mesh system attaches to the structural node fittings of the
concave face of the structure. In the packaged state the mesh is bundled at one
end of the packaged structure. It is pulled out by the deploying structure and
becomes taut in stable paraboloidal shape as the structure reaches full deploy-
ment.

The concept of deploying several such PETA structures, in space, and subse-
quently joining them to produce a single larger structure appears to have
potential and is presented in this study as an alternative to the DCM approach.

The first option to be considered is whether to use a minimum number of large
substructures (modules) or a larger number of smaller modules. The larger the
modules the fewer the number of structural interfaces but the greater will be
the risk associated with deployment of the individual modules. A basic objective of
the program is to establish reasonably small module sizes to reduce the cost and risk
of early test/development phases.

3.1.2 Mod-PETA MODULE DESIGN. Figure 3-4 illustrates some of the many
optional PETA modular patterns into which this reflector shape can be subdivided.
Figure 3-4(A) shows a single hexagonal module with six semi-hexagonal modules
joined at its periphery. Figure 3-4(B) presents eight, constant thickness modules
that stow longitudinally in the payload bay. They deploy to the full width of
the reflector and present straight-line joining interfaces. Figure 3-4(C) uses
six equal, triangular modules of maximum size. Figure 3-4(D) is the same
approach but with a larger number of smaller modules. Two of these approaches
are presented in this study.

STRUCTURAL
MODULE, FEMALE

STRUCTURAL
MODULE, MALE

100m DIA
NOMINAL

108m
(8) MODULES

4.05m
(13.29 FT)

13.7 m (45 FT)
NOM. TYP

CONCAVE FACE

CONVEX FACE

10   0   10 20   30   40 50   60   70 80   90 100
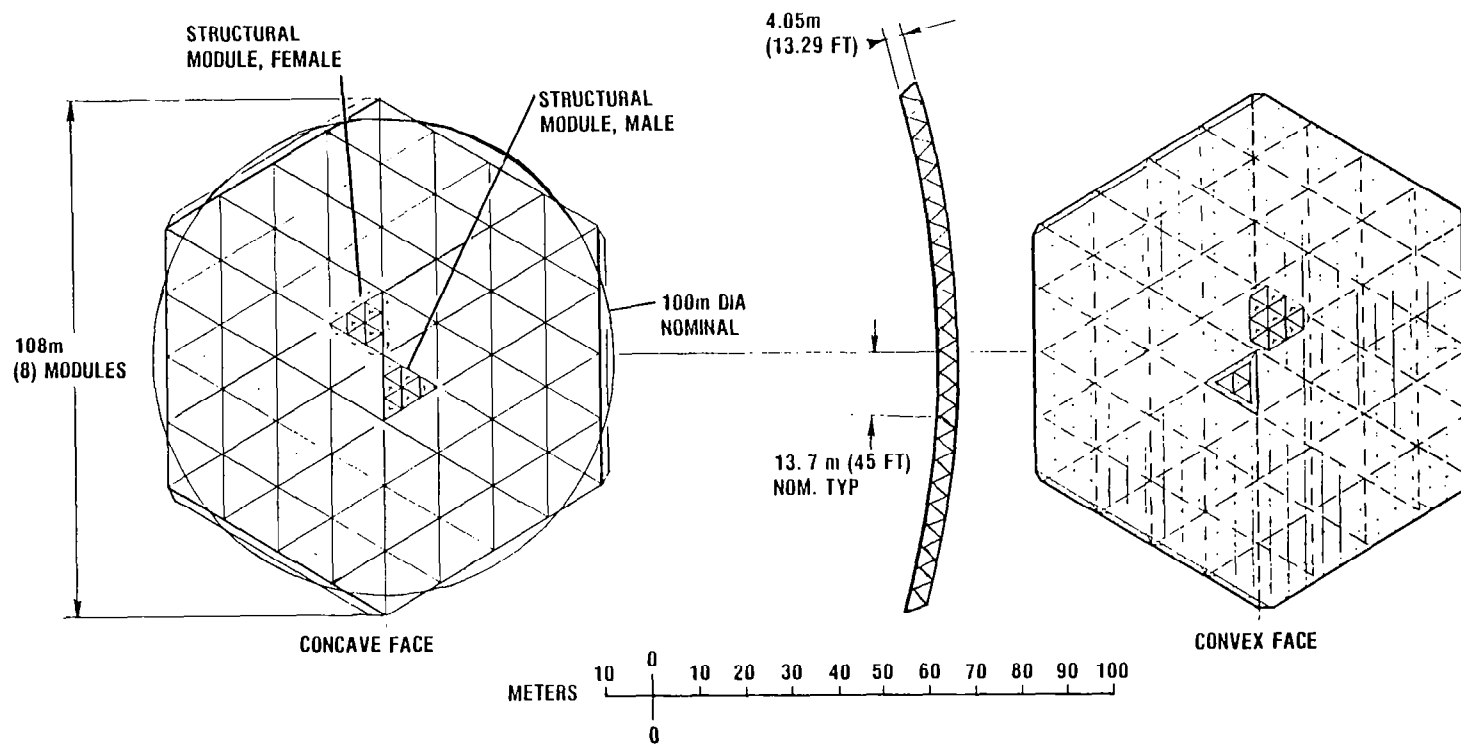METERS

0

Figure 3-1. Modularized PETA – 100-meter, (96) Module, Reflector – Study Case 'H'
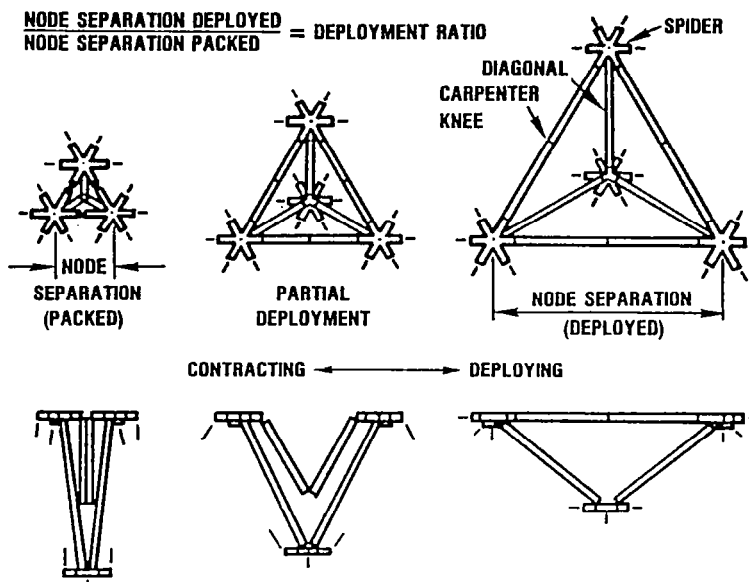
Figure 3-2. The Elemental Structure of Six Struts Deploys by
Extending from a Compact Bundle to Form the
Elemental Tetrahedron
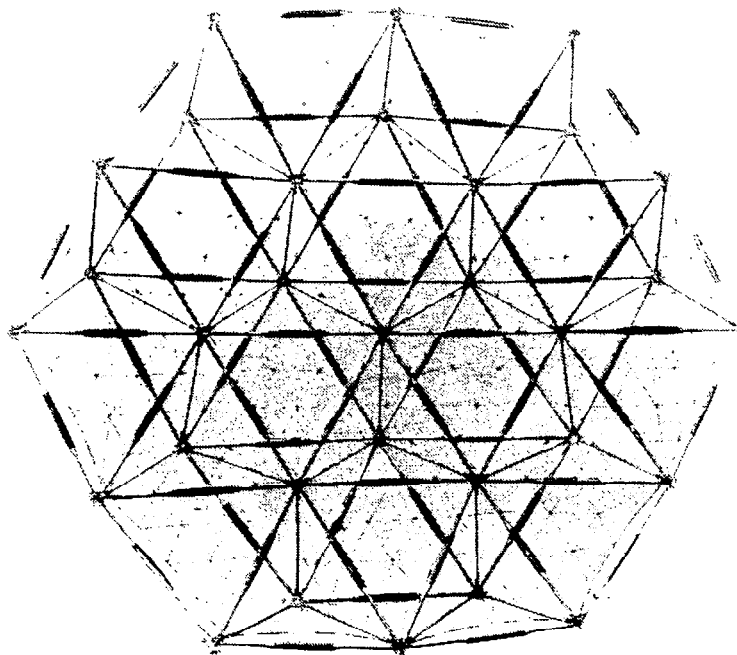
Figure 3-3. A Typical Full PETA Structure Consists of a
Multiplicity of Elemental Tetrahedrons
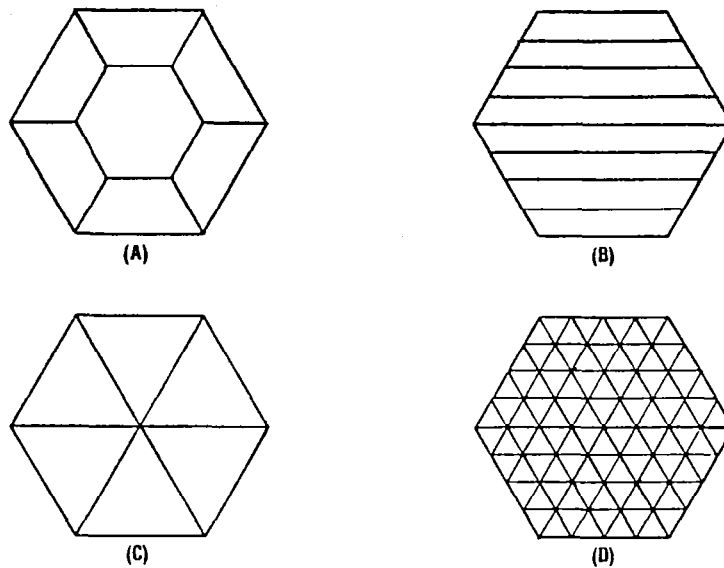
Figure 3-4. Options in Modular Subdivision

Study Case H uses the geometry shown in Figure 3-4(D) dividing the reflector into 96 modules. The configuration of its typical "male" module is shown in Figure 3-5 and the "female" module in Figure 3-6. Each module is of tetrahedral truss configuration, is approximately 13.7m (45 ft) in size, and is provided with a flexible mesh membrane stretched across its concave face. This membrane, which serves as the RF reflective surface, is suspended in near paraboloidal shape by a system of tie lines and standoffs.

Study Case J uses the geometry shown in Figure 3-4(B) with 48 "plank" shaped modules as described in Section 3.1.5. The reflective mesh installation is similar, in principle and in detail, to that used for the J modules.

The typical packaged configuration of the module is shown in Figure 3-7.

As in the DCM study, graphite epoxy composite is the selected primary struc-tural material, by virtue of its beneficial physical properties.

The Mod-PETA structure differs from the DCM structure by having pivotal joints at the mid-point of many of its component struts. These joints are of titanium and are included in the thermal compensation design technique for achieving zero (theoretical) CTE, as described in Section 2.2.1. The material property values defined in Section 2.2.1 are equally applicable to Mod-PETA performance analysis.
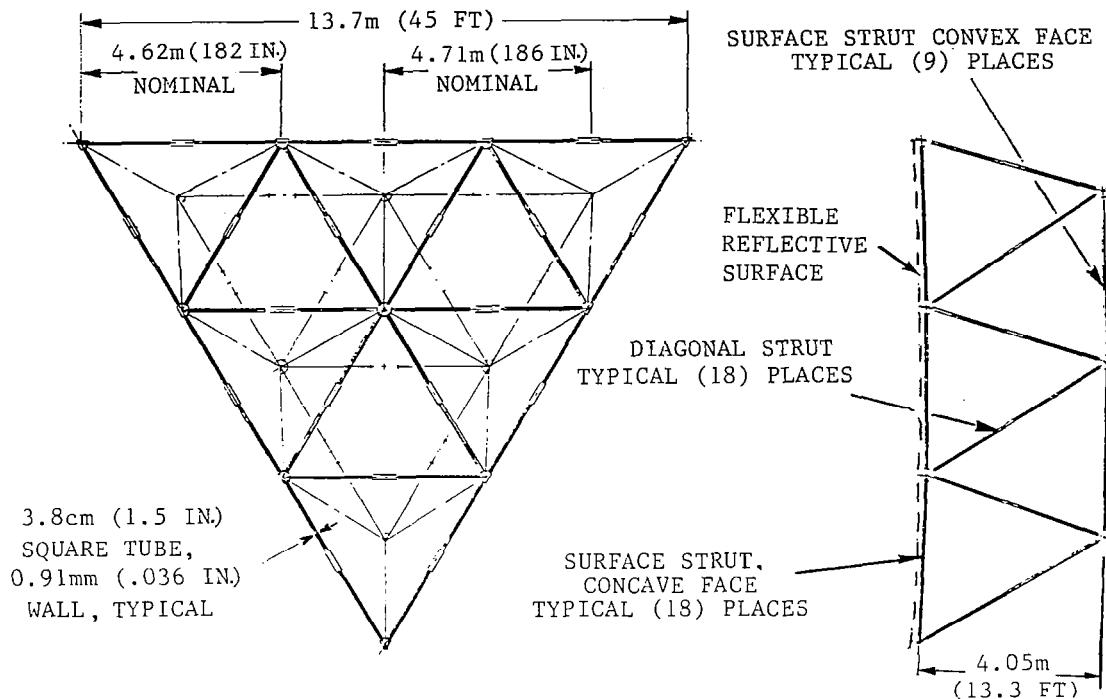
Figure 3-5. Male Module (three bays), Mod-PETA, Study Case H
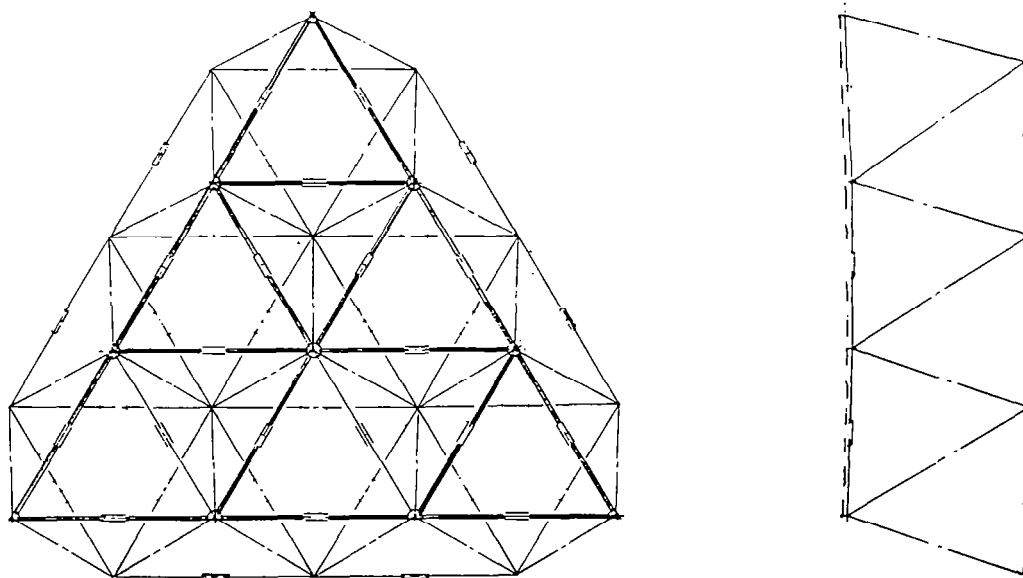
Figure 3-6. Female Module (three bays), Mod-PETA, Study Case H
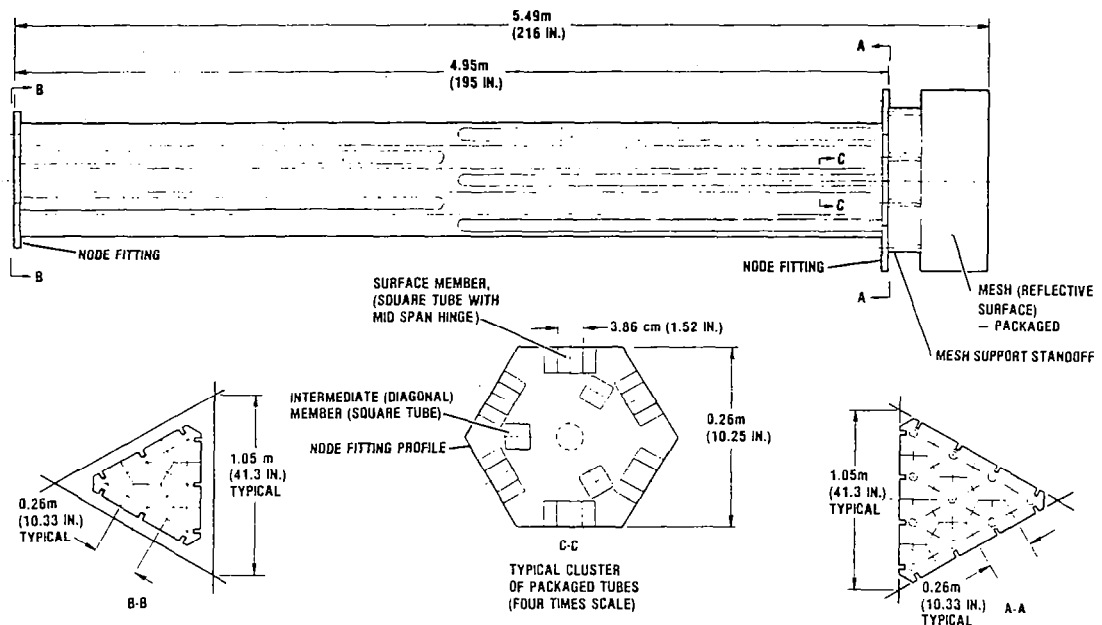
Figure 3-7. Each Module Packages into a Bundle Typically 13 Times Smaller than its Deployed Area (Mod-PETA, Study Case H)

As seen in Figure 3-5, the length of the face members is typically 4.6 meters. The typical member section, giving $L/\rho = 300$, is illustrated in Figure 3-8.

LENGTH (L) = 4.62m (182 IN.)

WALL (t) = 0.91mm (.036 IN.)

WIDTH (b) = 3.8cm (1.5 IN.)

RADIUS (r) = 3.0mm (.12 IN.)

L/ρ = 300

P_{CR} = 3895 N (652 LB)

WEIGHT = 0.92 K_g (2.02 LB)

Figure 3-8. Typical Structural Section Geometry

Note

Although in this concept the intermediate (diagonal) elements typically are more lightly loaded than the inner and outer surface members, they are assumed to be of the same stock section as the surface members, for practical reasons, and are so defined for the Mod-PETA Study Cases H and J.

3.1.3 QUANTITIES AND MASS PROPERTIES. The mass properties of the PETA concept, Study Case H (Figure 3-1) are presented in Table 3-1. Material properties input, consistent with those derived in Section 2.2.1 are listed with other input data in both metric and English units in Table 3-2.

The geometry of the total 24 bay reflector is shown in the "bore axis" view presented in Figure 3-9.

Table 3-1. Tetrahedral Truss Structures Synthesizer Output Provides the Mass Properties and Dimensional and Part Count Data for the 24 bay, 100m Reflector, Mod-PETA Study Case H

```
TRUSS PARAMETERS  24 BAY 56.84 DEG AN    95.3 M (   312.6 FT )ACROSS FLATS
                  XXXXXX L/RHO XXXXXX D/T 1.050 F/D     0.0 % CONTINGENCY
----------------------------------------------------------------------------
                       UNIT WEIGHT       NUMBER          WEIGHT
COMPONENTS         KILOGRAMS (POUNDS) REQUIRED KILOGRAMS    (POUNDS )
----------------------------------------------------------------------------
  STRUTS               .17E+01 ( .38E+01 ) 3852  .66115E+04 ( .14578E+05 )
   UPPER SURFACE       .15E+01 ( .33E+01 ) 1332  .19761E+04 ( .43572E+04 )
    TUBES              .13E+01 ( .29E+01 ) 1332  .17819E+04 ( .39290E+04 )
    HINGES             .94E-01 ( .21E+00 ) 1332  .12500E+03 ( .27563E+03 )
    END FITTINGS, PINS .15E-01 ( .33E-01 ) 2664  .40031E+02 ( .88269E+02 )
    BEARINGS           .11E-01 ( .24E-01 ) 2664  .29163E+02 ( .64305E+02 )
   DIAGONALS           .21E+01 ( .47E+01 ) 1296  .27850E+04 ( .61409E+04 )
    TUBES              .21E+01 ( .46E+01 ) 1296  .26971E+04 ( .59472E+04 )
    END FITTINGS, PINS .20E-01 ( .43E-01 ) 2592  .50816E+02 ( .11205E+03 )
    BEARINGS           .14E-01 ( .31E-01 ) 2592  .37020E+02 ( .81629E+02 )
   LOWER SURFACE       .15E+01 ( .33E+01 ) 1224  .18505E+04 ( .40803E+04 )
    TUBES              .14E+01 ( .30E+01 ) 1224  .16720E+04 ( .36868E+04 )
    HINGES             .94E-01 ( .21E+00 ) 1224  .11487E+03 ( .25329E+03 )
    END FITTINGS, PINS .15E-01 ( .33E-01 ) 2448  .36785E+02 ( .81112E+02 )
    BEARINGS           .11E-01 ( .24E-01 ) 2448  .26799E+02 ( .59091E+02 )
  SPIDER ASSEMBLY      .11E+01 ( .24E+01 )  901  .96818E+03 ( .21348E+04 )
   UPPER SPIDER        .10E+01 ( .23E+01 )  469  .48961E+03 ( .10796E+04 )
   LOWER SPIDER        .10E+01 ( .23E+01 )  432  .45099E+03 ( .99442E+03 )
   STANDOFFS           .59E-01 ( .13E+00 )  469  .27584E+02 ( .60822E+02 )
  MESH INSTALLATION                            .54527E+03 ( .12023E+04 )
   MESH                                        .45439E+03 ( .10019E+04 )
   MESH CONTROL SYSTEM                         .90878E+02 ( .20039E+03 )
  CONTINGENCY                             0.          (0.           )
----------------------------------------------------------------------------
TOTAL WEIGHT                                   8125. (    17916. )
----------------------------------------------------------------------------
X-C.G. CENTIMETERS (INCHES)                    .18307E-08 ( .72076E-09 )
Y-C.G. CENTIMETERS (INCHES)                    .14252E-07 ( .56109E-08 )
Z-C.G. CENTIMETERS (INCHES)                    .11231E+03 ( .44218E+02 )
IXX KILOGRAM METER SQ. (SLUG FT2)              .53109E+07 ( .39141E+07 )
IYY KILOGRAM METER SQ. (SLUG FT2)              .53109E+07 ( .39141E+07 )
IZZ KILOGRAM METER SQ. (SLUG FT2)              .10517E+08 ( .77509E+07 )
IXZ KILOGRAM METER SQ. (SLUG FT2)              .10709E-06 ( .78929E-07 )
IXY KILOGRAM METER SQ. (SLUG FT2)              .21008E-07 ( .15483E-07 )
IZY KILOGRAM METER SQ. (SLUG FT2)             -.12868E-05 (-.94834E-06 )

MISCELLANEOUS GEOMETRY     UPPER SURFACE     DIAGONAL      LOWER SURFACE
STRUT DIAMETER CM (IN)      4.79 (  1.88 )  4.79 (  1.88 )  4.79 (  1.88 )
STRUT THICKNESS CM (IN)    .1170( .04606) .15270( .06012) .1170( .04606)
AVG. STRUT LENGTH M (IN)    4.62 (  182. )  4.84 (  190. )  4.71 (  186. )
HINGE LENGTH CM (IN)       48.2 (  19.0 )   0.0 (   0.0 )  48.2 (  19.0 )
MAX. STRUT LENGTH CM (IN)                    481.9 (      189.7 )
MESH AREA SQ METERS (SQ YDS)                 7974.0 (     9537.1 )
PACKAGE DIA. CM (IN) A, B          708.3 (  278.9 )   379.0 (  149.2 )
PACKAGE HEIGHT CM (IN) A, B        558.0 (  219.7 )  1050.5 (  413.6 )
CRITICAL LOAD (PCR) NEUTONS (POUNDS)         2563.8 (      576.4 )
```
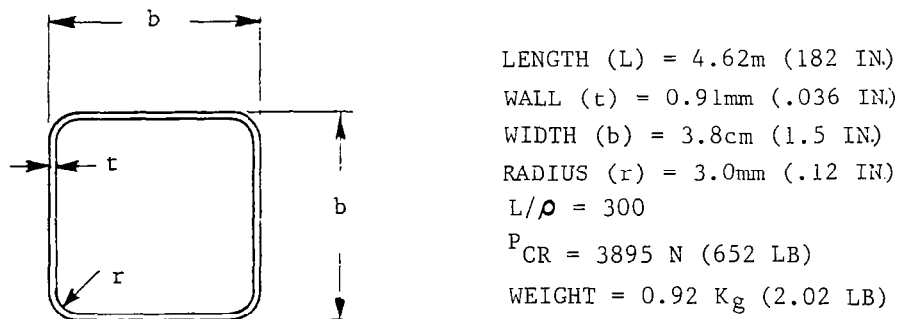
3-7

Table 3-2. Input Data (Metric and English Units) Fully Defines the
Mod-PETA (H) Reflector and its Structure

LASS PREPROCESSOR REAL MODEL INPUT ITEMS IN METRIC (S.I.) UNITS   INPUT DATA IN CONVENTIONAL (ENGLISH) UNITS

Metric Value	#	Name	Description	English Value	#	Name	Description
* 95.270	1	RFDM	-RADIO FREQUENCY DIAMETER (METERS)	* 312.56	23	RFD	-RADIO FREQUENCY DIAMETER (FEET)
* 1.0000	2	SHAPE	-SHAPE FLAG: 1=PARABOLA, 2=SPHERE, 3=FLAT	1.0000	19	ANP	-SHAPE FLAG: 1=PARABOLA, 2=SPHERE, 3=FLAT
* 1.0500	3	FOUERD	-FOCAL LENGTH TO RF DIAMETER RATIO	* 1.0500	17	FCN	-FOCAL LENGTH TO RF DIAMETER RATIO
24.000	4	NBAYS	-NUMBER OF BAYS IN REAL DISH STRUCTURE	24.000	18	ANBAYS	-ANALYSIS NUMBER OF BAYS
24.000	5	ANBAYS	-ANALYSIS NUMBER OF BAYS	56.838	21	AN	-DIAGONAL ANGLE TO SURFACE (DEGREES)
.99200	6	THETA	-DIAGONAL ANGLE TO SURFACE (RADIANS)	10.157	22	SOD	-MESH STAND-OFF DISTANCE (INCHES)
.25800	7	SODM	-MESH STAND-OFF DISTANCE (METERS)	3.0000	27	MF	-DISH MOUNTING FLAG: 0=APEX, 1=EDGE, 3=FREE
3.0000	8	MOUNTF	-DISH MOUNTING FLAG: 0=APEX, 1=EDGE, 3=FREE	0.	5	FLAG	-STRUT REMOVE FLAG: 0=NO, 1=NEW SET, 9=REPEAT
0.	9	REMOUF	-STRUT REMOVE FLAG: 0=NO, 1=NEW SET, 9=REPEAT	7.0000	20	NM	-NUMBER OF MODE SHAPES (0=NO SAP MODELS)
7.0000	10	NMODE	-NUMBER OF MODE SHAPES (0=NO SAP MODELS)	0.	28	XANAC	-X COORDINATE FOR ANGULAR ACCELERATION (INCHES)
0.	11	XANACM	-X COORDINATE FOR ANGULAR ACCELERATION (METERS)	0.	29	YANAC	-Y COORDINATE FOR ANGULAR ACCELERATION (INCHES)
0.	12	YANACM	-Y COORDINATE FOR ANGULAR ACCELERATION (METERS)	0.	30	ZANAC	-Z COORDINATE FOR ANGULAR ACCELERATION (INCHES)
0.	13	ZANACM	-Z COORDINATE FOR ANGULAR ACCELERATION (METERS)	0.	39	TUBES	-STRUT TYPE: 0=L/R, 1=EULER, 2=ISOG, 3=TRUSS
0.	14	TUBTYP	-STRUT TYPE: 0=L/R, 1=EULER, 2=ISOG, 3=TRUSS				
1.00000E+06	15	SLOR	-SURFACE STRUT LENGTH OVER RADIUS OF GYR RATIO	1.00000E+06	11	TRRS	-SURFACE STRUT LENGTH OVER RADIUS OF GYR RATIO
* 1.00000E+06	16	SDOT	-SURFACE STRUT DIAMETER OVER THICKNESS RATIO	1.00000E+06	13	TTRS	-SURFACE STRUT DIAMETER OVER THICKNESS RATIO
* 1.54620E+11	17	SSYRM	-SURFACE STRUT YOUNGS MODULUS (NEWTONS/SQUARE METER)	* 2.24200E+07	25	SSM	-SURFACE STRUT YOUNGS MODULUS (POUNDS/SQUARE INCH)
* 4.78600E-02	18	SMINDM	-SURFACE STRUT MINIMUM DIAMETER (METERS)	* 1.8842	33	DMINS	-SURFACE STRUT MINIMUM DIAMETER (INCHES)
* 1.17000E-03	19	SMINTM	-SURFACE STRUT MINIMUM THICKNESS (METERS)	* 4.60630E-02	34	TMINS	-SURFACE STRUT MINIMUM THICKNESS (INCHES)
1.0000	20	SPCRM	-SURFACE STRUT EULER LOAD FOR DESIGN (NEWTONS)	.22482	41	PCR	-SURFACE STRUT EULER LOAD FOR DESIGN (POUNDS)
.50000	21	SHAR	-SURFACE STRUT HINGE AREA RATIO	.50000	8	SPLAR	-SURFACE STRUT HINGE AREA RATIO
.10000	22	SHLR	-SURFACE STRUT HINGE LENGTH RATIO	.10000	9	HLR	-SURFACE STRUT HINGE LENGTH RATIO
1.11700E+11	23	SHMOD	-SURFACE STRUT HINGE MODULUS OR TRUSS LACE MODULUS	1.61970E+07	24	HM	-SURFACE STRUT HINGE MODULUS OR TRUSS LACE MODULUS
1.00000E+06	24	DLOR	-DIAGONAL STRUT LENGTH OVER RADIUS OF GYR RATIO	1.00000E+06	12	TRRD	-DIAGONAL STRUT LENGTH OVER RADIUS OF GYR RATIO
1.00000E+06	25	DDOT	-DIAGONAL STRUT DIAMETER OVER THICKNESS RATIO	1.00000E+06	14	TTRD	-DIAGONAL STRUT DIAMETER OVER THICKNESS RATIO
* 1.31350E+11	26	DSYRM	-DIAGONAL STRUT YOUNGS MODULUS (NEWTONS/SQUARE METER)	* 1.90460E+07	26	DSM	-DIAGONAL STRUT YOUNGS MODULUS (POUNDS/SQUARE INCH)
* 4.78600E-02	27	DMINDM	-DIAGONAL STRUT MINIMUM DIAMETER (METERS)	* 1.8842	32	DMIND	-DIAGONAL STRUT MINIMUM DIAMETER (INCHES)
1.52700E-03	28	DMINTM	-DIAGONAL STRUT MINIMUM THICKNESS (METERS)	6.01180E-02	35	TMIND	-DIAGONAL STRUT MINIMUM THICKNESS (INCHES)
1.0000	29	DPCRM	-DIAGONAL STRUT EULER LOAD FOR DESIGN (NEWTONS)	.22482	43	DPCR	-DIAGONAL STRUT EULER LOAD FOR DESIGN (POUNDS)
0.	30	DIFROD	-DIAGONAL STRUT PIN-ENDED (ROD) FLAG: 0=BEAM, 1=ROD	0.	40	FROD	-DIAGONAL STRUT PIN-ENDED (ROD) FLAG: 0=BEAM, 1=ROD
3.03380E+10	31	DSSM	-DIAGONAL STRUT SHEAR MODULUS (N/M**2) USED IF DIFROD=0.	4.39900E+06	38	GSM	-DIAGONAL STRUT SHEAR MODULUS (PSI) USED IF FROD=0.
1836.0	32	SRHO	-SURFACE STRUT DENSITY (KILOGRAMS/CUBIC METER)	6.63290E-02	1	RHOT	-SURFACE STRUT DENSITY (POUNDS/CUBIC INCH)
5.81000E-03	33	SSBRW	-SURFACE STRUT BEARING REFERENCE WEIGHT (KILOGRAMS)	1.28110E-02	2	UBST	-SURFACE STRUT BEARING REFERENCE WEIGHT (POUNDS)
5.81000E-03	34	SEFRW	-SURFACE STRUT END FITTING REFERENCE WEIGHT (KILOGRAMS)	1.28110E-02	36	USE	-SURFACE STRUT END FITTING REFERERENCE WEIGHT (POUNDS)
4429.0	35	SHLACE	-SURFACE STRUT HINGE OR LACE DENSITY (KILOGRAMS/METER**3)	.16001	7	SPLR	-SURFACE STRUT HINGE OR LACE DENSITY (POUNDS/CUBIC INCH)
1874.0	36	DRHOM	-DIAGONAL STRUT DENSITY (KILOGRAMS/CUBIC METER)	6.77030E-02	44	DRHOT	-DIAGONAL STRUT DENSITY (POUNDS/CUBIC INCH)
7.58000E-03	37	DSBRW	-DIAGONAL STRUT BEARING REFERENCE WEIGHT (KILOGRAMS)	1.67140E-02	3	UBDT	-DIAGONAL STRUT BEARING REFERENCE WEIGHT (POUNDS)
7.58000E-03	38	DEFRW	-DIAGONAL STRUT END FITTING REFERENCE WEIGHT (KILOGRAMS)	1.67140E-02	37	UDE	-DIAGONAL STRUT END FITTING REFERENCE WEIGHT (POUNDS)
4429.0	39	DLACE	-DIAGONAL STRUT TRUSS LACING DENSITY (KILOGRAMS/METER**3)	6.10720E-02	4	UUSTO	-UNIT WEIGHT OF STAND-OFF (POUNDS/FOUR INCHES)
2.28000E-02	40	UUSTOM	-UNIT WEIGHT OF STAND-OFF (.1 METERS LONG) (KILOGRAMS)	1.4774	10	SRW	-SPIDER REFERENCE WEIGHT (POUNDS)
.67000	41	SRWM	-SPIDER REFERENCE WEIGHT (KILOGRAMS)	1.6809	15	UUMSY	-UNIT WEIGHT OF MESH (OUNCES/SQUARE YARD)
5.70000E-02	42	UUMESH	-UNIT WEIGHT OF MESH (KILOGRAMS/SQUARE METER)	1.2000	16	UUMCSR	-MESH SYSTEM TO MESH ONLY WEIGHT RATIO
1.2000	43	UUMCSR	-MESH SYSTEM TO MESH ONLY WEIGHT RATIO	0.	6	CONTPR	-WEIGHT CONTINGENCY (ALL WEIGHT=(1+CONTPR))
0.	44	UTCONT	-WEIGHT CONTINGENCY (ALL WEIGHT=(1+UTCONT))	0.	42	ANSM	-MESH ON BACK FLAG: (=1, ONLY IF FLAT) 0=FRONT
0.	45	MESHBK	-MESH ON BACK FLAG: (=1, ONLY IF FLAT) 0=FRONT	1.0000	31	RRATIO	-RATIO OF REAL TO ANALOGOUS MODEL NUMBER OF BAYS

*Modified to compensate for geometry aberration; does not correspond to actual parameter.
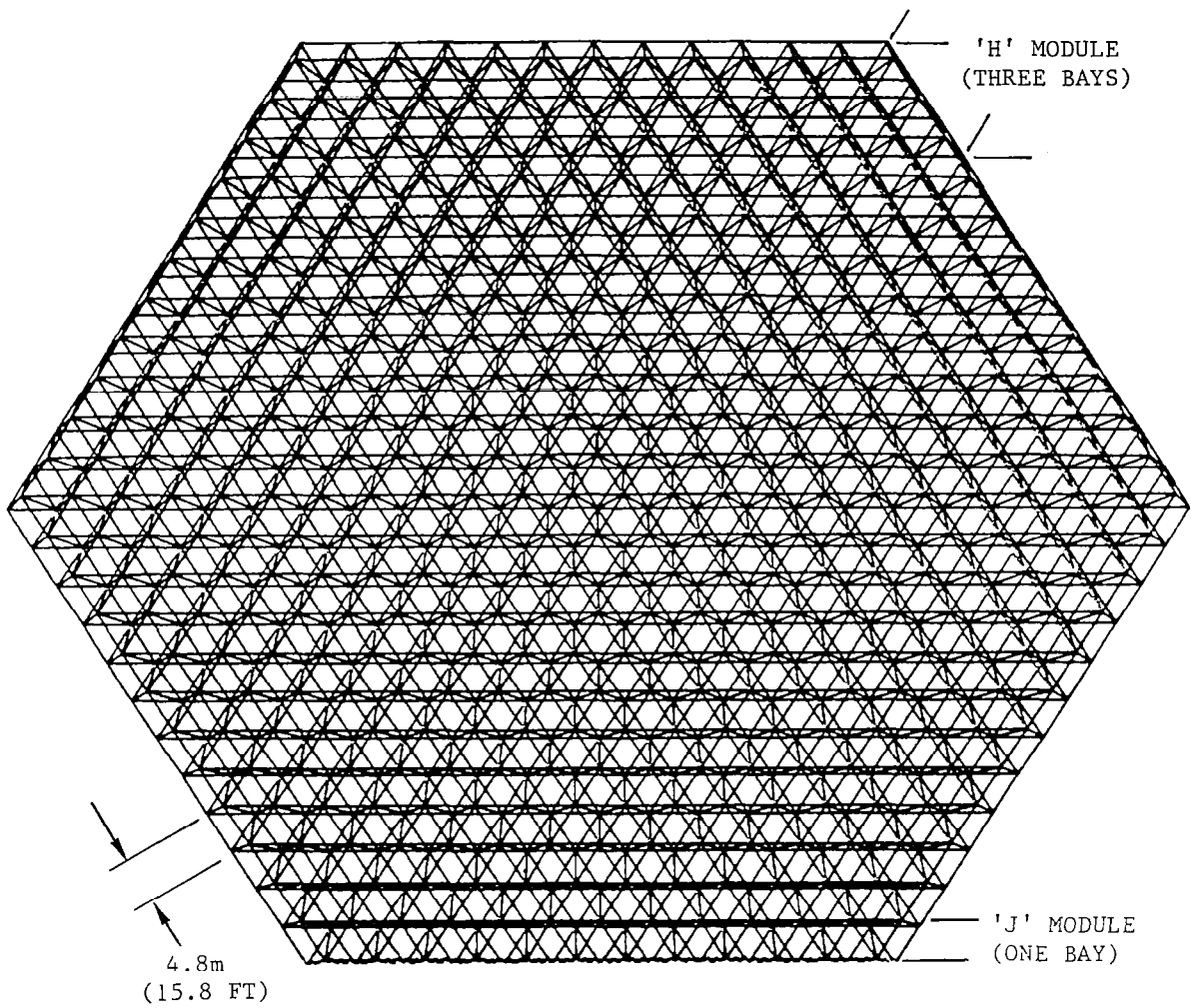
Figure 3-9. Mod-PETA Study Case H Geometry Viewed on Z Axis

3.1.4 METHODOLOGY, AND PROVISIONS FOR CONSTRUCTION OF THE REFLECTOR BY DISPENSING, DEPLOYING, AND JOINING PETA MODULES (STUDY CASE H).

As with the DCM concept studies it is assumed that 10% of the Orbiter payload bay length is reserved for support equipment, leaving 16.46m (54 ft) available for stowage of the packaged reflector. Thus, the PETA reflector structure described above stows in clusters, with 24 modules per cluster as shown in Figure 3-10. This arrangement permits three clusters to be accommodated within a single payload. A second flight is required for the fourth cluster. Total stowage space required, therefore, is equivalent to 1.3 payload bays.

It is conceivable that all four clusters can be accommodated in one payload (Study Case H-1, Figure 3-11) by shortening each packaged module to 4.1m (162 in.) While such shortening is feasible it must be considered that this results in corresponding reduction of deployed structural depth, structural stability (dynamic and thermal), surface shape accuracy and, therefore, potential RF capability.

Figure 3-11 presents three typical cases, Study Cases H-1, H-2, and H-3, to illustrate the relationship between payload volume (length) and deployed structural depth for a 100 meter structure. It will be noted that reducing structural depth also results in a significant increase in component part count, due to corresponding increase in the number of structural bays.

To facilitate comparison the general characteristics of these three cases are listed in Table 3-3. It is seen that Orbiter flights required are 1, 2, and 4, respectively.

As described above, the Mod-PETA reflector, Study Case H, consists of 48 female modules and 48 male modules, 96 total. They are stowed in a cradle in identical packages, 24 per package, occupying the full diameter of the Orbiter payload bay (Figure 3-10).

As shown in Figure 3-12 the clusters of modules are restrained in their stored locations by circumferential straps (two per cluster) that compact the aligned nodal fittings of the modules against support cradle interfaces. The module nodal fittings have interlocking profiles that provide restraint in the fore and aft directions.

The cradle also extends into the foremost 10% of the payload bay to support the manipulator unit, which consists of two manipulator arms and associated support equipment. Each arm is provided with a grappling device at its end that permits attachment to the center nodal fitting at the near end of each packaged module. The manipulators dispense the modules by lifting them one-by-one from their stowed locations and moving them outside the Orbiter for deployment. When all 24 modules of the first package have been expended, the manipulator unit travels approximately 4 meters (13 feet) aft, on a wheel/track system installed in the cradle, and proceeds to unload the second package — and so on to the third cluster until all modules have been removed, deployed, and added to the evolving structure.
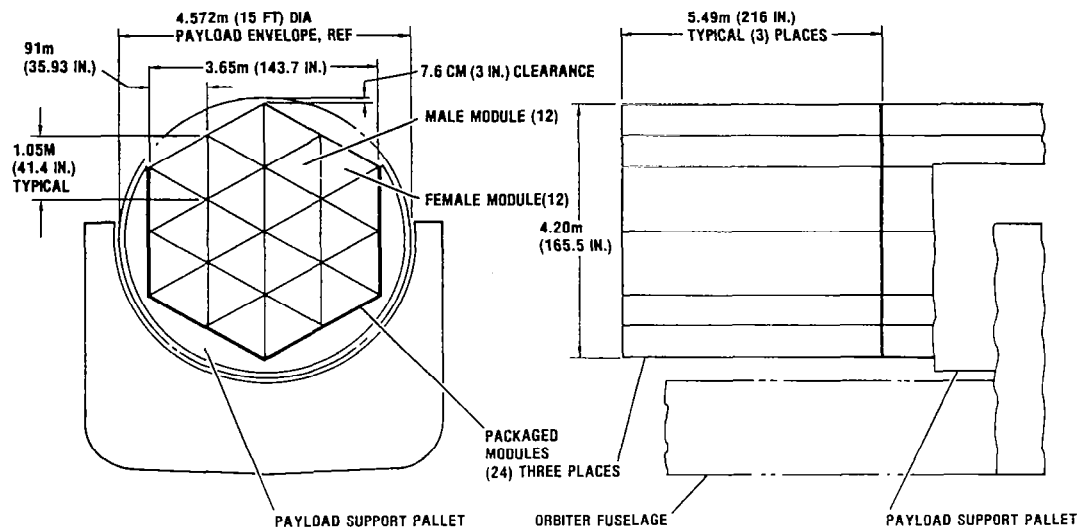
Figure 3-10. Orbiter Payload Bay Diameter Accommodates 24 Packaged
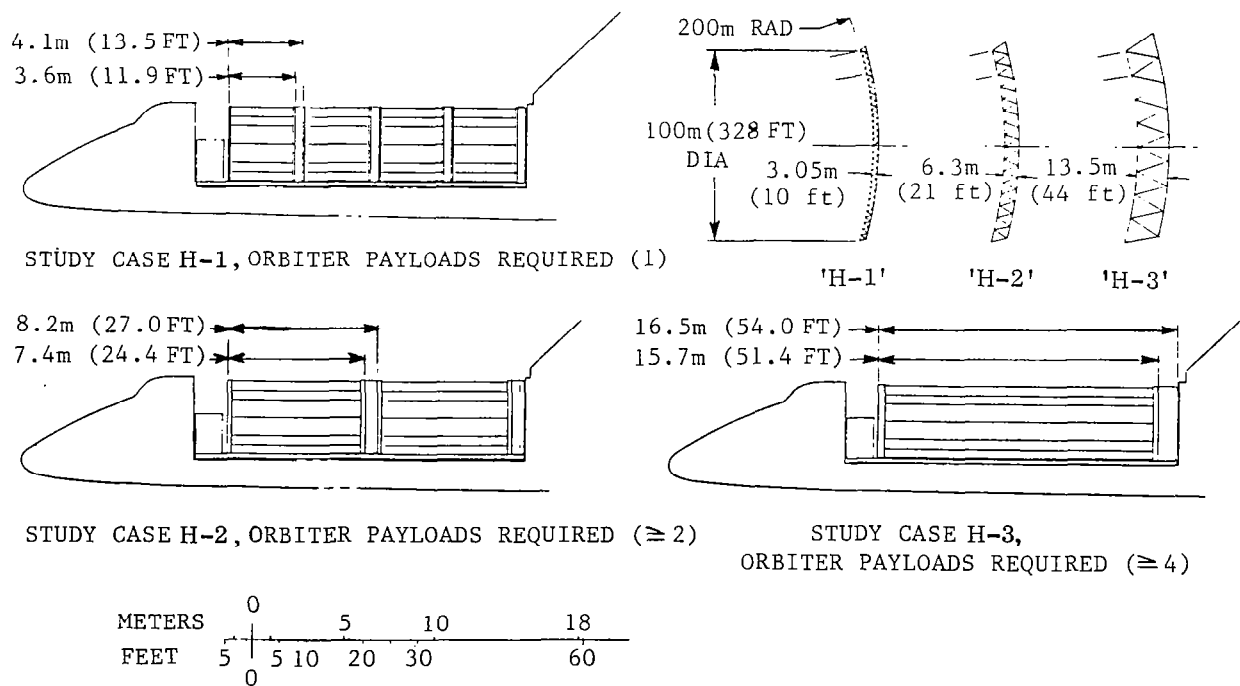Modules Stacked as Shown (Mod-PETA, Study Case H)

Figure 3-11. Stowed Configurations Mod-PETA Concept, Study
Cases H-1, H-2 and H-3

Table 3-3. Analysis of Modularized PETA

Study Case Definition	H-1	H-2	H-3
RF Diameter, meters (ft)	100 (328)	100 (238)	100 (238)
Focal Length/RF Diameter	1.0	1.0	1.0
Number of Bays Across Flats	32	16	8
Structural Bays per Module	4	2	1
Total Number of Modules	96	96	96
Structural Depth, meters (ft)	3.06 (10.0)	6.29 (20.6)	12.95 (42.5)
Strut Length (L)/Radius of Gyration (ρ)	286	286	286
Tubular Element Wall Thickness, mm (in.)	0.914 (0.036)	1.83 (0.072)	3.66 (0.144)
Outputs from Analysis			
Total Mass, kilograms (lb)	7150 (15,766)	-----	------
Average 'Concave' Strut Length, meters (ft)	3.47 (11.42)	6.9 (22.8)	13.8 (45.9)
Average 'Convex' Strut Length, meters (ft)	3.52 (11.50)	7.0 (23.0)	14.1 (46.0)
Diagonal Length, meters (ft)	3.64 (11.9)	7.4 (24.4)	15.7 (51.4)
Overall Package Height, meters (ft)	4.12 (13.5)	8.2 (27.0)	16.5 (54.0)
Surface Strut Critical Load, newtons (lb)	2312 (520)	... -- .	--------
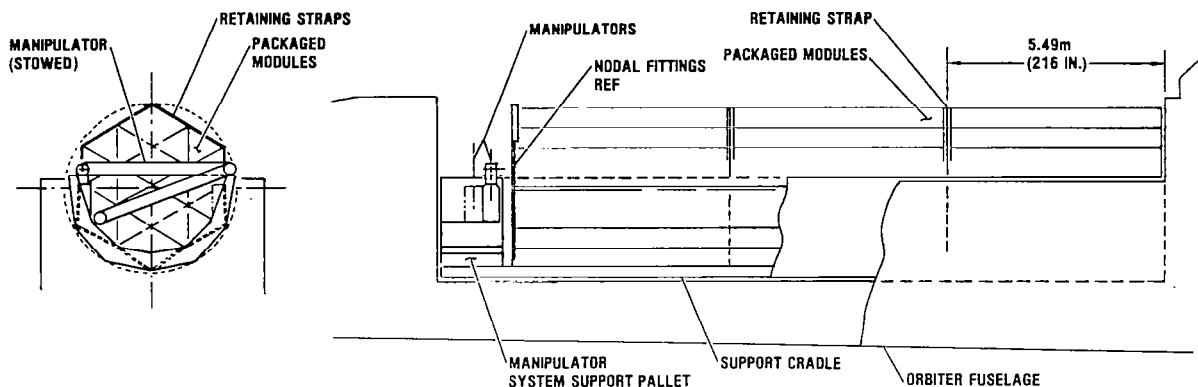
Figure 3-12. Orbiter Payload Bay Accommodates Three of the Four
Stacks of Packaged Modules plus Support Equipment
(Mod-PETA, Study Case H)

It is typical of the PETA structure that elastic energy can be stored in the sur-
face member mid-span joints during the folding (packaging) phase. This energy
provides the modules with self-energized deployment capability. To effect deploy-
ment it is therefore necessary only to release the lanyards that restrain the
structure in its packaged configuration. This is accomplished by firing a pyro-
technic to sever the lanyards. To ensure that the deploying structure adequately
clears the Orbiter the manipulator is extended to maximum reach and the module
held at optimum attitude, as shown in Figure 3-13. When the second module is
deployed, the selected deployment position and attitude has also to consider the
presence of the already deployed module No. 1 (Figure 3-14).

Typical structural detail of a Study Case H (male) module is shown in Figure
3-5, above.

The initial stage of modular construction of the reflector is shown in Figure
3-15, where each manipulator has dispensed and deployed a module. The manipu-
lator attaches to the center node point on the back side of the male modules and
to a near center node in the case of the female modules. The shoulder, elbow,
and wrist joints of the manipulators are now used to bring the two modules into
approximate attitude and alignment for joining. The standard RMS is used to
support structural joining at the mating node fittings. It does this by means of
a special mechanical effector mounted at its tip. It operates from the convex
side of the reflector and mechanically joins each pair of matching node fittings,
in turn, at both the convex and concave structural faces. It performs this task
by first securing the two nodal fittings to be joined and then moving them into
proper relative alignment for joining, within 1.0 cm (0.39 inch) of their final,
locked location. (Note: It is assumed that the two principal manipulators de-
scribed above will be limited in their ability to precisely relate the two separated
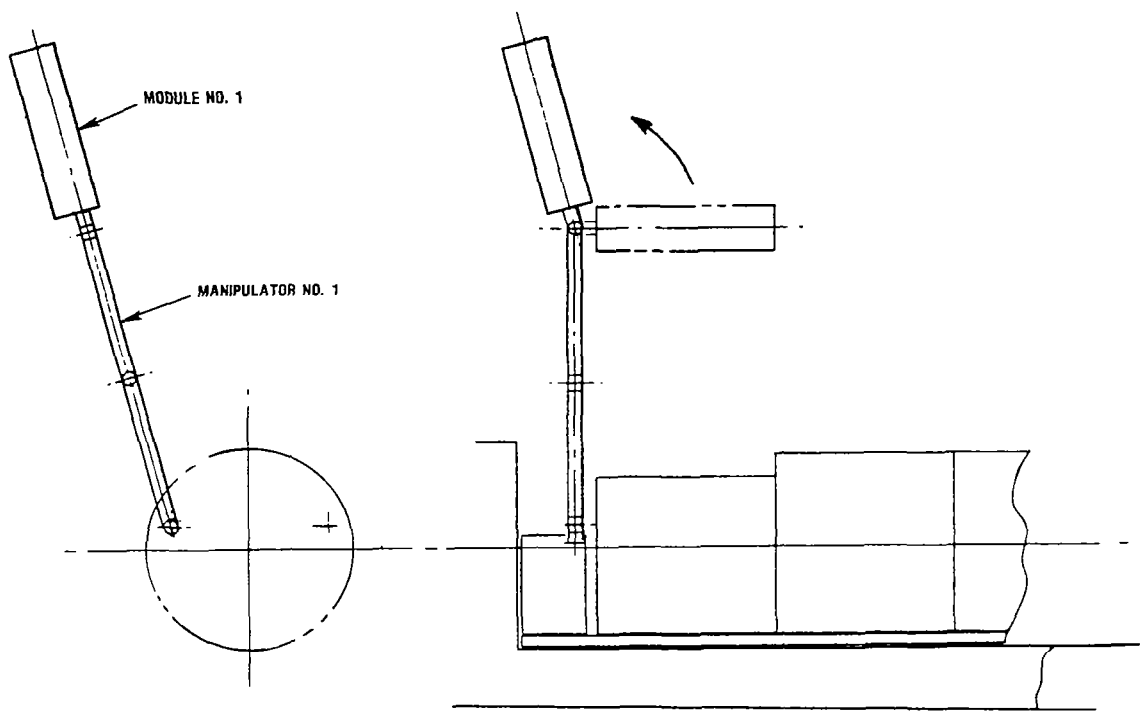structures and that the initial alignment error will be at least 5.0 cm.)

3-13

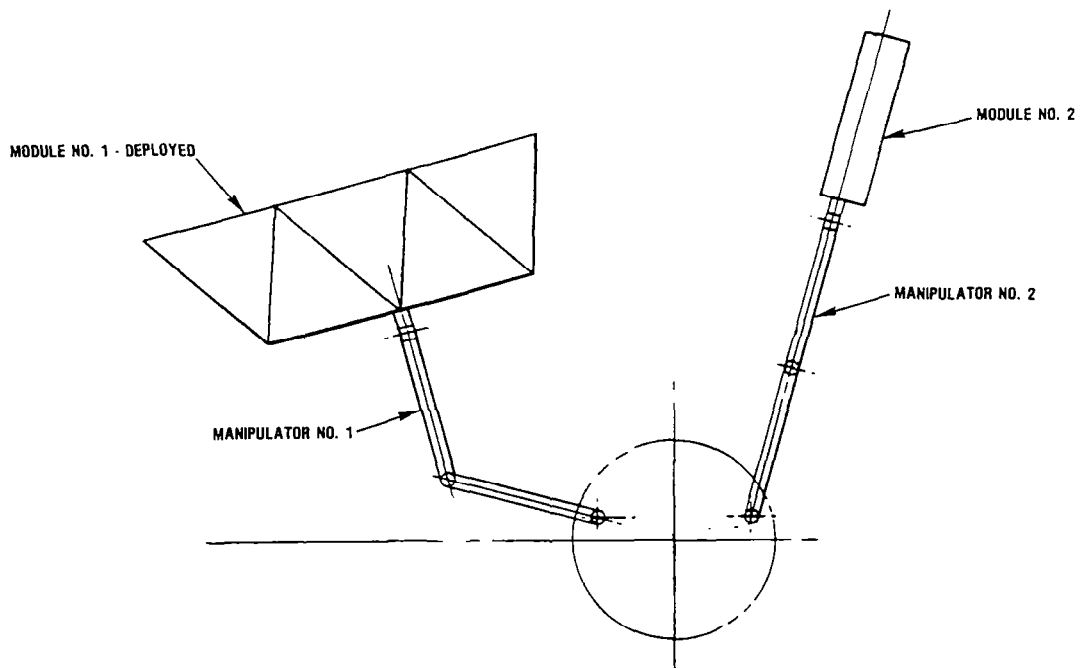Figure 3-13. Manipulator No. 1 Moves Packaged Module out of Payload Bay

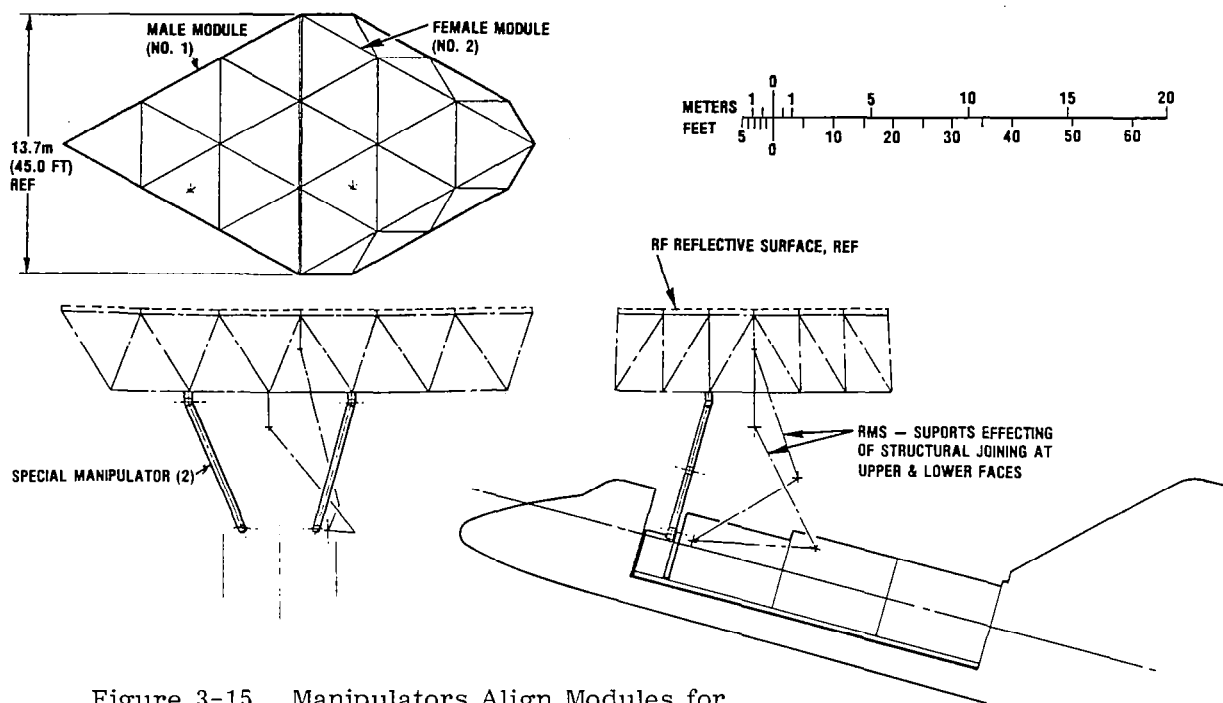Figure 3-14. Module No. 1 Deploys; Manipulator No. 2 Moves Packaged Module No. 2 out of Payload Bay

Figure 3-15. Manipulators Align Modules for Mating; RMS Joins Structural Node Fittings

With alignment and positioning accomplished the mechanical effector now actuates the locking device, which pulls the nodes into firm engagement and effects the structural joint.

Figure 3-16 shows the progressive assembly of the first six modules. Figures 3-16A and B correspond to Figures 3-13 and 3-14, respectively. It is seen that the two manipulators alternate in their functions. While one is disconnected from the structure and reaching back into the Orbiter for the next module, the other is rotating the structure in preparation for the addition of the next module. In Figure 3-16 six modules have been joined forming a hexagonal structure 27 meters (88 feet) in size. This represents only one-sixteenth of the payload in the Orbiter bay. The remaining 90 modules are assembled, as shown in Figure 3-17 sequence H through L, to produce the full 108 meter (354 foot) structure. Note that in Figure 3-16 the structure is assumed to be rotating relative to a fixed Orbiter, while in Figure 3-17 the opposite assumption is made.
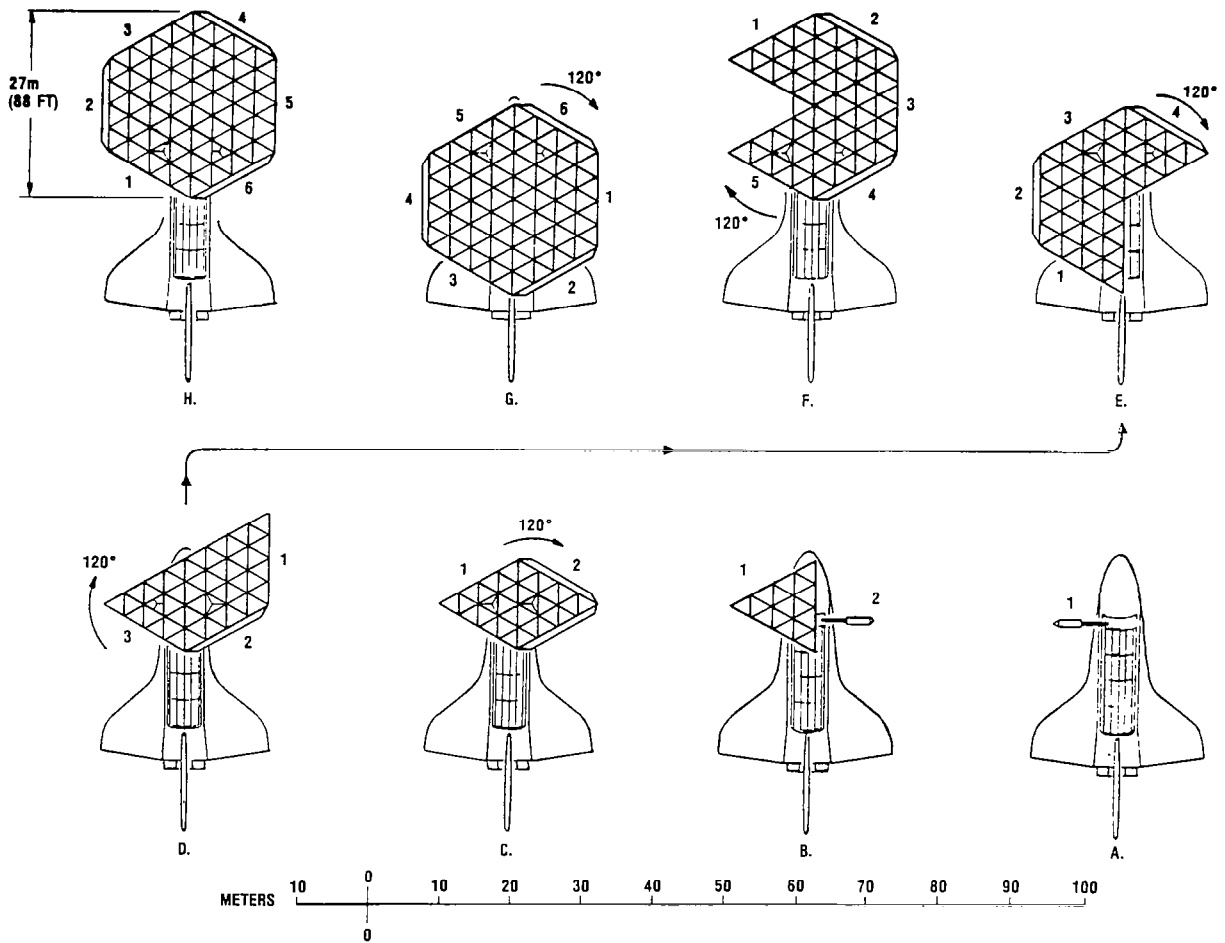
Figure 3-16. Initial Assembly Stages Require Intermittent Rotation of Assembly as Each Module is Joined, Mod-PETA, Study Case H
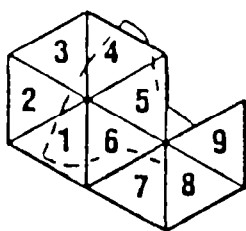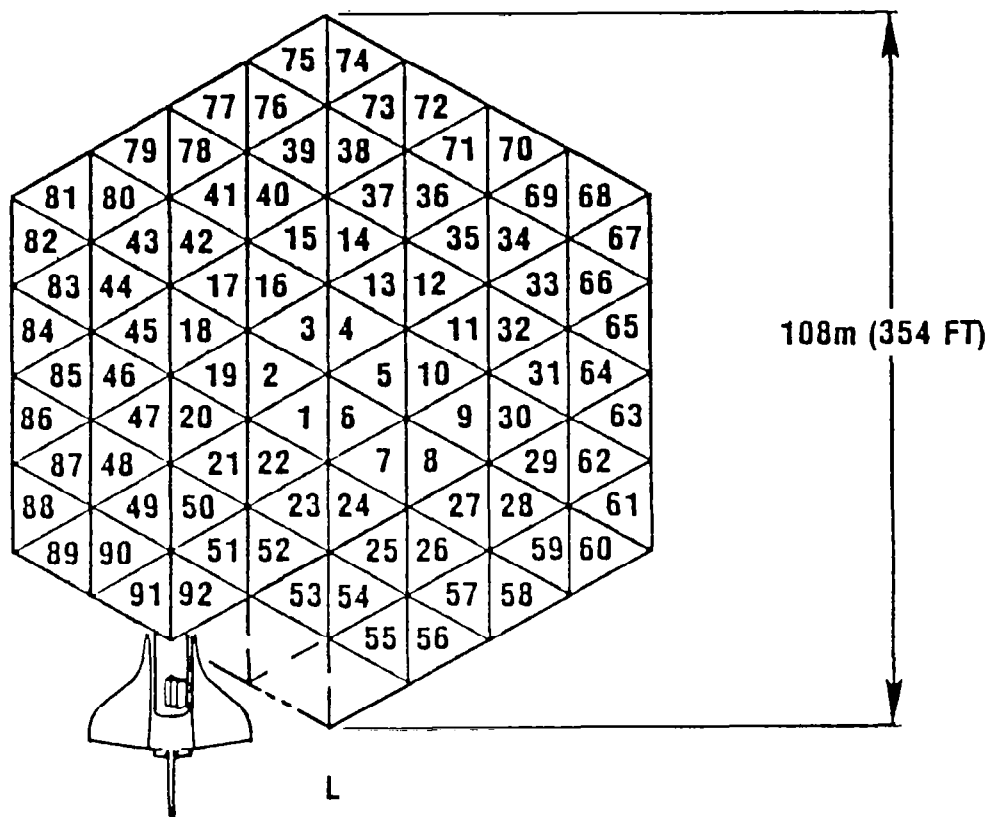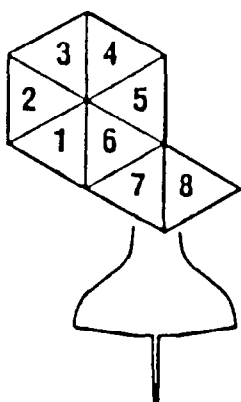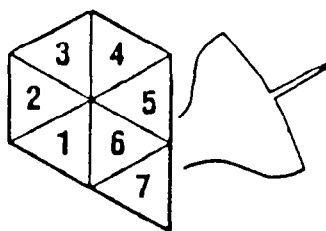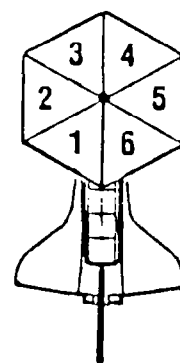
Figure 3-17. Manipulation Continues until all 96 Modules are Deployed and Attached

3.1.5 <u>AN ALTERNATIVE APPROACH TO MODULAR ASSEMBLY (STUDY CASE J)</u>.
This section presents a method of stowage and assembly of the PETA reflector
that differs from the method presented in Section 3.1.4.

The significant features of this alternative method, Study Case J, presented
below, are:

a. The basic mode of modular subdivision is shown in Figure 3-4(B), i.e.,
high aspect ratio beams joined in parallel.

b. Forty-eight flat modules are stacked in four hexagonal packages occupy-
ing two Orbiter payload bays.

c. All module handling, deployment and joining is performed immediately
above the Orbiter payload bay by articulated handling and joining
mechanisms (HJM) mounted immediately forward of each module package.

d. The two HJMs perform the following functions:

   1. Removal of individual modules from stowed stack to location outside
   payload bay.

   2. Support of individual modules during deployment.

   3. Alignment and positioning of adjacent modules for joining and
   lateral translation as joining proceeds.

   4. Effecting the structural joining (latching) of individual interface
   node points.

   5. Supporting the evolving structure as modules are added one by one.

The initial Orbiter flight produces one-half of the reflector. The second flight
produces the second half. Integration of the two halves is a final function per-
formed by the second flight, or integration can be performed concurrently with
assembly of the second half.

Figure 3-18 shows the stowed arrangement typical for both flights, except the
modules carried by the second flight are of the opposite hand (1B through 24B).

In Figure 3-19 the initial stages of erection are shown. The forward HJM is seen
to have engaged module 1A preparatory to removing it from the payload bay.
The aft HJM has already removed module 2A and has positioned it ready for
deployment. In the right-hand view of Figure 3-19 this module is shown sup-
ported vertically on six finger probes. (The other six finger probes, shown
clustered at the left-hand end of the deployment guide rail, are unused for this,
shorter module.)

Figure 3-20 illustrates the first increment of deployment of the module. This
step repeats, bay-by-bay (see Figure 3-21), until the fully deployed module
extends in cantilever fashion, from the guide rail. The left-hand view of
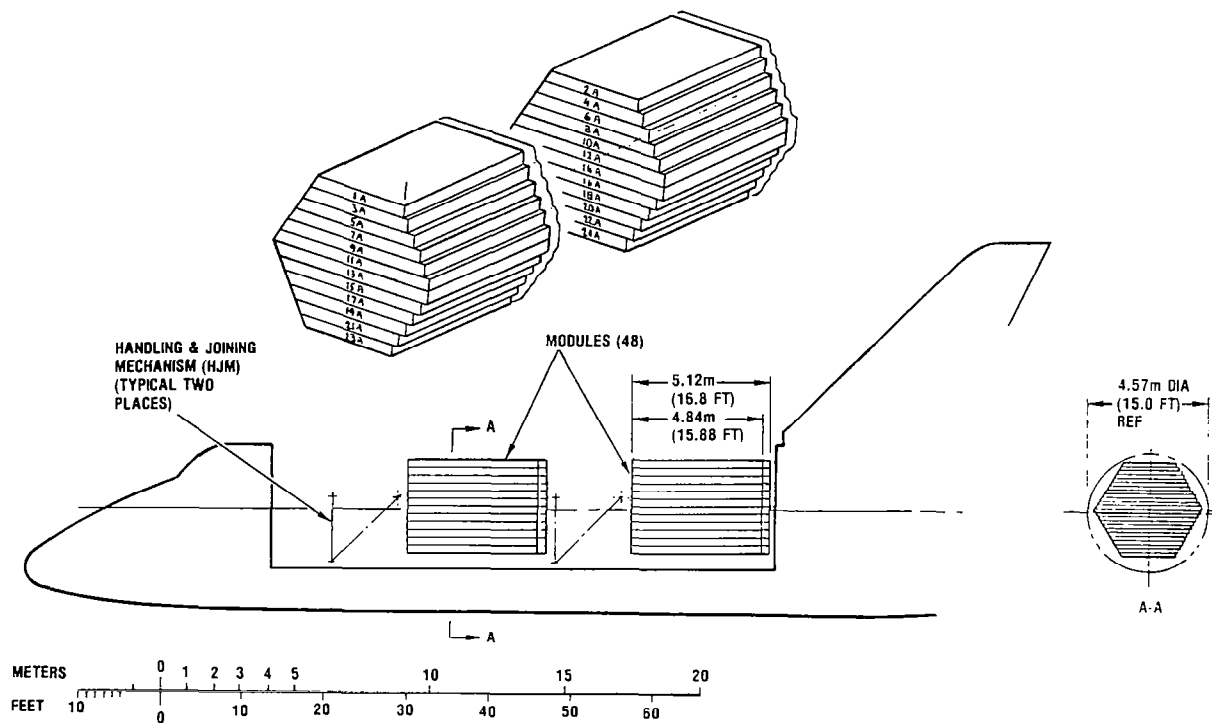Figure 3-20 shows the deployed section shape of the module.

Figure 3-18. Stowed Arrangement of Stacked Modules and Handling
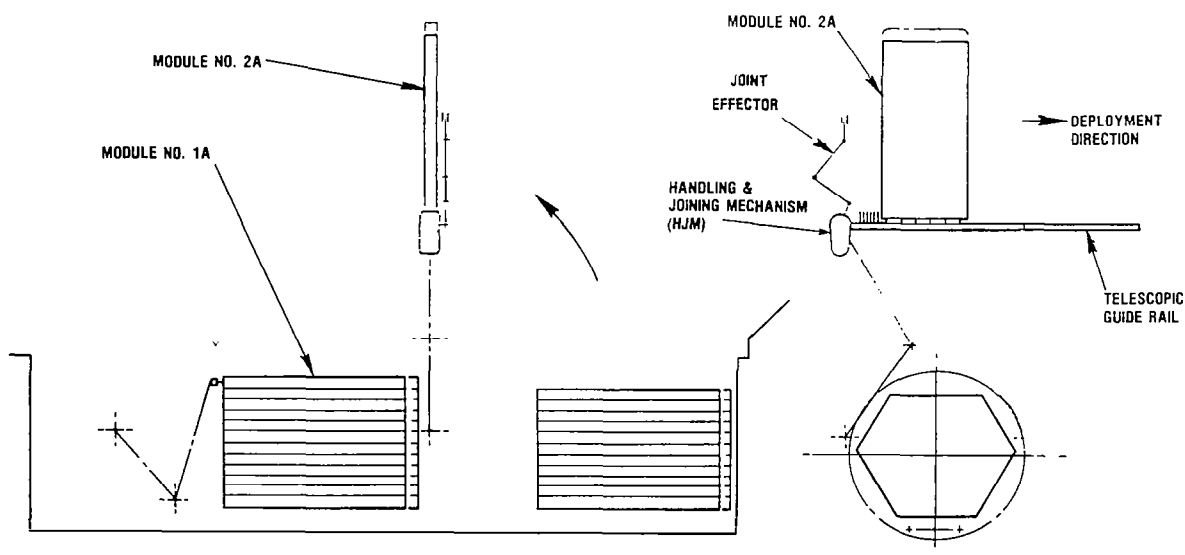Equipment (Typical for Both Flights), Mod-PETA, Study Case J

Figure 3-19. HJMs Remove Modules from Payload Bay and Erect Them
Preparatory to Deployment, Mod-PETA, Study Case J
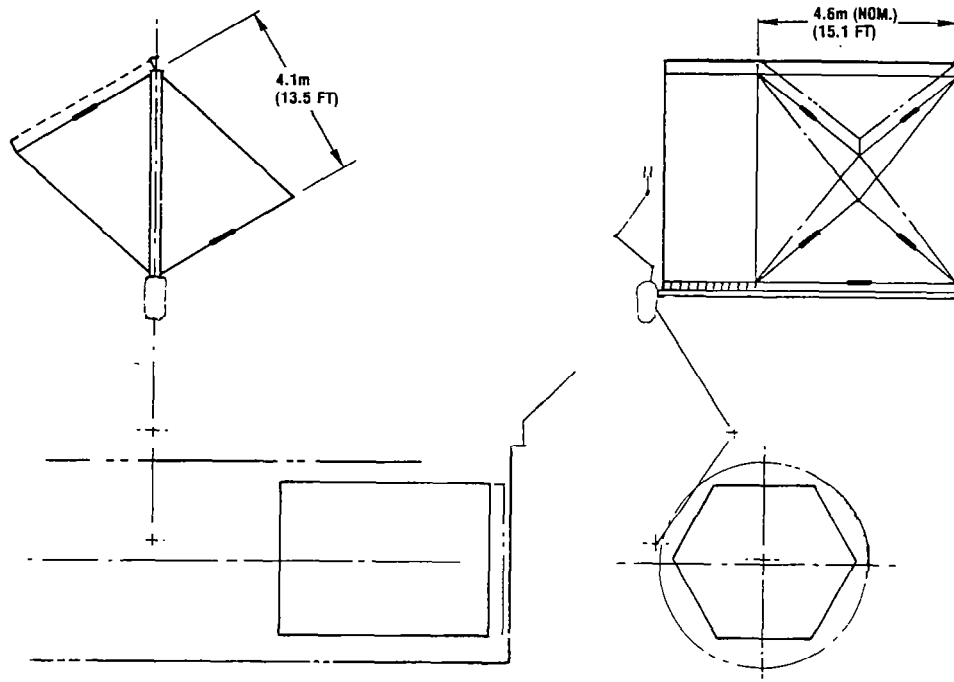
3-19

Figure 3-20. Module Deploys in Two Steps: First Expanding to Diamond Shape, then Incrementally Extending Bay-by-Bay, Mod-PETA, Study Case J
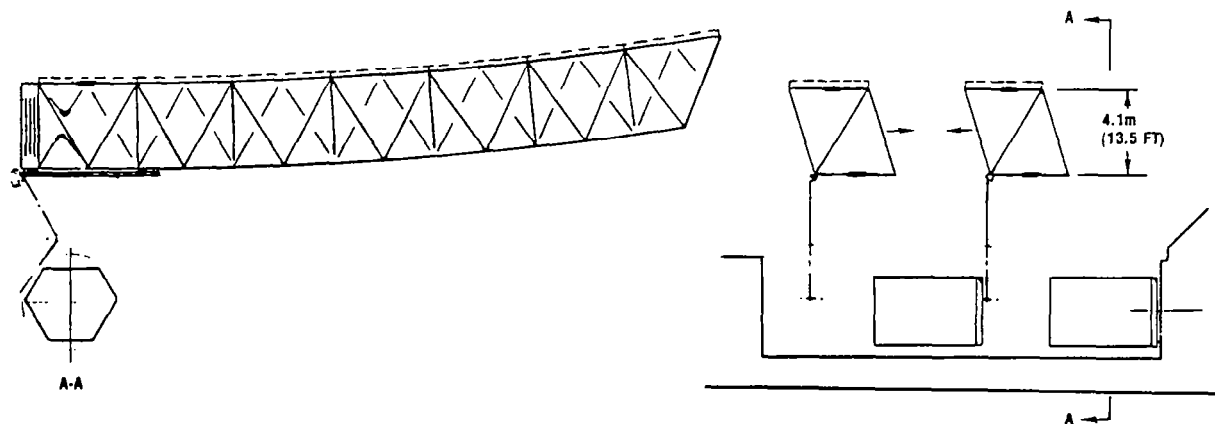

Figure 3-21. First Two Modules are Deployed Individually, then Moved Together for Joining, Mod-PETA, Study Case J

As shown in Figure 3-22, the two deployed modules (1A and 2A) are rotated to a suitable orientation for joining (see Figure 3-23).
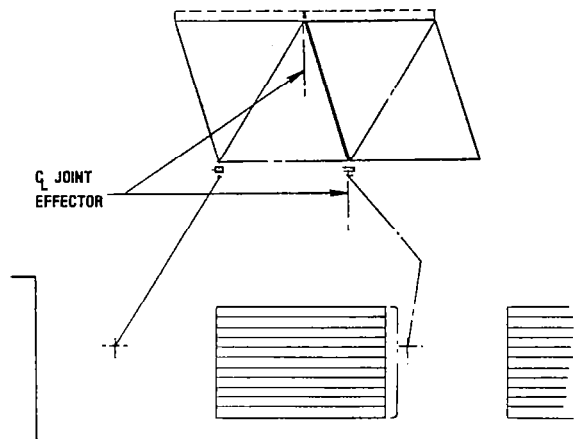

Figure 3-22. Mating Node Fittings are Joined by Effector Device
that Extends from Aft HJM, Mod-PETA, Study Case J

The aft HJM differs from the forward HJM in that it is provided with an effector subsystem capable of reaching both the lower and the upper node fittings of the interface and of performing the structural joining of the mating node fittings. This function is shown in Figure 3-15, as applied to the Mod-PETA 'H'.

Joining of all node fittings along the interface is accomplished by laterally translating the modules across the payload bay by hand-over-hand operation of the two HJMs. The third module is deployed in the opposite direction to the first two modules and the construction thus proceeds in a zig-zag mode as indicated in Figure 3-23 where the reflector is shown a little more than quarter complete. Thirteen modules have been deployed and joined, and the fourteenth is deployed and about to be joined. Note: This stage of construction is also illustrated in the frontispiece of this report. When twenty-four modules have been joined, the reflector is half complete and the initial payload is exhausted. The second flight assembles the other half of the reflector in similar fashion and integrates the two half structures.

This "beam" type module is not an entirely new concept. The same basic idea of "minimum" section tetrahedral truss has received in-depth study during the last two years under General Dynamics independent research and development (IRAD) programs. Figure 3-24 shows existing hardware built to demonstrate the fully controllable, step-by-step deployment capability of the beam. The sequence of views shows the progressive stages between the compact, stowed stage (that corresponds to Figure 3-19), and full, cantilevered deployment (that corresponds to Figure 3-21).
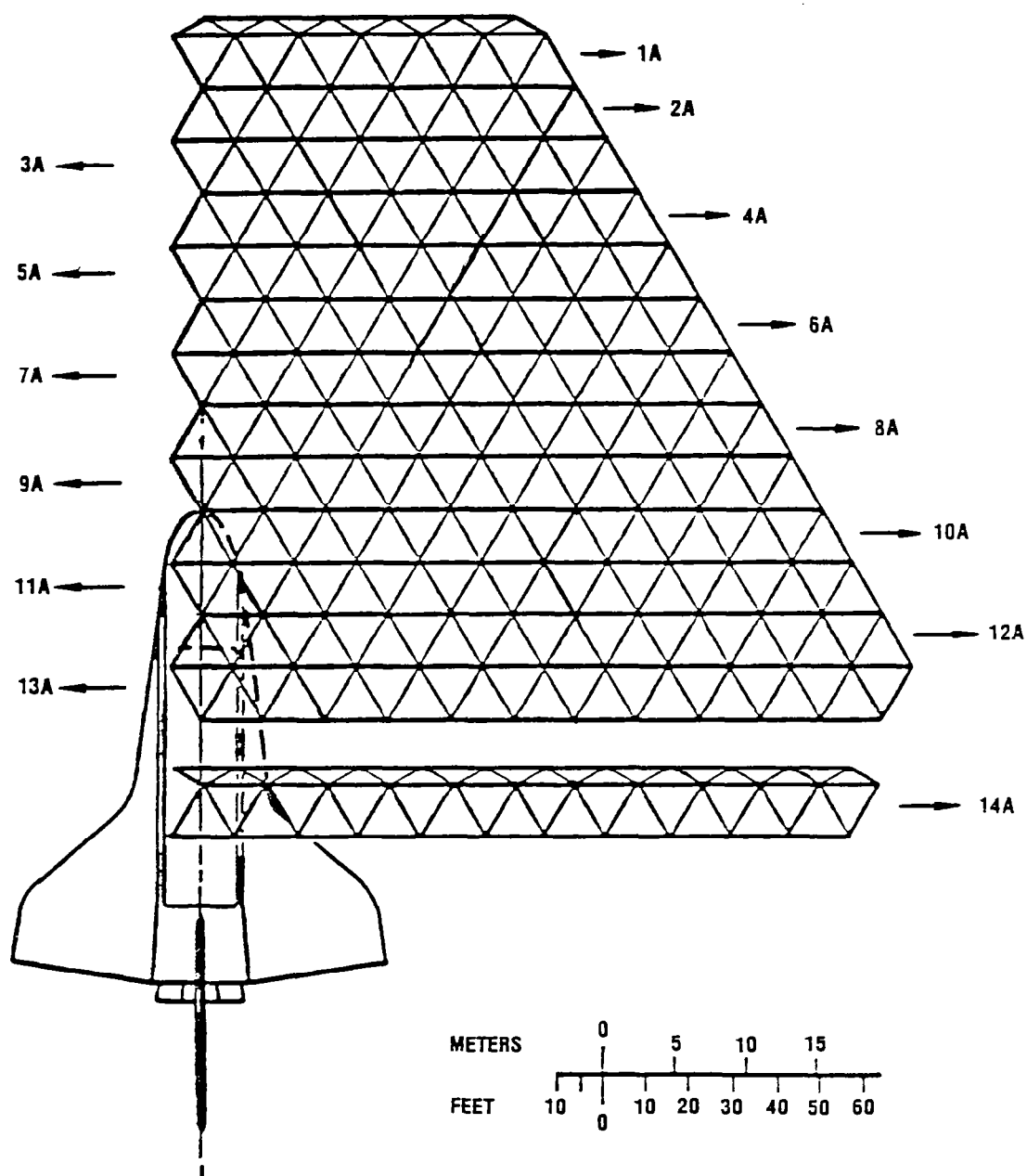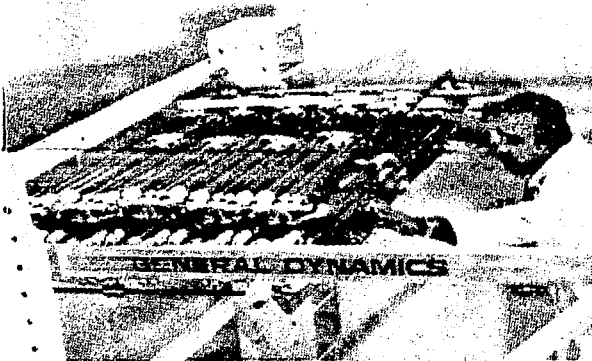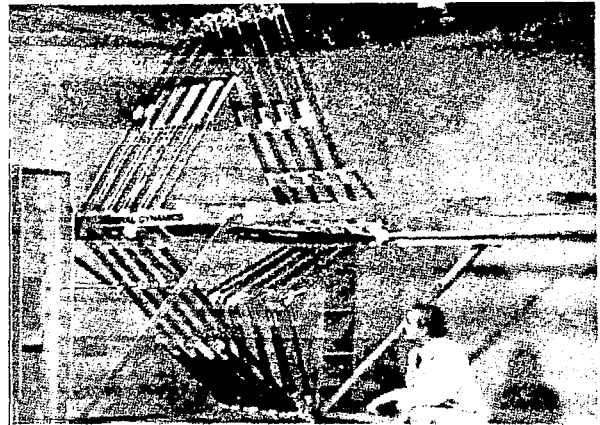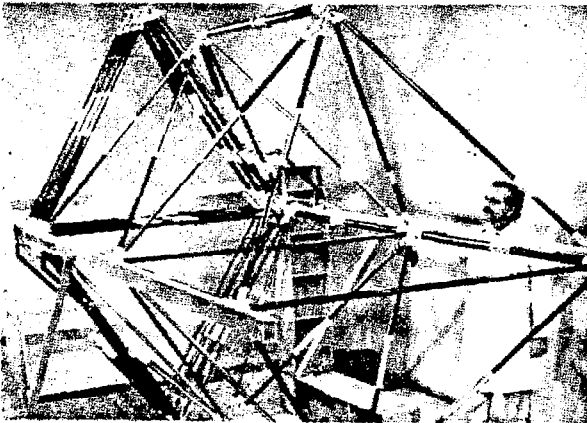
3-21

Figure 3-23. Half Reflector is Assembled by Deploying and Joining
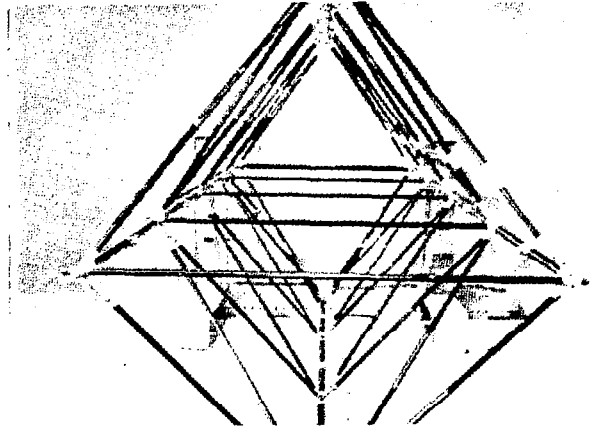Modules 1A through 24A, Mod-PETA, Study Case J

CVC800222
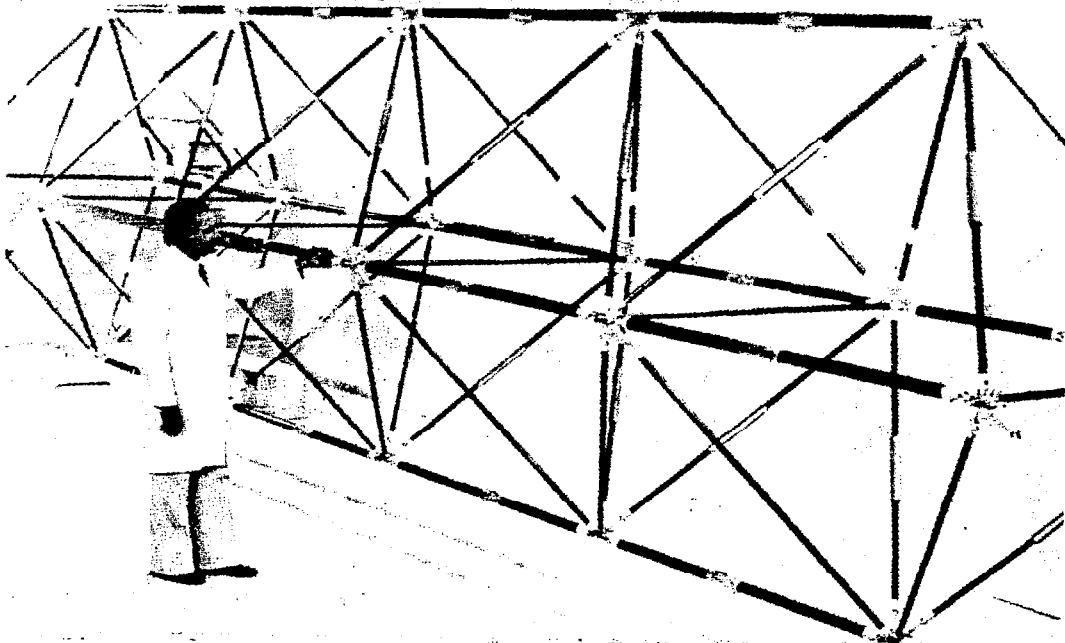
CVC800105

CVC800230

CVC800234

CVC800236

Figure 3-24. Stowed Beam Initially Expands Vertically, then Extends Horizontally in Bay-by-Bay Increments

3-23

3.1.6 ANALYSIS AND EVALUATION OF THE COMPLETED MOD-PETA REFLEC-
TOR. The modularized PETA reflector concept is basically equivalent to the
DCM in general structural application, but is significantly different in most other
respects. Within the limitations imposed by the Orbiter payload envelope, the
Mod-PETA concept has considerable design flexibility offering many sizing options.
The initial design step in sizing is to increase the structural bay size until the
flat facets of reflective mesh reach the budgeted limits of shape accuracy. In
Mod-PETA Study Cases H and J, this optimization enables reduction of bay
count across the total structure to 24 from the 31 minimum for the DCM.

The Mod-PETA structure can be packaged to a high degree of compactness with
all elements lying in parallel orientation. Number of Orbiter flights required to
enable construction of a 100 meter reflector varies between 1.0 and 4.0, depend-
ing upon selected structure depth and mode of modularization (H or J).

In Study Case H the 96 male and female modules are of triangular shape, and in
Study Case J the 48 modules are minimum width "planks." In both cases, struc-
tural duplication exists at the intermodular interfaces. Design development
could reduce the degree of duplication with attendant weight saving but in the
analyses presented in this study, full duplication is assumed at all modular
interfaces.

The deploying, handling, and joining methodology presented as Mod-PETA Study
Case J outlines a basic approach that incorporates deployment methodology already
developed for existing, deployable beam truss, demonstration hardware. Although
there appears to be no fundamental flaw in the overall sequence of operations
outlined, adequate assurance of feasibility requires greater depth of study with
attention to each of the successive steps.

Compared to the DCM, the modules and intermodular connection points are fewer.
However, the individual modules are larger and their deployment is a more com-
plex operation. Deployment of each Mod-PETA J module, therefore, may re-
quire a time period approaching two hours. A further two hours per module
could be required to effect the module-to-module interface joining. Total assem-
bly time could, therefore, approach 200 hours assuming all operations to be fully
automated.

The mode of modularization H or J does not significantly affect the structural
characteristics of the completed Mod-PETA structure, and the estimated data
presented in Figure 3-25 can be considered generally typical for large, hexa-
gonal, modular Mod-PETA reflectors and platforms.

Structural thermal stability is more than adequate for operation at 1 GHz, but
marginal at 15 GHz. Table 3-4 presents achievable overall shape accuracy (ex-
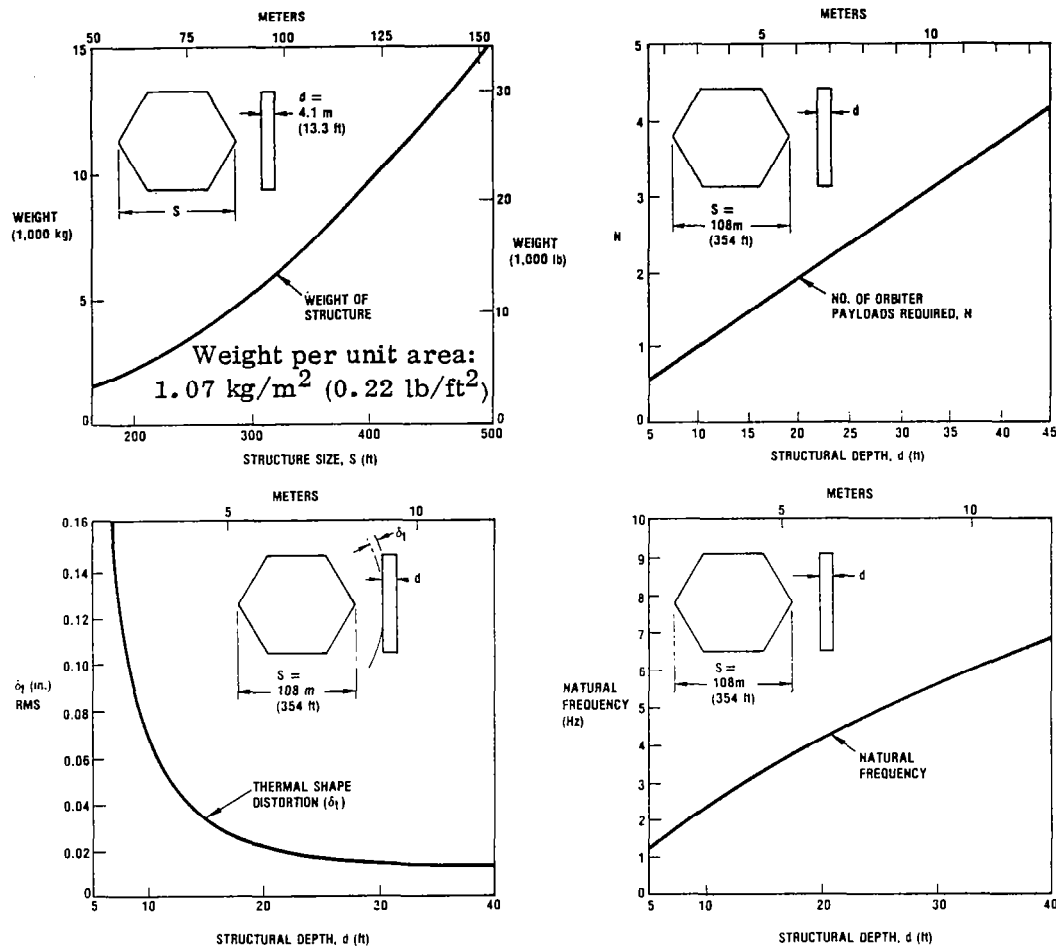cluding static loading which will vary according to mission).

Figure 3-25. The Mod-PETA Concept Provides Large Structures
of Outstanding Performance

3.1.6.1 Modeling. The LASS computer program (Section 2.6.1) was written specifically for analysis of the PETA tetrahedral truss, and is thus directly applicable to Mod-PETA analysis due to the basic geometric similarity. However, allowances are made for characteristics peculiar to modularization such as duplication of structural members. Also, certain additonal members exist at the periphery of the Mod-PETA reflector structure.

3.1.6.2 Thermal Distortion Analysis (Study Case H). The LASS computer program analysis of Mod-PETA Study Case H was performed per the input data presented above in Section 3.1.3, and for the thermal condition defined in Section 2.6.1.2. As for all candidate concepts, the selected structural material is graphite epoxy composite material with the mechanical properties given in Section 2.2.1.

The input values for solar absorption (α_s) and emissivity (ε) are 0.91 and 0.81, respectively, which represent the surface characteristics of bare (uncoated) graphite epoxy with a roughened (diffused) surface texture.

3-25

Table 3-4. Error Budget and Achievable Shape Accuracy - Mod-PETA (H)

Item	δ mm (inch) RMS
1. Geometry (design)	
— Common flat facets	1.14 (0.045)
2. Thermal Strains	
— Structure	1.12 (0.044)
— Mesh system (10%)	0.11 (0.004)
3. Static Loading Strains	—
4. Measurement Accuracy	0.03 (0.001)
5. Adjustment Accuracy	0.25 (0.01)
6. Repeatability	0.76 (0.03)
Total RSS (half path error)	1.79 (0.070)
RSS correction (10%)	0.18 (0.007)
Adjusted total RSS (δ)	1.61 (0.063)
=	$\lambda/187$ at 1 GHz
=	$\lambda/12.5$ at 15 GHz

For the thermal condition defined above (Section 2.6.1.2), the thermal analysis determined that temperatures experienced by the front face struts ranged from 76°K (-197°C) to 302°K (29°C); 30% of the front face struts were below 78.6°K and 1% were above 301.0°K. Temperatures of the back face ranged from 61°K to 303°K, with 15% below 78.6°K and 20% above 301.1°K. Temperatures for the intermediate (core) struts ranged from 61.0°K to 304°K, with 18% below 73.2°K and 14% above 301.0°K.

Figure 3-26 presents, in contour form, the normal surface displacements of the concave face of the structure with respect to a best-fit paraboloid.

The overall best-fit error (δ) is then: δ = 1.12 mm (0.044 inch) RMS.

Change in focal length (de-focus), best-fit versus nominal, is: $\Delta f = 0.21m$ (8.33 inches).

CONTOUR LEVELS

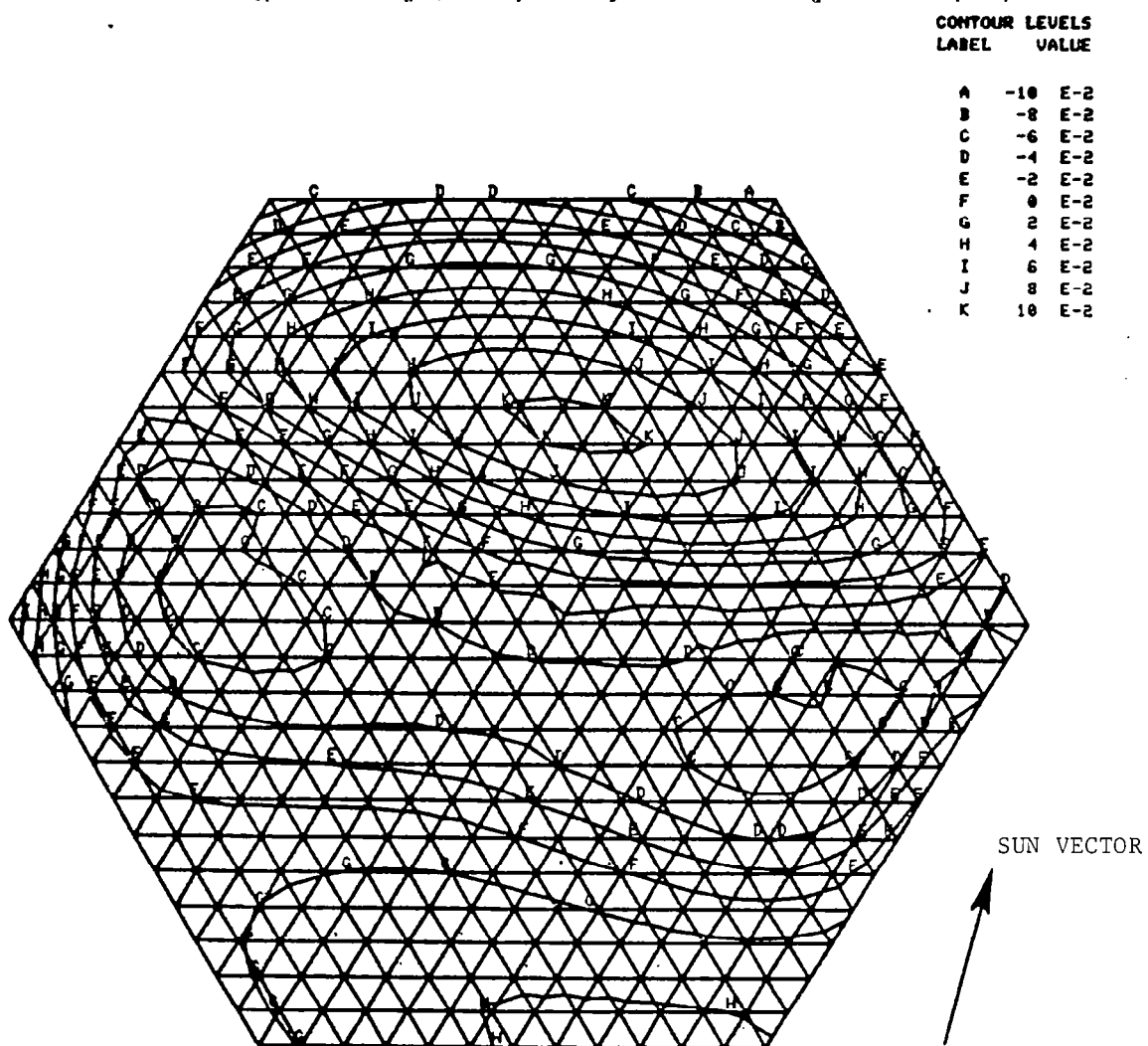| LABEL	VALUE	
A	-10	E-2
B	-8	E-2
C	-6	E-2
D	-4	E-2
E	-2	E-2
F	0	E-2
G	2	E-2
H	4	E-2
I	6	E-2
J	8	E-2
K	10	E-2

SUN VECTOR

Figure 3-26. Contours of Deviations of Surface from "Best-Fit" Paraboloid in Direction Normal to Surface, Mod-PETA Study Case H

3.1.6.3 <u>Determination of Fundamental Frequency of Mod-PETA Reflectors.</u> Using the analytical method applied to the DCM in Section 2.6.1.3, and the input parameters listed in Table 3-5:

$$D_t = \frac{3\sqrt{3}}{8} \cdot E_f \cdot A_f \cdot L_f \left[\left(\frac{L_c}{L_f}\right)^2 - \frac{1}{3} \right]$$

$$= \frac{3\sqrt{3}}{8} (1.314 \times 10^{11})(0.000135)(4.66)\left[\left(\frac{4.84}{4.66}\right)^2 - \frac{1}{3}\right]$$

$$= 4.0 \times 10^7$$

Natural frequency $(f_1) = \frac{25.93}{2\pi D^2}\sqrt{\frac{D_t\, g_\varepsilon}{(M/A)_{system}}} = \frac{25.93}{2\pi(108)^2}\sqrt{\frac{(4.0 \times 10^7)(1)}{8125/7854}}$

$$= \underline{2.20\ Hz}$$

3.2 MODULAR EXTENDABLE PARABOLOIDAL ANTENNA (META) CONCEPT

The assembled geometry of the META reflector is identical to that of the basic PETA, i.e., a tetrahedral truss. It is modularized by subdividing into elemental, structural modules that are equivalent in size, shape, and function to DCM modules.

META modules differ from DCM modules by having three intermediate struts per module, instead of columns and cross ties, as shown in Figure 3-27. Stowage, dispensing, handling, and assembly techniques are also essentially the same as for the DCM concept (Section 2).

The weight summary for the META reflector is presented in Table 3-6. Material properties are assumed to be the same as for the DCM and Mod-PETA cases (Section 2.2.1).

The structure is directly applicable to analysis by the LASS computer program, needing no program modification. For the thermal condition defined in Section 2.6, the estimated shape deviation, due to thermal distortion, is: $\delta = 1.75$ mm (0.069 inch) RMS. This degree of thermal stability is adequate for operation at 1 GHz but marginal at 15 GHz. Table 3-7 presents achievable overall shape accuracy (excluding static loading, which will vary according to mission).

As with the DCM concept, META modules are limited in size by the available diameter of the Orbiter payload bay so that a minimum of 721 is required to assemble a 100 meter reflector, and deployed structure depth is 3.10 meters (maximum). Since the META module uses tubes (instead of the less bulky tension ties of the DCM module) the packaged thickness of the META module is greater by 49%; therefore, 3.9 Orbiter flights are required to provide a 100-meter reflector, versus 2.6 for the DCM.

Table 3-5. Input Parameters for Analysis of the Mod-PETA H (and J)

Parameter		Metric Units (SI)	English Units
Maximum Dimension (D)		108m	4251.97 in.
Equivalent Aperture Dia (D_a)		100m	3937.0 in.
Equivalent Aperture Area (A)		7584 m^2	1.217×10^7 in^2
Face Struts			
Young's Modulus (E_f)		1.314×10^{11} N/m^2 i.e., 131 G Pa)	19.05×10^6 lb/in^2
Diameter	(d_f)	0.0479m	188 in.
Wall	(t_f)	0.000914m	0.036 in.
Sec. Area	(A_f)	0.000135 m^2	$\pi(1.88)$ 0.036 = 0.21 in^2
Length	(L_f)	4.66m	184 in.
Density	(ρ_f)	1836 kg/m^3	0.06633 lb/in^3
Core Struts			
	(E_c)	1.314×10^{11} N/m^2 (i.e., 131 G Pa)	19.05×10^6 lb/in^2
	(d_c)	0.0479m	1.88 in.
	(t_c)	0.000914m	0.036 in.
	(A_c)	0.000135 m^2	0.21 in^2
	(L_c)	4.84m	1.90 in.
	(ρ_c)	1836 kg/m^3	0.06633 lb/in^3
Gravity	(g_c)	1	32.2×12 in/sec^3 = 386
Structural Mass	(M_s)	7552 kg	$\dfrac{16,653 \text{ lb}}{32.2\,(12)\ in/sec^2}$
Parasitic Mass	(M_p)	573 kg	$\dfrac{1263 \text{ lb}}{32.2\,(12)\ in/sec^2}$
Total System Mass	(M_T)	8125 kg	$\dfrac{17,916 \text{ lb}}{32.2\,(12)\ in/sec^2}$

THREE MODULE STRUCTURAL INTERCONNECT POINT (TYPICAL)

MODULE No. 1

MODULE No. 3

MODULE No. 2

FOLDING MEMBER, WITH MID-SPAN JOINT

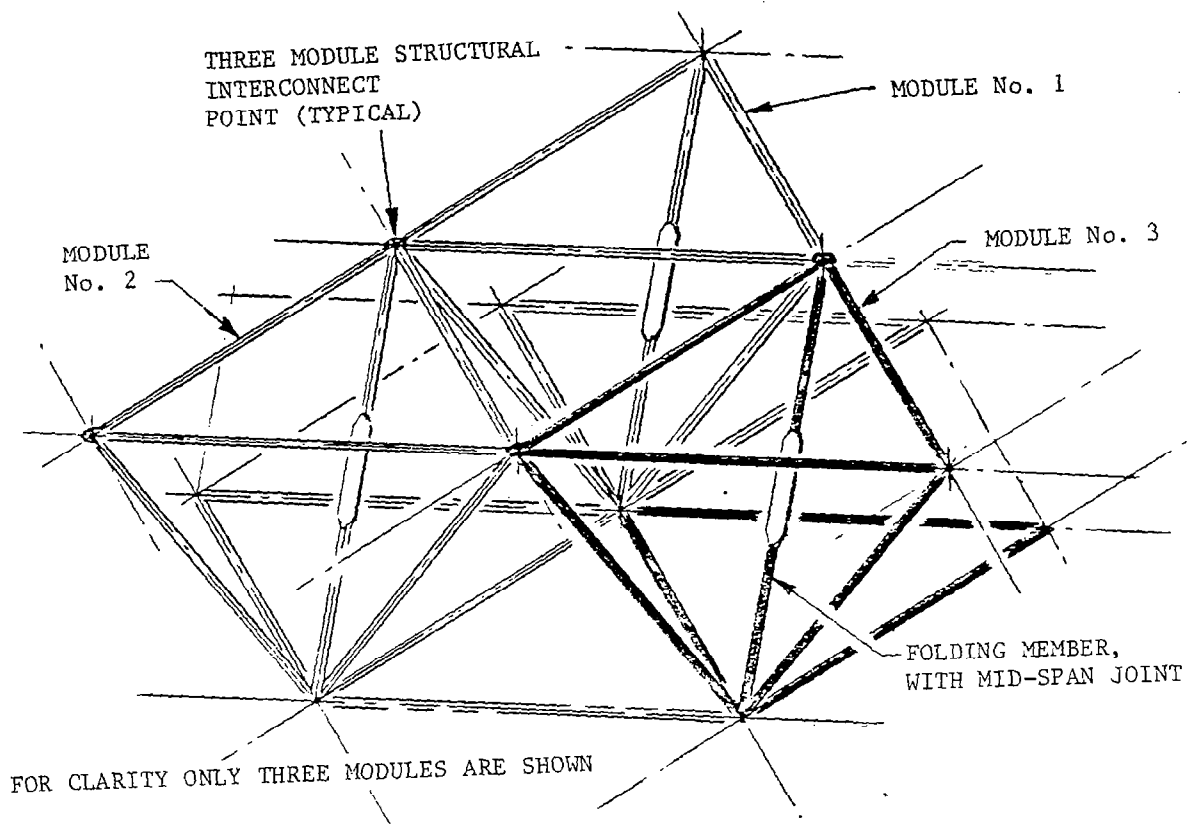FOR CLARITY ONLY THREE MODULES ARE SHOWN

Figure 3-27. Modular Expandable Truss Antenna (META)

The fundamental frequency of the META Reflector is determined using the analytical method applied to the DCM in Section 2.6.1.3, and the input parameters listed in Table 3-8.

$$D_t = \frac{3\sqrt{3}}{8} E_f \cdot A_f \cdot L_f \left[\left(\frac{L_c}{L_f} \right)^2 - \frac{1}{3} \right]$$

$$= \frac{3\sqrt{3}}{8} (1.314 \times 10^{11})(1.06 \times 10^{-4})(3.645)\left[\left(\frac{3.80}{3.645} \right)^2 - \frac{1}{3} \right]$$

$$= 2.485 \times 10^7$$

Natural frequency (f_1)

$$= \frac{25.93}{2\pi D} \sqrt{\frac{D_t \, g_c}{(M_t/A)/system}}$$

$$= \frac{25.93}{2\pi 108^2} \sqrt{\frac{2.485 \times 10^7 \, (1)}{7517/7854}}$$

$$= \underline{1.80 \, Hz}$$

3-30

Table 3-6. Weight Summary — META Concept

Components	Unit Weight kg	Unit Weight (lb)	Number Required	Weight kg	Weight (lb)
Struts				4656	(10,269)
Upper Surface	0.73	(15)	2163	1552	(3,423)
Core	0.73	(15)	1442	1035	(2,282)
Core (folding)	1.46	(30)	721	517	(1,141)
Lower Surface	0.73	(15)	2163	1552	(3,423)
Spider Assembly				1964	(4,330)
Upper Spider	1.3	(2.8)	768	982	(2,165)
Lower Spider	1.3	(2.8)	768	982	(2,165)
Mesh Installation				895	(1,974)
Mesh				454	(1,002)
Mesh Control System				441	(972)
			Total Weight	7517	(16,573)

In summary — the META concept is functionally very similar to the DCM. The most significant difference is its tetrahedral truss structural geometry, which is generally accepted to be a highly efficient and stable structural form.

The absence of tie lines avoids possible concerns over the performance of such elements in primary structure, and over structural integrity being independent on sustained preloading.

As with the DCM concept, the META modularization approach does not result in structural duplication. META has a lower part count than the DCM (6489 tubes versus 10,815 tubes and ties).

The principal disadvantages of the concept are its low packaging density, requiring 3.9 Orbiter flights to construct the full 100-meter reflector, its high module count (721), and its relatively small structural depth, which is limited to 3.1 meters compared to 3.5 meters for the DCM.

Although mechanical movements involved in deployment of the typical META module are different to those for deploying the DCM, the overall time required to deploy/assemble the full 100-meter META structure is estimated to be similar, i.e., 240 hours, approximately.

Table 3-7. Error Budget and Achievable Shape Accuracy — META

	Item	δ mm (inch) RMS
1.	Geometry (design) — Common Flat Facets	2.6 (0.102)
2.	Thermal Strains — Structure	1.75 (0.069)*
	— Mesh System (10%)	0.18 (0.007)*
3.	Static Loading Strains	—
4.	Measurement Accuracy	0.03 (0.001)
5.	Adjustment Accuracy	0.25 (0.01)
6.	Repeatability	0.76 (0.03)
	Total RSS (half path error)	3.24 (0.127)
	RSS correction (10%)	0.32 (0.013)
	Adjusted total RSS (δ)	2.92 (0.114)
	=	$\lambda/103.6$ at 1 GHz
	=	$\lambda/6.9$ at 15 GHz

*Estimated values

Table 3-8. Input Parameters for Analysis of the META Reflector

Parameter		Metric Units (SI)	English Units
Maximum Dimension (D)		108m	4251.97 in.
Equivalent Aperture Dia (D_a)		100m	3937.0 in.
Equivalent Aperture Area (A)		7854 m^2	1.217×10^7 in^2
Face Struts — Young's Modulus (E_f)		1.314×10^{11} N/m^2 (i.e., 131 G Pa)	19.05×10^6 lb/in^2
— Diameter	(d_f)	0.0369m	1.45 in.
— Wall	(t_f)	0.000914m	0.036 in.
— Sec. Area	(A_f)	0.000106 m^2	$\pi(1.45)0.036=0.164$ in^2
— Length	(L_f)	3.645m	143.5 in.
— Density	(ρ_f)	1836 kg/m^3	0.06633 lb/in^3
Core Struts	(E_c)	1.314×10^{11} N/m^2 (i.e., 131 G Pa)	19.05×10^6 lb/in^2
	(d_c)	0.0369m	1.45 in.
	(t_c)	0.000914m	0.036 in.
	(A_c)	0.000106m^2	0.164 in^2
	(L_c)	3.8m (equiv.)	150 in. (equiv.)
	(ρ_c)	1836 kg/m^3	0.06633 lb/in^3
Gravity	(g_ϵ)	1	32.2×12 in/sec^3=386
Structural Mass	(M_s)	6622 kg	$\dfrac{14{,}600 \text{ lb}}{32.2 \ (12) \text{ in/sec}^2}$
Parasitic Mass	(M_p)	898 kg	$\dfrac{1973 \text{ lb}}{32.2 \ (12) \text{ in/sec}^2}$
Total System Mass	(M_T)	7517 kg	$\dfrac{16{,}573 \text{ lb}}{32.2 \ (12) \text{ in/sec}^2}$

SECTION 4

RF DESIGN AND PERFORMANCE

The ground rule for this study is that the baseline antenna configuration is a 100 meter symmetrical paraboloid reflector with a feed supported on the primary axis, 100 meters from the vertex.

Radiometry and communications are the two prime applications envisioned for the large modular antenna. The radiometer application is the more exacting in terms of required reflective surface accuracy and structural stability. Typically, the operating frequency range would be from 1 to 15 GHz and might require a surface shape accuracy of $\lambda/50$, i.e., ≤ 0.4 mm (0.0157 inch) RMS, for the 15 GHz case. Figure 4-1 gives idealistic performance values. The lower curve (solid) relates RF frequency to gain (60% efficiency) for a 100 meter diameter, solid surface modularized into 4.5 meter facets. Surface accuracy of individual facets is taken to be 0.38 mm (0.015 inch) RMS and facet-to-facet alignment error. It is also assumed that the reflector surface need not be physically continuous, but that the gap between facets is small enough to be not significant to RF performance. The dotted line indicates the drop off in performance at higher frequencies that is characteristic of mesh surfaces, as opposed to solid surfaces.

$$G = \eta_T \left(\frac{\pi D}{\lambda} \right)^2 \text{EXP}^{-(4\pi\delta/\lambda)^2}, - \text{RUZE}$$

WHERE D = 100 METER DIAMETER
λ = WAVELENGTH

η_T = 100%

δ = 0

PRACTICAL LIMIT OF 32 GAUGE MESH

η_T = 60%

δ = 0.38 mm (0.015 INCHES) RMS

GAIN (dB)

3 dB BEAMWIDTH (DEG)

FREQUENCY (GHz)
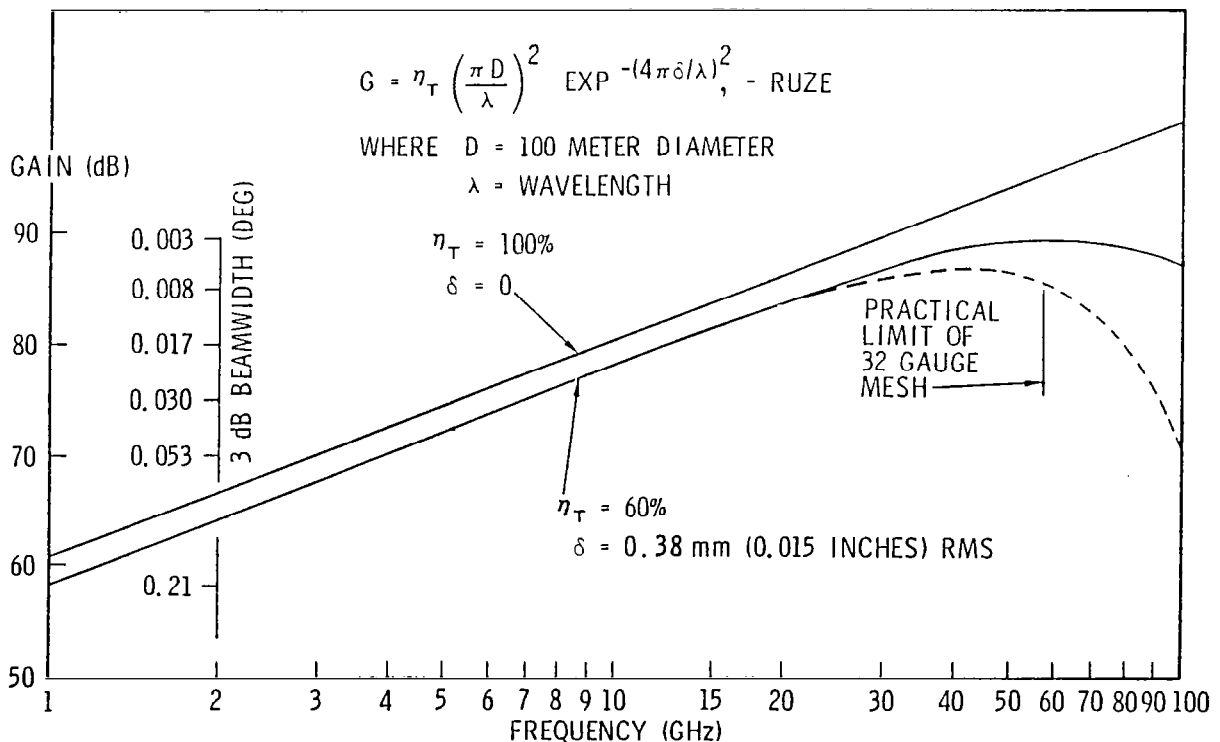
Figure 4-1. Theoretical Performance of a 100-meter (328-foot) Diameter Reflector

There is the consideration that an offset feed antenna would be preferable for applications sensitive to aperture blockage. For radiometry, for example, high beam efficiencies are required, and signal degradation due to side lobes, caused by aperture blockage, must be minimized. The total absence of blockage, which is characteristic of the offset feed antenna, eliminates such losses. Such alternative configurations are likely to impose more severe structural requirements, slightly larger structural sizes, and some loss of structural stiffness.

4.1 EFFECTS OF USING FLAT, HEXAGONAL FACETS TO SIMULATE A PARABOLOIDAL REFLECTIVE SURFACE

This is an extension to Astro Report ARC-R-1008.

The potential advantages of using flat facets as opposed to mean spherical facets include reduced cost, reduced weight, and increased density of packaging. The most significant disadvantage is the greater deviation from the ideal paraboloid and hence, lower achievable RF operating frequencies. This becomes more severe when the focal length/reflector diameter (f/d) ratio is small and when the number of component flat facets comprising the reflector surface is also small.

In comparing a flat, hexagonal facet to a parabolodial surface, the mean error and the standard deviation of the error over the surface are computed. The latter is the 'best fit' RMS error for this symmetrical figure of revolution and is limited to the desired fraction of wavelength ($\delta = \lambda/n$) by adjusting the minor diameter (d) of the hexagonal facet. Maximum values of d, beyond which the limiting values of d are exceeded, are presented below in graphical form for parametric values of F/D (0.5, 0.75, 1.00), D (30, 100, 300m), N (10, 50), and J (0.1 to 100.0 GHz). Figure 4-2 gives limiting values of d for $\delta = \lambda/10$, and Figure 4-3 gives the same for $\delta = \lambda/50$.

In design cases where the ideal curvature of the facet is close to flatness, actual deviations of the facet from theoretical flatness could then produce greater errors than would be attributable to theoretical flatness versus the ideal curvature Figure 4-4 . Ideal curvature would approach flatness if the F/D ratio were large or if the facet were small compared to D.

Deviations from theoretical flatness would result from manufacturing tolerances, initial misalignment, thermal distortion, creep, and maneuvering or environmental accelerations. Such deviations can be classified using the equation:

$$\delta = D \cdot 10^{-Q}$$

which, thus, expresses surface accuracy as a function of reflector diameter (D).

In practice a surface shape accuracy where Q = 3 is readily obtainable. An accuracy of Q = 4 is difficult to achieve, and Q = 5 would demand extreme manu-
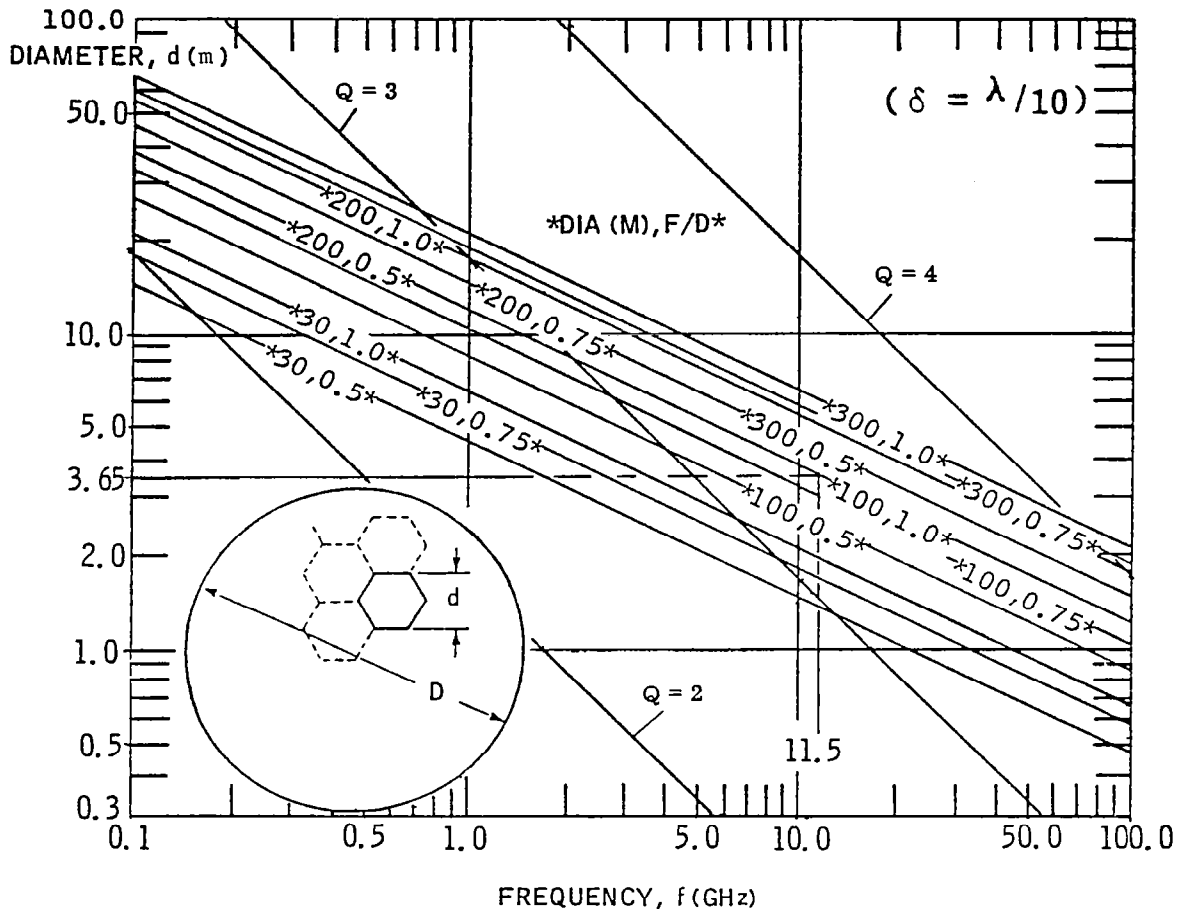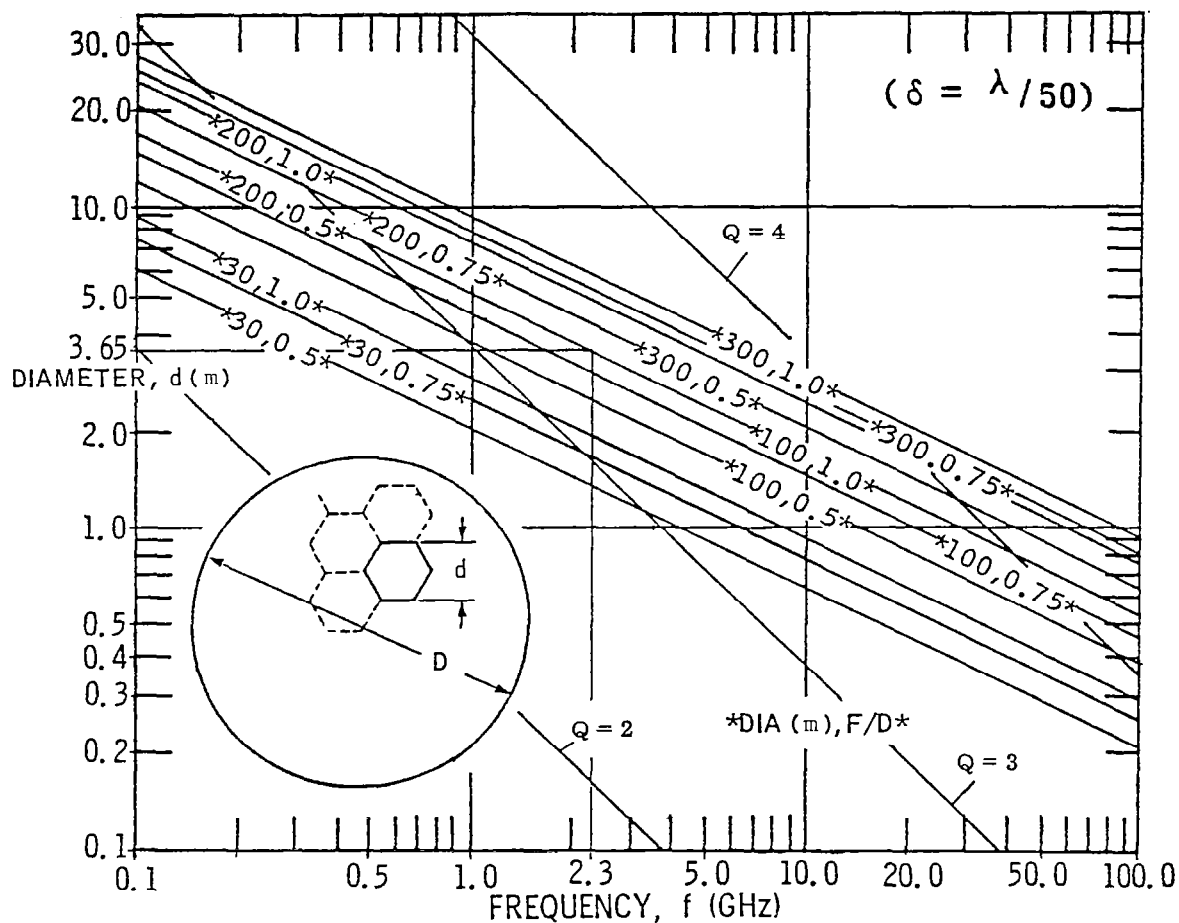
Figure 4-2. Maximum Diameter of Flat Facets, for 30-, 100-, 200-,
and 300 meter Diameter Paraboloid Reflectors, to
Limit Surface Deviation to 1/10 the Wavelength

facturing precision. Figures 4-2 and 4-3 are seen to be augmented to include
the sensitivity of maximum d allowable to Q, the surface figure and alignment
criterion, where $\delta = d \cdot 10^{-Q}$. For example, from Figure 4-2, a Q of 4 would
indicate a deviation (δ) of ±1.0 mm in a 10m diameter 'flat' facet surface.

The error resulting from the flat approximation to the parabolic surface clearly
dominates at lower frequencies. We are particularly interested in the 3.6M-
diameter panel that stacks conveniently in the Orbiter payload bay.

Flat error and manufacturing tolerance are assumed to be uncorrelated. Then
δ for flat error and δ for manufacturing and alignment can be combined by root
sum square. The result is equated to allowable δ and the equation is evaluated
at d = 3.6 meters.

Figure 4-3. Maximum Diameter of Flat Facets, for 30-, 100-, 200-,
and 300-meter Diameter Paraboloid Reflectors, to
Limit Surface Deviation to 1/50 the Wavelength

Figure 4-4 shows the maximum allowable frequency as a function of Q for N = 10
and 50, respectively. The data shows that at 1/10 wavelength allowable distor-
tion, the 100m, F/D = 1.0 reflector peaks at 9.4 GHz, with a surface accuracy
requirement of Q = 3.5 (distortions of 1.1 mm maximum tilt, displacement, warp-
age, RMS surface). At 1/50 wavelength, the same panels can be used at 2.2
GHz if a Q of 4 can be achieved. An improvement in Q beyond 4 does not increase
performance significantly, as shown in Figure 4-6.
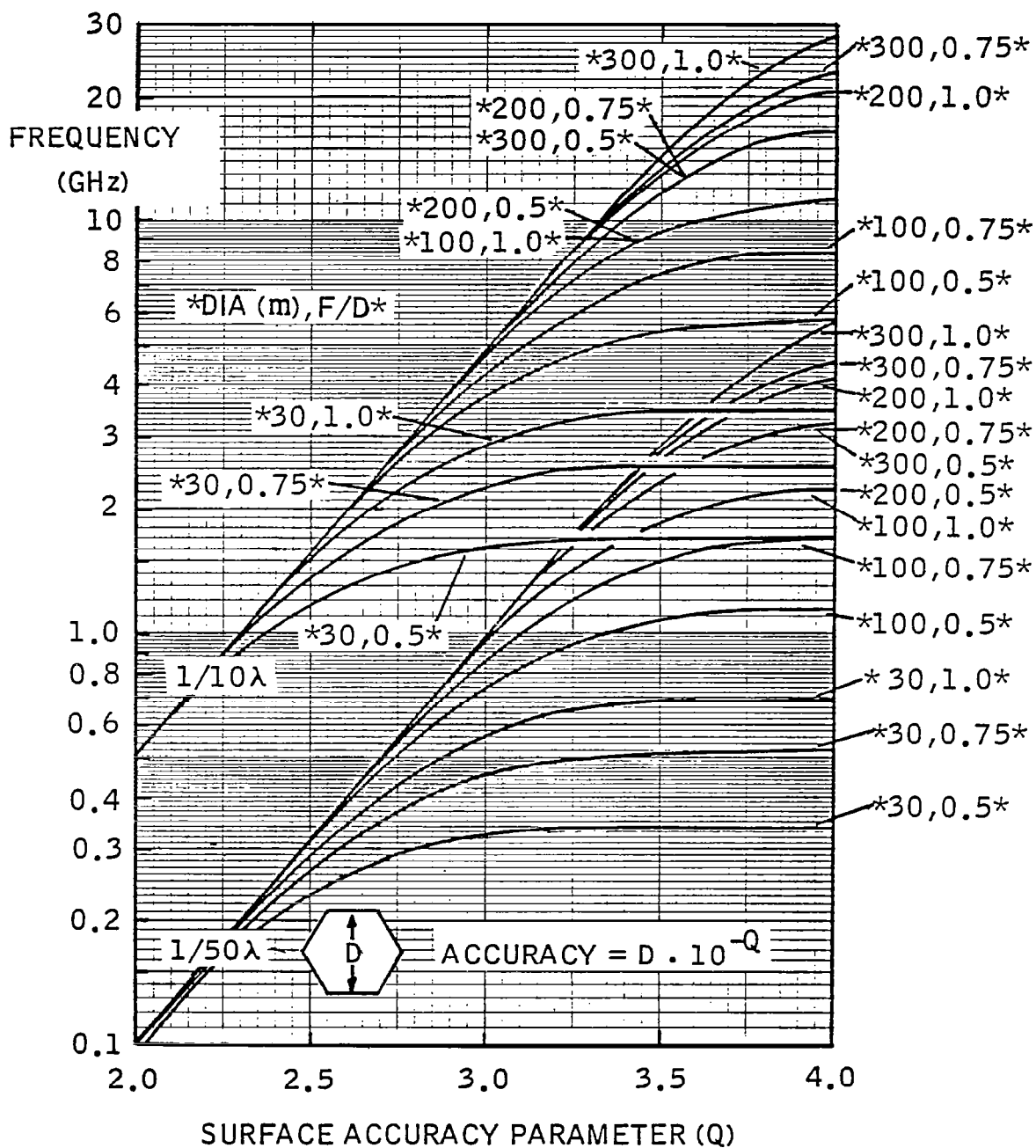
Figure 4-4. Frequency Capabilities of the 3.6m, STS Compatible,
Hexagonal Panel at 1/10 and 1/50 Wavelength Accuracy,
versus Variable Surface Accuracy Parameter Q

4-5
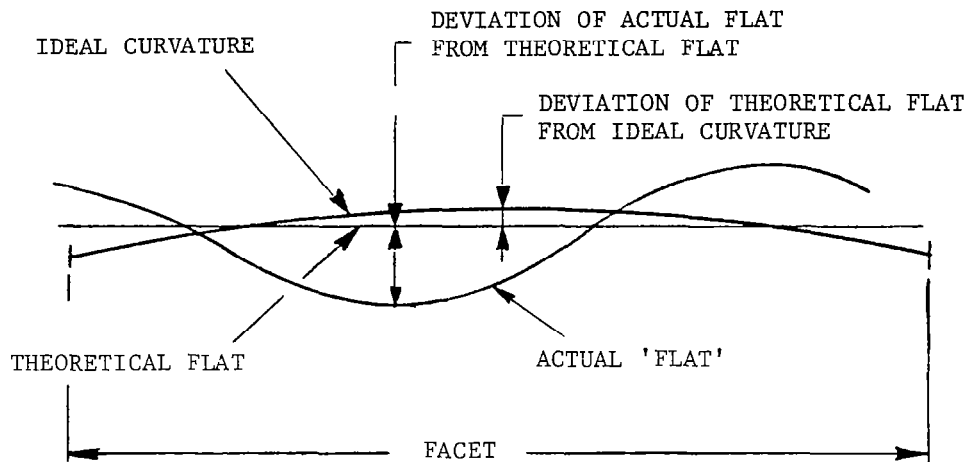
Figure 4-5. Actual Deviations from Flatness have Greater Error
Significance when Ideal Curvature is Small
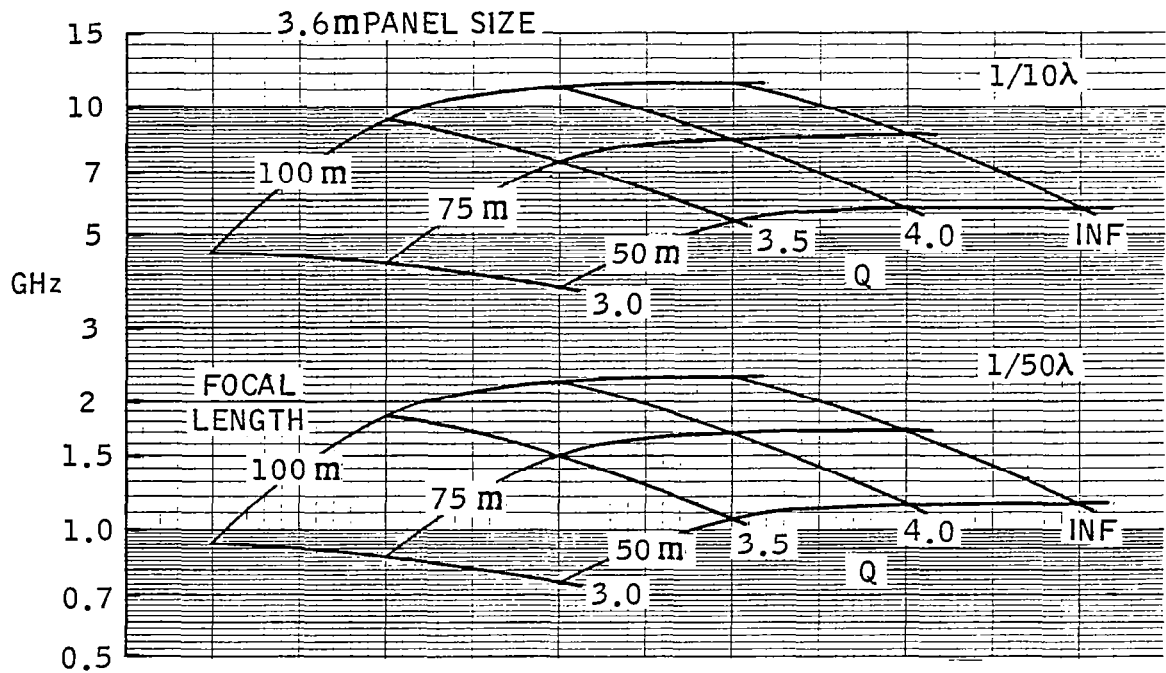
Figure 4-6. For Constant Panel Size, Maximum Operating Frequency
is Reached for a Surface Accuracy Q = 4

4.2 REFLECTIVE SURFACES FOR THE THREE CONCEPTS

4.2.1 SPHERICAL FACETS FOR DCM AND META

4.2.1.1 Theory and Design Approach. A first compromise between the desirability of perfect shape and the practicality of simplifying fabrication and reducing costs is offered by the concept of designing all facets with identical, spherical curvature. The spherical radius of this common curvature approximates the mean radius of curvature of the theoretical paraboloid. The inherent residual shape error involved is small compared to the other items in the overall error budget and results in very little degradation of RF performance capability. Upon assembly of the full reflector each component facet is positioned to 'best fit' the ideal paraboloid.

For the 100 meter, F/D = 1.0, 721 module reflector shown in Figure 2-1, the magnitude of deviation of the typical spherical facet (Figure 4-7) can be determined from the Astro Research Corp. Report ARC-R-1008, and is found to be δ_{RMS} = 0.09 mm (0.004 inch). If no other contributors to shape distortion exist, this degree of shape accuracy permits operation at frequencies up to 68.0 GHz, (with an accuracy of $\delta_{RMS} = \lambda/50$).

4.2.1.2 Design Development. Metallic meshes serve well as RF reflector surfaces. They are lightweight and their open surface minimizes shadowing of the backup structure. For relatively low RF frequencies the mesh can be correspondingly coarse.

The spacing of the elements of the mesh generally should not exceed $\lambda/10$. Thus, for 1 GHz applications, a spacing of up to $\dfrac{3 \times 10^8}{10 \ (1 \times 10^9)}$ = 0.03 meter = 3 cm (1.18 inches) is acceptable. This coarseness, plus the double curvature of its preformed shape gives the mesh a certain stiffness and, to a degree, makes it self supporting against the 1g environment and the accelerations of the launch phase.

In designs where the span length of unsupported mesh is large enough that curvature reversal could occur, additional mesh support may be required. Figure 4-8 shows a simple mesh backup system consisting of a hexagonal, peripheral frame plus (9) stiffening ribs arranged in hexagonal pattern. If this span is still excessive, the backup support can be designed to a finer (hexagonal) pattern.

4.2.2 FLAT FACETS FOR DCM AND META

4.2.2.1 Theory and Design Approach. A further, more drastic compromise in the direction of shape approximation is to flatten the entire modular facet. Compared to the 'mean spherical' approach this results in inherent errors at least an order of magnitude greater, which thus become a significant item in the error budget.
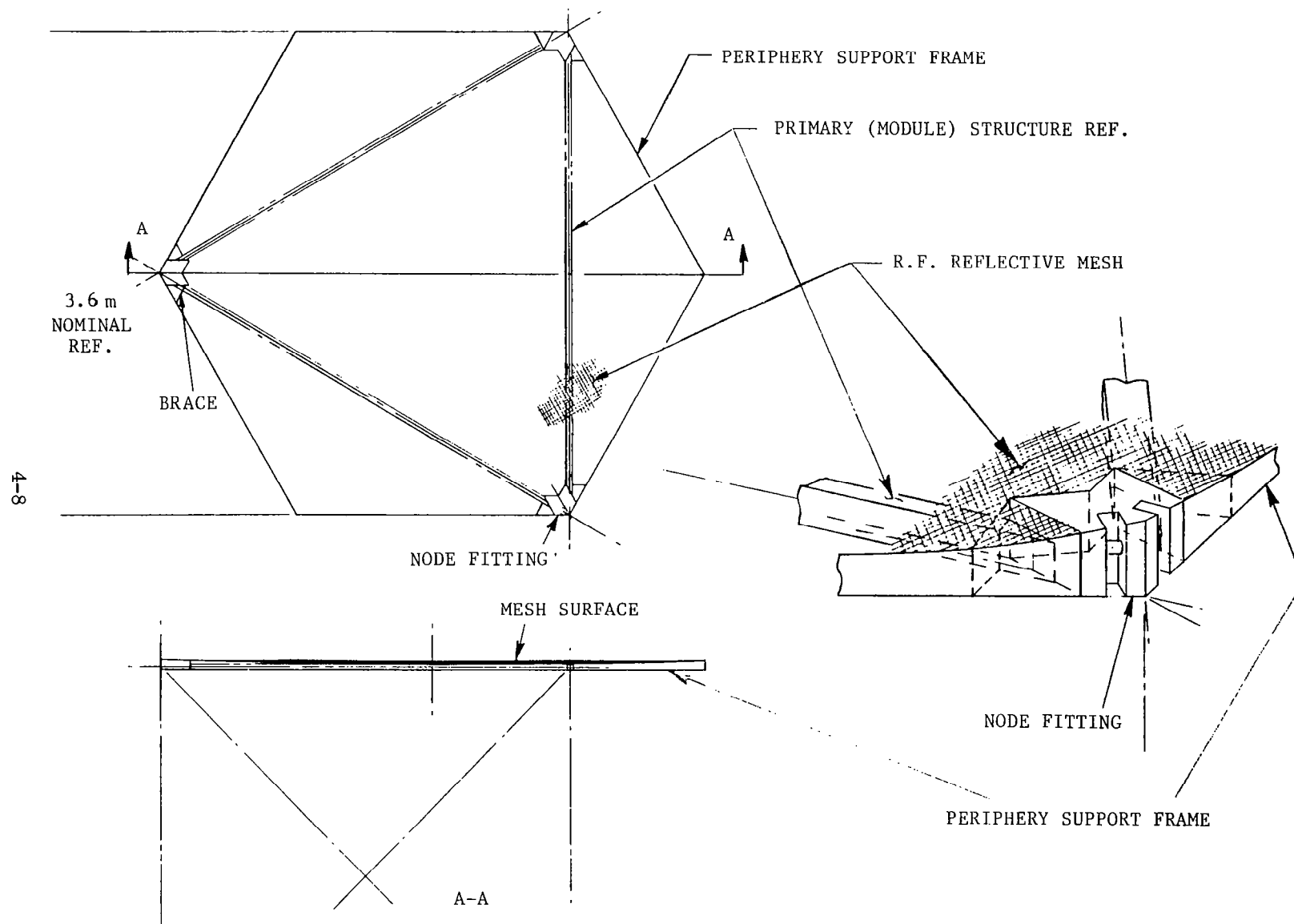
PERIPHERY SUPPORT FRAME

PRIMARY (MODULE) STRUCTURE REF.

A

3.6 m
NOMINAL
REF.

BRACE

R.F. REFLECTIVE MESH

A

NODE FITTING

MESH SURFACE

NODE FITTING

PERIPHERY SUPPORT FRAME

A-A

Figure 4-7. Spherical, Rigid Mesh Facet Supported at Periphery Only

MESH SUPPORT STIFFENERS

MESH

MESH PERIPHERY SUPPORT FRAME

MODULE STRUCTURE, REF.

3.6 m
NOMINAL,
REF

2.08
REF

1.20 m
(47.2 INCHES)

MESH SURFACE

MODULE STRUCTURE, REF.
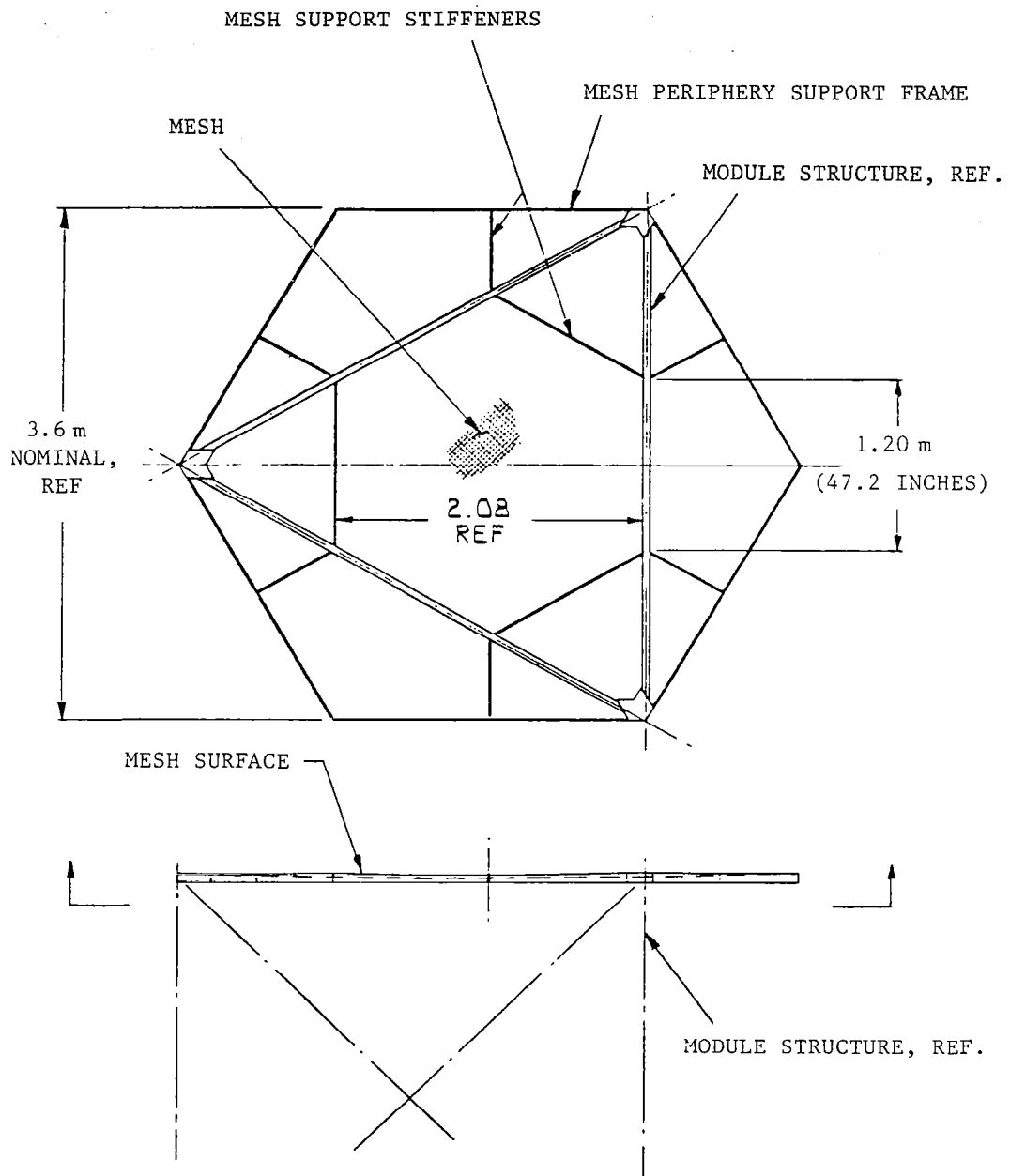
Figure 4-8. Spherical, Rigid Mesh Facet Supported at the
Periphery and by Internal Stiffeners

However, when the intended RF operating frequency is low enough to tolerate such shape deviation, this approach offers great simplification of design and fabrication, denser packaging potential, reduced weight, and drastically reduced cost.

Table 4-1 presents equations for determination of the inherent shape error that results from 'best fitting' flat facets to the theoretical ideal shape (spherical radius, R):
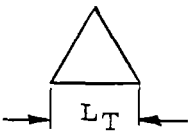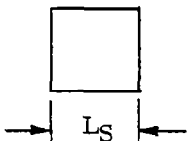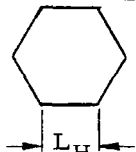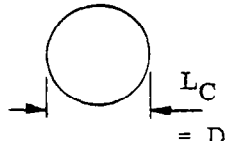
For operation at an RF frequency of 1 GHz the maximum tolerable deviation of the reflective surface shape from the ideal paraboloid is given by:

$$\delta_{RMS} = \lambda/10 = \frac{3 \times 10^8}{1 \times 10^9} \: /10 = 0.03 \text{ meter} = 30.0 \text{ mm} \: (1.18 \text{ inches})$$

or

$$\delta_{RMS} = \lambda/50 = \frac{3 \times 10^8}{1 \times 10^9} \: /50 = 0.006 \text{ meter} = 6.0 \text{ mm} \: (0.24 \text{ inch})$$

Table 4-1. Best Fit Deviations of Flat Facets

Flat Facet Shape	Deviation (RMS)	Values of L for Equal RMS
L_T	$.0322 \dfrac{L_T^2}{R}$ $\left(.0460 \dfrac{L_T^2}{R}\right)*$	1.00
L_S	$.0528 \dfrac{L_S^2}{R}$	0.78
L_H	$.1222 \dfrac{L_H^2}{R}$ $\left(.1767 \dfrac{L_H^2}{R}\right)*$	0.513
$L_C = D$	$.0361 \dfrac{L_C^2}{R}$	0.94

*Applicable when quilting occurs.

4-10

Deviation of a flat hexagonal facet is:

$$\delta_{RMS} = 0.1222\, L_H^2/R \text{ (see Table 4-1).}$$

Thus, where R = local radius of curvature of the ideal paraboloid = 200 meters,

$$L_H = \sqrt{\frac{200\,(0.03)}{0.1222}} = 7.01 \text{ meters, maximum for } \lambda/10$$

$$= \sqrt{\frac{200\,(0.006)}{0.1222}} = 3.13 \text{ meters, maximum for } \lambda/50$$

Figures 2-3 and 2-4 show the value of L_H for the maximum size facet stowable in the Orbiter to be 2.07 meters (i.e., well within the limiting values determined above for 1 GHz operation). Actual shape deviation of this flat, maximum size, hexagonal facet from the ideal curvature is given by:

$$\delta_{RMS} = 0.1222\, L_H^2/R = 2.6 \text{ mm } (0.102 \text{ inch})$$

Table 2-5, in Section 2.6.2, presents this deviation together with other items in the total error budget. The net deviation is seen to be less than $\lambda/50$ at 1 GHz, and the concept of a flat facet for the DCM module is therefore shown to be feasible.

4.2.2.2 Design Development. Options in facet design for various degrees of accuracy are summarized in Table 4-2.
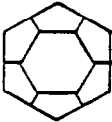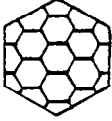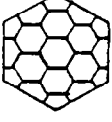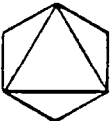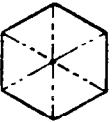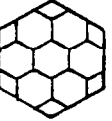
The facet installation selected is similar to that shown in Figure 4-7, except that the facet surface is a flexible, knitted, metallic mesh stretched taut and flat within the peripheral frame (See Table 4-2, item 5.) As shown in Figure 4-7, the frame is made of thin, thermally stable graphite-epoxy laminate and is in three segments integrally bonded to the three node fittings of the module structure.

A simple method of improving the effective accuracy of the flat facet, should it be required, is to displace the center point of the facet in a direction normal to the surface so that the surface 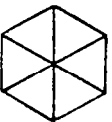creases into six smaller triangular zones as shown in Figure 4-9 (see Table 4-2, item 7). 'Best fitted' to the ideal paraboloid this would reduce the deviation to:

$$\delta_{RMS} = 0.0460\, L_T^2/R = 0.98 \text{ mm } (0.039 \text{ inch})$$

where 0.0460 is the constant, appropriate to triangular facets "quilted" at the corners (see Table 4-1).

Table 4-2. Summary of Facet Concepts for DCM and META

Facet Type (DCM/META)		RMS Shape Deviation mm (inches)	Ref. Figure No.
1. Spherical, rigid mesh facet		.09 (.004)	
2. Same, except mesh stiffeners added		ditto	
3. Same, except more stiffeners		ditto	
4. Flexible mesh taut (flat) within stiffeners		0.24 (.009)	—
5. Flexible mesh taut (flat) within periphery		2.60 (.102)	—
6. Flexible mesh taut (flat) within (4) zones		2.10 (.080)	
7. Flexible mesh pulled down at center point (quilted)		0.98 (.039)	
8. Flexible mesh taut (flat) within (6) zones		0.69 (.027)	—
9. Flexible mesh taut (flat) within (13) zones		0.29 (.011)	

$L_T = 2.07$ m
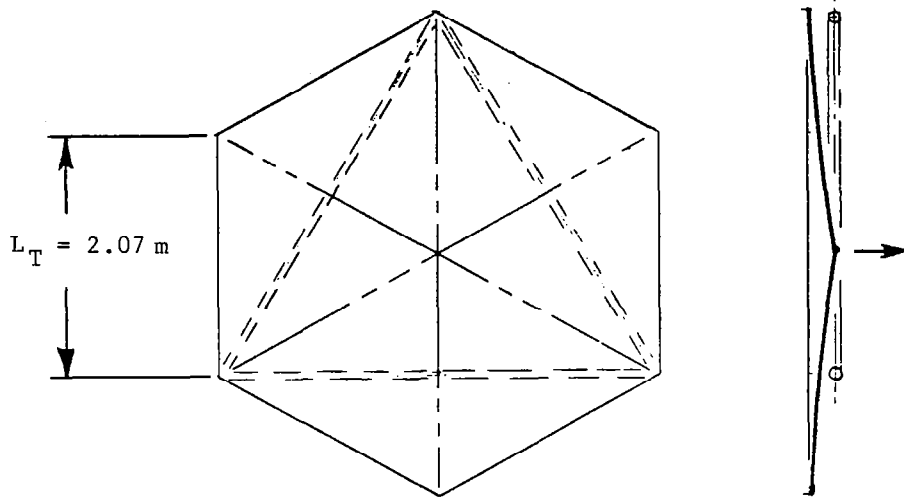
Figure 4-9.   Surface Shape Deviation is Reduced by Depressing
             Center Point to Produce Six Equal, Triangular
             Facets

This represents a simple but crude means of achieving a significant reduction
of shape error. A further improvement can be achieved by a refinement that
corrects the "quilting" (reverse curvature) that occurs around the point of
attachment. This is accomplished by adding six radial stiffeners or taut wires
(Table 4-2, item 8). The mesh surface is thus divided into six, *flat*, triangular
zones.

Then: $\delta_{RMS} = 0.0322 \, L_T^2/R = 0.69$ mm (0.027 inch).

These facet designs (Table 4-2) are applicable to both the DCM and META con-
cepts. They are installed on the structural module in preassembled, finished
shape before launch and are not disturbed or affected by subsequent, in-space
deployment of the modules.

4.2.3 FLAT FACETS FOR PETA

4.2.3.1 Theory and Design Approach. The PETA structure typically deploys in the radial direction, i.e., in a plane parallel to the reflective surface. The preinstallation of rigid (non-deployable) facets such as those described above (for DCM/META) is therefore not practical for PETA unless they are installed as a separate operation after structural deployment has been performed.

A more practical technique is to use an integral, flexible mesh system that deploys with the PETA structure, becoming taut between structural node points at the moment of full deployment. The mesh is pulled down into approximate paraboloidal shape by control lines that attach to the structural node points. Theoretically, to produce a perfect paraboloid an infinite number of control lines is required. Achievable surface accuracy is therefore limited by the maximum number of control wires considered practical.

With a finite number of control lines attached in triangulated pattern to discrete points on the taut mesh, there is a tendency for the mesh to develop "quilting" (dimpling) at the attach points. This effect can be almost eliminated by overlaying the mesh with a triangulated wire grid and attaching the control lines to the cross-over node points of the grid wires as shown in Figure 4-10. With this arrangement the wires assume much of the tension loading, being considerably stiffer than the mesh. The wires thus pull straight between attach points and the mesh lies taut against the wires in a series of triangular flats.
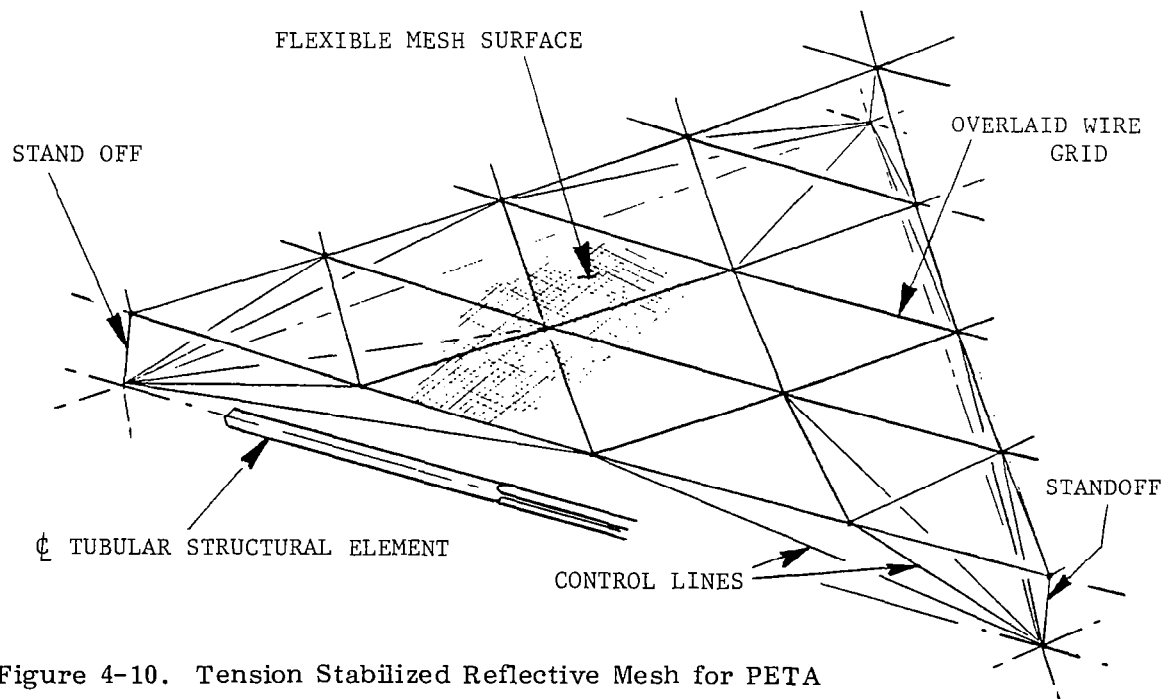

Figure 4-10. Tension Stabilized Reflective Mesh for PETA

A further design development is to thread the grid wires through the mesh in such a way that the cross-over nodes of the wire grid are on the back of the mesh. With the control lines attached to these grid wires nodes, the flexible mesh creases into a barely discernable hexagonal pattern, with each hexagon essentially flat (Figure 4-11).

Each of these progressive phases of design refinement produces improved over-all surface accuracy.

FLEXIBLE MESH SURFACE
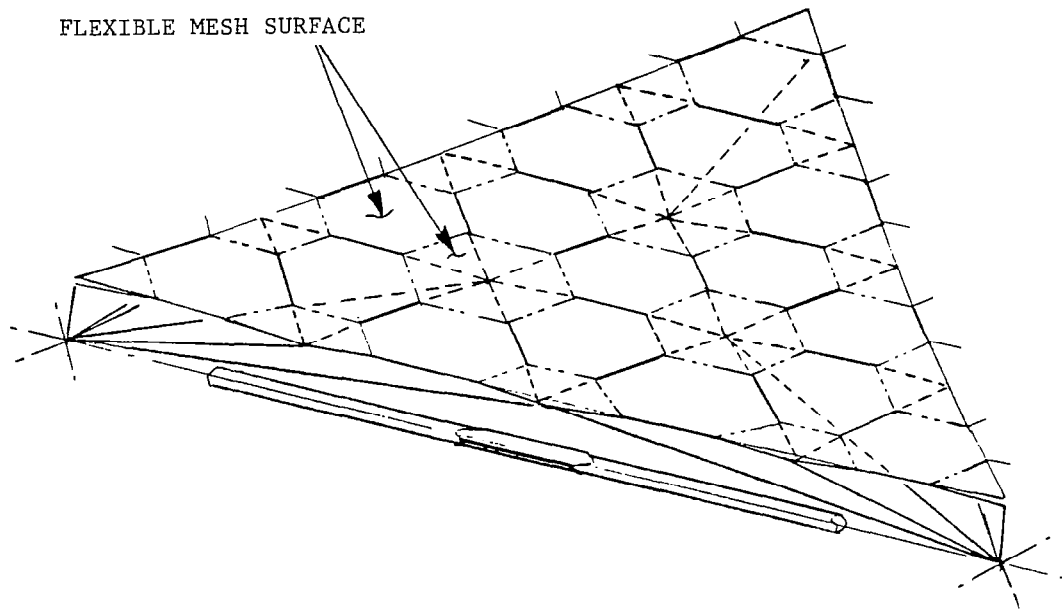
Figure 4-11. Weaving Grid Lines Produces Hexagonal Facets

4.2.3.2 Design Development. A typical reflective mesh installation applicable to Mod-PETA H modules (Figures 3-5 and 3-6) is shown in Figures 4-12 and 4-13. The flat hexagonal facets of the surface are sized for similarity with the facets derived above for the DCM design.

To assure flatness of the facets, the mesh is overlaid by a wire grid of matching hexagonal pattern, following the technique shown in Figure 4-11.

$$L_H = \frac{13.7}{3 \times 3} = 1.52 \text{ meters}$$

$$\text{and } \delta_{RMS} = 0.1222 (1.52)^2 / 200$$

$$= 0.00141 \text{ meter}$$

$$= 1.14 \text{ mm } (0.045 \text{ inch})$$

This is well within tolerable deviation for 1 GHz.

TAUT HEXAGONAL MESH FACETS

GRID WIRES

1.52 m
(5.0 FT)

13.7 m
(45.0 FT) REF

Mod - PETA MODULE STRUCTURE
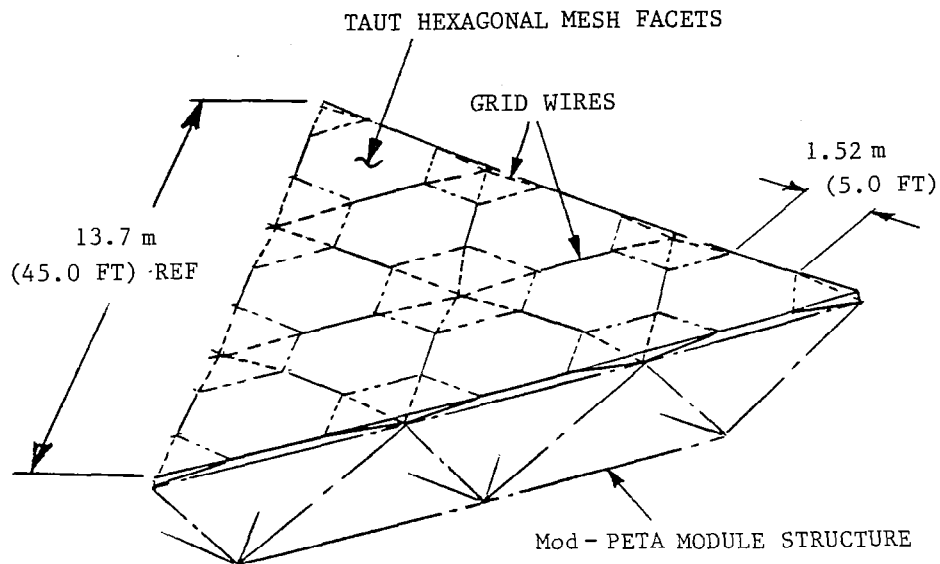
Figure 4-12.   PETA H Module with Hexagonal Pattern Surface
on a Three-Bay Structure

13.7 m
(45 FT) REF.

4.57 m
(15 FT)

STRUCTURAL NODE
FITTING (SPIDER)

STANDOFF

GRID WIRE

CREASE, TYPICAL

2.6 m
(8.7 FT)

1.5 m
(5.0 FT)
TYP.

STAND OFF, TYP.

MODULE STRUCTURE

GRID WIRES

MESH

MESH WITH
HEXAGONAL, FLAT ZONES

Mod - PETA MODULE
TRUSS STRUCTURE
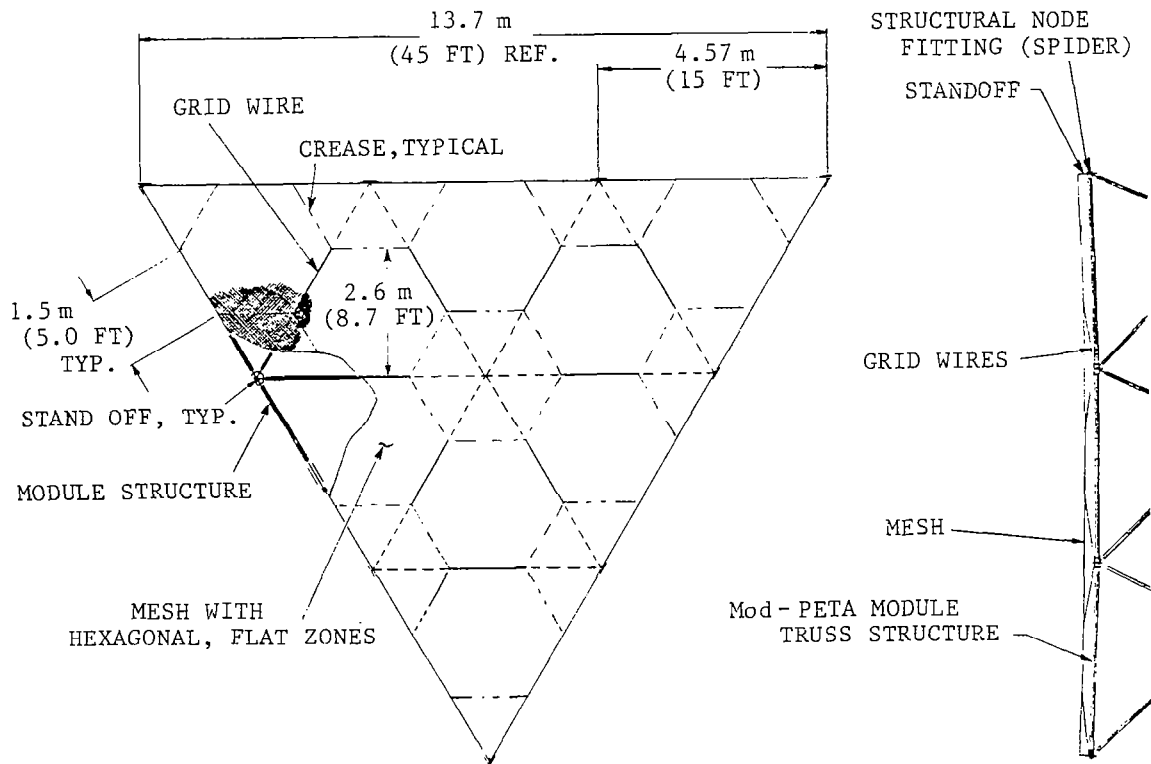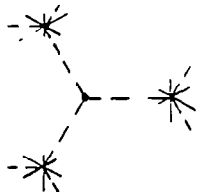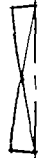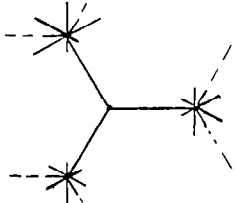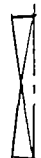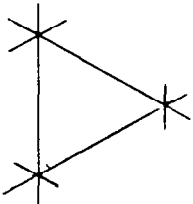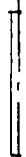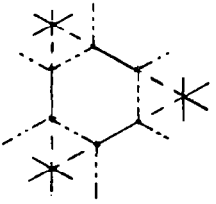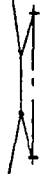
Figure 4-13.   1-GHz Capability is Provided by Simple Mesh Installation

4-16

The above flexible mesh installation designs are all applicable to Mod-PETA concept reflectors depending upon what degree of surface accuracy proves to be adequate for the applications. They package and deploy integrally with the structure and are pulled taut into defined shape by the structure at the moment of full deployment. Various available options exhibiting varying degrees of complexity and accuracy are summarized in Table 4-3.

Of these options, the design listed as item 4 in Table 4-3, and illustrated in Figures 4-12 and 4-13, is selected for the Mod-PETA analysis and evaluation.

Table 4-3. PETA Surface Options

Facet Type (PETA)		RMS Shape Deviation mm (inches) 3-bay
1. Flexible mesh with control lines, gives quilted surface.		5 mm, approx.
2. Same as 1, except quilting is eliminated by overlaying hex-pattern wire grid.		3.2 mm (.126 in.)
3. No control lines. Overlaying, triangulated, wire grid attaches to short standoffs at structural node points		2.52 mm (.099 in.)
4. Same as 3, except grid wires weave through mesh and attach to structural node points. (no standoffs, no control wires.)		1.14 mm (.045 in.) Ref. Fig. 4-12 and 4-13

SECTION 5

COMPARATIVE ANALYSIS OF CANDIDATE MODULAR CONCEPTS

5.1 SELECTION OF EQUIVALENT DESIGNS

The basic common objective to be satisfied by the three candidate concepts is that they shall be capable of space assembly from the Orbiter and shall provide an RF reflective surface of 100 meters effective diameter suitable for operation in the space environment at 1-GHz frequency. If each candidate design is individually optimized to best satisfy this specific objective, the designs can be said to be equivalent regardless of apparent dissimilarity of geometry, depth, element sizing, etc. This approach permits full development of characteristic advantages that one concept may have over another and also tends to make inherent, characteristic limitations more apparent. Conversely, the imposition of arbitrary equivalence by making certain key dimensions common would give only an illusion of equivalence and would, in fact, tend to conceal the very peculiarities that we wish to uncover.

Thus it is that the three concepts presented have differing structural depths, although it is known that thermal stability tends to be proportional to structural depth; they have varying bay counts although it is known that lower bay count sharply reduces component parts count and increases reliability; they have varying module count although it is known that lower module count reduces in-space assembly time. Primary parameters that are deliberately made common for all concepts are limited to those relating directly to RF performance, (e.g., the effective aperture diameter and the F/D ratio (curvature), to the selection of L/ρ of the component structural elements, and to the choice of structural material. Thermal stability of the candidate structures is an important consideration in their evaluation and is highly sensitive to material selection. All concepts are therefore given equal benefit of the properties of graphite-epoxy composite material.

For actual applications, the sizing of structural components would be dependent upon specific operational requirements; however, for the purposes of comparative evaluation, a common, typical, square section, tubular strut is selected. Its design is based upon existing hardware developed for similar applications and is characterized by minimum practical wall thickness, high slenderness ratio (L/ρ), and with graphite-epoxy as the selected primary material. Choice of graphite-epoxy is justified by its high specific strength and stiffness and its high thermal stability.

Table 5-1 summarizes these and other parameters considered common for the three concepts.

Table 5-1. Common Controlling Parameters

Nominal RF size	100 meter diameter
Structural size across flats	95.27 meters
Radius of curvature	200 meters
L/ρ of structural members	300
Wall thickness (t) of structural members	0.91 mm (0.036 inch)
Density of structural material	1874 kg/m^3 (0.0677 lb/in^3)
Modulus (E_{11}) of structural material	131 × 10^{11} N/m^2 (19.05 × 10^6 lb/in^2)
Effective thermal coefficient of structure	0.45 × 10^{-6} m/m/deg K * (0.25 × 10^{-6} in/in/deg F)

*Note: This low value is achieved by tailoring the coefficient of thermal expansion (CTE) of the graphite-epoxy subcomponents so that the net node-to-node CTE is theoretically zero. The value listed represents achievable accuracy of this technique.

5.2 CHARACTERISTIC DIFFERENCES BETWEEN THE THREE CONCEPTS

Whereas the Mod-PETA and META concepts provide structures with tetrahedral truss geometries, the DCM intermediate (core) structure is in the form of rectangular facets cross-braced with tension ties. The upper and lower elements of this geometry are the common, typical, surface strut elements discussed above. The vertical elements are spring columns.

These and certain other parameters that are peculiar to each of the three concepts are summarized in Table 5-2.

The cross-bracing ties are primary elements in the DCM structure, and their structural performance is therefore critical to the performance of the structure as a whole. The most attractive natural characteristic of the tie as a structural element is its high structural efficiency (strength/weight). However, for the subject application of RF reflector backup structure, high specific strength is not as significant a requirement as rigidity and high-dimension stability.

The META concept possesses a combination of the key characteristics of both the DCM and the PETA concepts. Individual modules are very similar to DCM modules in their general size and shape, in their manner of deployment, and in their reflective surface installations. The essential difference is found in the relative arrangement of their component structural elements. In META the structural component arrangement is directly related to the tetrahedral geometry

of the PETA. A reflector structure assembled from META modules produces an overall structure geometry basically identical to PETA structure.

Table 5-2. Peculiar Controlling Parameters

Parameter	DCM	PETA (H/J)	META
Number of structural bays	31 minimum	24	31 minimum
Structural depth (meters)	3.50m	4.05m	3.10m
Number of modules	721 minimum	96/48	721 minimum
Section size of tubular members	3.1 cm sq	4.2 cm sq	3.1 cm sq
Length of surface members	3.6m	4.6m	3.6m
Pre-load in inner surface members	41N (9.2 lb) (compression)	0	0
Pre-load in outer surface members	39N (8.8 lb) (compression)	0	0
Pre-load in diagonal elements	55N (12.4 lb) (tension)	0	0
Pre-load in buckled columns	76N (17.0 lb) (compression)	NA	NA

Note: The PETA concept offers significant freedom of choice of such parameters as number of structural bays, total number of modules, and structural depth; any depth up to 13.5 meters can be selected. The values listed here are selected and optimized to achieve equivalence with the DCM design.

As with the DCM, achievable deployed size of the META module is strictly limited by the diameter of the available payload envelope. It is more limited in this respect than is the DCM and also possesses a greater packaged length, which means lower packaging density. Its main virtues are its high overall structural efficiency when deployed and joined into a complete structure, the absence of ties or cables as structure elements, and the absence of structural duplication at the inter-modular structural interfaces. Due to its limited structural depth it may not have the potential of satisfying requirements for large, rigid reflectors, but could prove very attractive for smaller structures and/or where rigidity requirements are moderate.

Table 5-3 presents the input data upon which the analysis of the three concepts is based.

Table 5-3. Input Data for Concept Analysis

Input Parameters (actual)	Concept (study case)			
	DCM (C)	PETA (H)	PETA (J)	META
Equivalent RF dia, meters (ft)	100 (328)	100 (328)	100 (328)	100 (328)
Focal length/RF diameter	1.0	1.0	1.0	1.0
Number of structural bays	31	24	24	31
Number of modules	721	96	48	721
Structural bays per module	1 × 1	3 × 3	1 × 12 (max)	1 × 1
Strut length (L) Radius of Gyration (ρ)	300	300	300	300
Strut wall thickness, mm (in.)	0.914 (0.036)	0.914 (0.036)	0.9.4 (0.036)	0.914 (0.036)
Coefficient of thermal expansion, (Strain/deg K)	0.45×10^{-6}	0.45×10^{-6}	0.45×10^{-6}	0.45×10^{-6}

5.3 EVALUATION AND CONCLUSIONS

Table 5-4 presents analytical output including LASS computer data.

The total number of individual tubular elements in the Mod-PETA (Study Case H) is 5440 versus 10,815 tubes and ties in the DCM. The PETA H and J require 1.3 and 2.0 Orbiter flights, respectively, versus 2.6 for the DCM. Total number of in-space structural connections to be effected for PETA (H and J) is approximately 2200 and 900, respectively, versus 8460 for the DCM. The total weight of PETA Study Case H is 8125 kg (17,916 lb), versus 9399 kg (20,725 lb) for the DCM and 7515 kg (16,573 lb) for the META.

Table 5-5 presents judgment scoring of the three candidate concepts against pertinent evaluation factors. Weighting factors are presented in the final column and are applied prior to summation. In all columns, higher values indicate superiority and lower values inferiority.

The data indicates the Mod-PETA to be the superior concept despite its structural duplication and the relatively greater challenge of manipulating and joining its large modules.

Table 5-4. Output Data of Concept Analysis

Output Data	Concept Study Case			
	DCM (C)	PETA (H)	PETA (J)	META
Orbiter payloads required	2.6	1.3	2.0	3.9
Total reflector weight, kg (lb)	9399 (20,725)	8125 (17,916)	8183 (18,043)	7515 (16,573)
Structural depth, m (ft)	3.5 (11.5)	4.05 (13.3)	4.05 (13.3)	3.10 (10.17)
Fundamental frequency (f_1), hertz	1.78	2.20	2.20	1.80
Surface accuracy, RMS, mm (in.)	2.83 (0.11)	1.61 (0.063)	1.61 (0.063)	2.92 (0.114)
Surface accuracy at 1 GHz	$\lambda/107.4$	$\lambda/187$	$\lambda/187$	$\lambda/103.6$
Surface accuracy at 15 GHz	$\lambda/7.2$	$\lambda/12.5$	$\lambda/12.5$	$\lambda/6.9$
Length of packaged module, m (ft)	0.07 (0.23)	5.49 (18.0)	5.49 (18.0)	0.1 (0.34)
Surface strut column strength, newtons (lb)	2131 (480)	2895 (652)	2895 (652)	2131 (480)
Average 'concave strut length, m (ft)	3.62 (11.8)	4.62 (15.2)	4.62 (15.2)	3.52 (11.50)
Average 'convex' strut length, m (ft)	3.68 (12.1)	4.71 (15.5)	4.71 (15.5)	3.58 (11.55)
Average 'diagonal' strut length, m (ft)	5.05 (16.6)	4.84 (15.8)	4.84 (15.8)	3.8 (12.5)
Number of surface struts	4326	3610	3361	4326
Number of 'diagonal' struts	0	1830	2112	2163
Number of cross bracing ties	4326	0	0	0
Number of spring loaded columns	2163	0	0	0
Number of 'in-space' structural connections	8460	2200	900	8460

Table 5-5. Comparative Evaluation of the Three Concepts

Item	DCM (C)	PETA (H/J)	META	Weighting Factor	Remarks
● Shape accuracy					
– as manufactured	5	5	5	8	Flat facetted surfaces on all concepts
– as assembled in space	3	7	3	5	PETA has fewer intermodular joints
– in-space correction	10	10	10	8	All concepts can be "shape tuned"
– effect of time	4	7	7	5	DCM structure is in constant stress state
● Thermal stability	9	10	8	8	META has the least structural depth
● Dynamic stability	8	10	8	8	PETA has greatest structural depth
● Bending strength	9	10	8	8	Tends to be proportional to structural depth
● Density of packaging	7	10	3	10	META has lowest packaging density
● Reliability of deployment	9	8	10	8	PETA modules are few but more complex
● Reliability of assembly	5	5	5	8	DCM and META very repetitive. PETA more complex
● Ease of assembly	8	5	8	10	PETA modules are large
● Minimized assembly time	5	5	5	10	All require prolonged on-orbit time
● Minimized support equipment	5	5	5	8	All concepts require sophisticated provisions
● Low cost					
– fabrication	3	7	10	8	DCM has largest component part count
– in-space assembly	7	10	3	10	PETA requires fewest orbiter flights
● Surface continuity	10	5	10	5	PETA requires surface 'facet' peripheries to be joined, to close gaps
● Low total weight	8	9	10	5	META is lightest
Total	899	1000	892		

SECTION 6

RECOMMENDATIONS FOR FURTHER STUDY

This study has defined structural module shapes and sizes, the basic functions required to effect module deployment and joining, the dimensional limitations of the working environment, and has outlined the general physical relationship between the Orbiter and the evolving reflector structure.

The study has indicated that dispensing, deployment, and joining of reflector structural modules performed in an automated fashion from the Orbiter with no essential EVA participation is a feasible concept and is a cost effective, low risk approach to development of large space structures.

The merits of the approach may be summarized as follows:

- The cost of transporting the structure to orbit is minimized by the high packaging density of the candidate structural concepts, which approaches that of stacked stock material.

- The transition of a typical module from the packaged configuration to its stable, deployed geometry is a straightforward mechanical event in which the linked structural elements move in a coordinated manner. The characteristic benefits of deployable structure are evident in this phase — no joining is required, there are no loose parts, and deployment is essentially automatic, self energized and of high reliability.

- The mechanical operations required for deploying and joining the first two modules are typical of all subsequent operations. The completed multi-module structure results from continuing repetition of these initial operations. The overall task is therefore well suited to automation, with EVA limited to inspection and troubleshooting tasks.

- The repetitious nature of the overall task also permits low cost, low risk proof of concept, which can be adequately demonstrated by the successful deployment and joining of just two modules.

The degree of mechanical automation envisioned to effect deployment, handling, and joining of the modules requires relatively sophisticated support equipment including precise monitoring and positioning subsystems.

The logical next step in concept development, therefore, is to define the mechanical method and means, within this established framework, to a greater depth than has been possible within the relatively broad scope of this study.

Tasks suggested for this second phase of feasibility study include structural/ mechanical design studies of the provisions for:

1. Launch phase support of the stowed modules.

2. Release of individual modules from the stowage pallet.

3. Handling of the packaged module from stowage to a location for deployment.

4. Release of module restraints and performance of module deployment.

5. Accommodation of this initial module while handling and deployment of the second module is performed.

6. Docking of the two modules and alignment of structural interfaces.

7. Performance of structural integration of deployed modules by actuation of mechanical latches at each pair of mating node points.

8. Integration and alignment of reflective surface facets.

Performance of these eight tasks would permit realistic estimation of the magnitude of the engineering tasks involved and of the viability of this overall concept for construction of large structures in space.

1. Report No. NASA CR-3411	2. Government Accession No.	3. Recipient's Catalog No.
4. Title and Subtitle MODULAR REFLECTOR CONCEPT STUDY		5. Report Date March 1981
		6. Performing Organization Code
7. Author(s) D. H. VAUGHAN		8. Performing Organization Report No. GDC-ASP-79-003
		10. Work Unit No.
9. Performing Organization Name and Address General Dynamics Corporation Convair Division San Diego, California 92138		11. Contract or Grant No. NAS1-15753
		13. Type of Report and Period Covered Contractor Report (April 79 – Feb. 80)
12. Sponsoring Agency Name and Address National Aeronautics and Space Administration Washington, DC 20546		14. Sponsoring Agency Code

15. Supplementary Notes
Langley Technical Monitor: Michael F. Card Final Report

16. Abstract
    A study was conducted to evaluate the feasibility of space-erecting a 100-meter paraboloidal R.F. reflector by joining a number of individually deployed structural modules. Three module design concepts were considered: – 1) the Deployable Cell Module (DCM), 2) the Modular Paraboloidal Erectable Truss Antenna (Mod-PETA), and 3) the Modular Erectable Truss Antenna (META).

    With the space shuttle (STS) as the launch system, the methodology of packaging and stowing in the orbiter, and of dispensing, deploying and joining, in orbit, were studied and the necessary support equipment identified.

    The structural performance of the completed reflectors was evaluated and their overall operational capability and feasibility were evaluated and compared. The potential of the three concepts to maintain stable shape in the space environment was determined. Their ability to operate at radio frequencies of 1 GHz and higher was assessed assuming the reflector surface to consist of a number of flat, hexagonal facets.

    A parametric study was performed to determine figure degradation as a function of reflector size, flat facet size and f/D ratio.

17. Key Words (Suggested by Author(s)) Paraboloidal Reflector (1–15GHz) Space deployable/erectable Large modular structure	18. Distribution Statement Unclassified – Unlimited Subject Category 39

19. Security Classif. (of this report) Unclassified	20. Security Classif. (of this page) Unclassified	21. No. of Pages 118	22. Price A06